

Electronic Thesis and Dissertation Repository

3-28-2013 12:00 AM

Catalytic Conversion of Benzothiophene Over a H-ZSM5 Catalyst, Reactivity and a Kinetic Model

Saad A. Al-Bogami
The University of Western Ontario

Supervisor
Prof. Hugo de Lasa
The University of Western Ontario

Graduate Program in Chemical and Biochemical Engineering
A thesis submitted in partial fulfillment of the requirements for the degree in Doctor of Philosophy
© Saad A. Al-Bogami 2013

Follow this and additional works at: <https://ir.lib.uwo.ca/etd>

 Part of the [Catalysis and Reaction Engineering Commons](#)

Recommended Citation

Al-Bogami, Saad A., "Catalytic Conversion of Benzothiophene Over a H-ZSM5 Catalyst, Reactivity and a Kinetic Model" (2013). *Electronic Thesis and Dissertation Repository*. 1146.
<https://ir.lib.uwo.ca/etd/1146>

This Dissertation/Thesis is brought to you for free and open access by Scholarship@Western. It has been accepted for inclusion in Electronic Thesis and Dissertation Repository by an authorized administrator of Scholarship@Western. For more information, please contact wlsadmin@uwo.ca.

**CATALYTIC CONVERSION OF BENZOTHIOPHENE OVER
A H-ZSM5 CATALYST
REACTIVITY AND A KINETIC MODEL**

(Thesis format: Monograph)

by

Saad A. Al-Bogami

**Graduate Program in Engineering Science
Department of Chemical and Biochemical Engineering**

**A thesis submitted in partial fulfillment
of the requirements for the degree of
Doctor of Philosophy**

**The School of Graduate and Postdoctoral Studies
The University of Western Ontario
London, Ontario, Canada**

© Saad Al-Bogami 2013

ABSTRACT

Nowadays and due to environmental legislations, a world-wide attention has been given towards clean transportation fuels with emphasis on sulfur contents reduction. These efforts on the other hand are challenged by the poor qualities of crude oils. The existing desulfurization technologies such as hydrodesulfurization are not capable to cope with new firm standards. Hence, it is very desirable to develop a catalytic desulfurization process to meet both sulfur limits and refining economics. As one aspect of this objective, it is of great importance to study and comprehend the behavior and reactivity of individual sulfur species present in transportation fuels cuts. Zeolites namely, H-ZSM5 has shown a potential catalyst for a desulfurization process for gasoline fuel range. Acidity and shape selectivity of these zeolites make it viable for such a process eliminating the use of hydrogen.

With aiming to light diesel fraction desulfurization, this dissertation provides insights and understanding of benzothiophene sulfur species conversion over a H-ZSM5 zeolite catalyst. The H-ZSM5 particles were dispersed in an inert silica-alumina matrix to diminish possible cracking of diesel component. This catalyst was characterized using standard techniques including: a) NH_3 -TPD, b) N_2 adsorption, c) Particle size distribution, d) X-ray diffraction, e) SEM-EDX, and f) Pyridine FTIR. Catalytic and thermal runs were performed in the CREC Riser Simulator that mimics the industrial FCC unit. Mixtures containing 6 wt% benzothiophene dissolved in n-dodecane were reacted at close to atmospheric pressure, 350°C – 450°C temperatures, and 3, 5, 7 seconds reaction times. Thermal cracking was found to be negligible under the studied

reaction conditions. Experimental results from catalytic runs showed a higher benzothiophene conversion over n-dodecane conversion. This was true despite the difference in benzothiophene and n-dodecane molecular sizes.

The experimental results of this PhD dissertation are also supported with a molecular dynamics (MD) simulation study that investigates self diffusivity of benzothiophene and n-dodecane in ZSM-5 zeolite. In addition and using the obtained experimental data, a heterogeneous kinetic model is proposed for benzothiophene conversion over H-ZSM5 catalyst. Numerical non-linear regression leads to model parameters estimations with low confidence intervals suggesting the adequacy of this kinetic model.

Keywords

Diesel, Desulfurization, Zeolite, Catalyst, H-ZSM5, Benzothiophene, MD Simulation, Self Diffusivity, Kinetic modeling.

“Read! In the Name of your Lord, Who has created (all that exists). He has created man from a clot. Read! And your Lord is the Most Generous. Who has taught (the writing) by the pen. He has taught man that which he knew not” (The Noble Quran, Chapter 96, Verses 1-5).

Dedicated to My Parents, Wife, and Daughters (Sarah & Shatha)

ACKNOWLEDGMENTS

In the name of ALLAH, the Most Beneficent, the Most Merciful

First and foremost, praise and gratitude are due to ALLAH, the Almighty, who has blessed me and gave me the strength and patience to complete my PhD study.

I owe much gratitude to my supervisor Prof. Hugo de Lasa for giving me this unique opportunity to work in his group and learn from his vast knowledge and experience.

I would like to acknowledge Saudi Aramco Oil Company/Research and Development Centre for granting and providing the scholarship for my PhD program at University of Western Ontario.

I would like also to thank Dr. Maria Lujan Ferreira for her support and guidance during the Molecular Dynamics Simulation part of my thesis.

I am very appreciative for all my friends at CREC for surrounding me with a healthy research environment. Namely, I would like to recognize Engineer Jose Munoz for being of help all the time during my experimentations. Also, I especially thank my colleagues Sameer Al-Ghmadi, Jesus Moreira, and Mohammad Rezwanul Quddus, for their continuous help and fruitful technical discussions. In addition, I thank Mr. Pastor Solano for lending me a helping hand always when needed.

Last but definitely not least, my deepest gratitude goes to my parents, brothers, and sisters for their encouragement and support. I am very grateful to my wife and my daughters (Sarah and Shatha) for being beside me during the PhD journey.

TABLE OF CONTENTS

ABSTRACT	ii
AKNOWLEDGMENTS	vi
TABLE OF CONTENTS	vii
LIST OF TABLES	xii
LIST OF FIGURES	xiii
LIST OF APPENDICES	xvii
NOMENCLATURE	xviii
CHAPTER 1. INTRODUCTION	1
CHAPTER 2. LITERATURE REVIEW	4
2.1 Introduction.....	4
2.2 Sulfur Compounds in Transportation Fuels.....	4
2.3 Reactivity of Sulfur Compounds	5
2.4 Benzothiophene	6
2.4.1 Methods for Benzothiophene Removal from Transportation Fuels.....	7
2.4.1.1 Hydrodesulfurization (HDS).....	7
2.4.1.2 Oxidative Desulfurization (ODS)	9
2.4.1.3 Biodesulfurization.....	11
2.4.1.4 Adsorption Methods.....	11
2.4.1.5 Desulfurization Using Zeolites	11
2.4.1.5.1 Transformation Studies.....	12
2.4.1.5.2 Adsorption Studies of Benzothiophene on Zeolites	14
2.5 H-ZSM5 Zeolite as A Desulfurization Catalyst	15
2.6 Kinetics of Benzothiophene Reactions	18

2.7 Zeolites Catalysts	21
2.8 Zeolite Properties	22
2.8.1 Acidity	22
2.8.2 Shape Selectivity	25
2.9 Pore Size and Molecular Diameters	27
2.10 ZSM-5 Zeolite	30
2.11 Conclusions.....	33
CHAPTER 3. SCOPE OF RESEARCH.....	36
CHAPTER 4. MOLECULAR DYNAMICS SIMULATION	38
4.1 Introduction.....	38
4.2 Diffusion in Zeolites	38
4.2.1 Self Diffusivity and Transport Diffusivity	39
4.2.2 Factors Influencing the Diffusivity	40
4.2.2.1 Adsorbate Concentration	40
4.2.2.2 Temperature	41
4.2.2.3 Zeolite Crystal Size	42
4.2.2.4 Si/Al Ratio	42
4.3 Methods for Determining the Diffusion in Zeolites	42
4.3.1 Molecular Dynamics (MD) Simulation.....	43
4.3.1.1 Molecular Dynamics Studies of Hydrocarbons Diffusion in ZSM-5	44
4.3.1.2 Flexibility of Zeolite Framework in MD Simulation.....	50
4.4 Methodology	51
4.5 Results and Discussion	55
4.5.1 Self Diffusivity Calculations Stability	55
4.5.2 Self Diffusivity of n-Dodecane	57

4.5.2.1 Temperature Effect on n-Dodecane Self Diffusivity	58
4.5.2.2 Molecule Loading Effect on n-Dodecane Self Diffusivity	59
4.5.3 Self Diffusivity of Benzothiophene.....	61
4.5.3.1 Temperature Effect on Benzothiophene Self Diffusivity	61
4.5.3.2 Molecule Loading Effect on Benzothiophene Self Diffusivity	63
4.6 Significance of the Results Obtained for the Catalytic Desulfurization of Light Diesel.....	65
4.7 Conclusions.....	65
CHAPTER 5. EXPERIMENTAL METHODS	67
5.1 Introduction.....	67
5.2 Catalyst Preparation and Materials	67
5.3 Catalyst Characterization.....	69
5.3.1 Apparent Bulk Density and Particle Size Distribution.....	69
5.3.2 X-Ray Diffraction (XRD)	70
5.3.3 SEM-EDX	72
5.3.4 NH ₃ -TPD.....	72
5.3.5 Pyridine FTIR.....	74
5.3.6 N ₂ Adsorption.....	75
5.4 Reaction System	78
5.4.1 The Riser Simulator	78
5.4.2 Experimental Procedure	83
5.4.3 Analytical System	85
5.4.4 Quantification of Carbonaceous Material in Spent Catalyst Samples	89
CHAPTER 6. RESULTS AND DISCUSSION	91
6.1 Introduction.....	91

6.2 Catalyst Characterization.....	91
6.2.1 ABD and PSD	91
6.2.2 XRD	92
6.2.3 SEM-EDX.....	94
6.2.4 NH ₃ -TPD.....	95
6.2.5 Pyridine FTIR.....	97
6.2.6 N ₂ Adsorption.....	99
6.3 Catalyst Stability	103
6.4 Thermal and Catalytic Runs	106
6.4.1 Thermal Cracking.....	107
6.4.2 Catalytic Runs	107
6.4.2.1 Benzothiophene Conversion	107
6.4.2.2 Conversion of n-Dodecane.....	112
6.4.3 Products Distributions	115
6.5 Benzothiophene Adsorption Selectivity	120
6.6 Effect of Reactants Initial Concentrations on Catalytic Conversion	121
6.7 Conclusions.....	124
CHAPTER 7. KINETIC MODELING	126
7.1 Introduction.....	126
7.2 Benzothiophene Reaction Mechanism	126
7.3 Kinetic Model Development.....	128
7.4 System of Ordinary Differential Equations	133
7.5 Kinetic Parameters Estimation	138
7.6 Conclusions.....	144
CHAPTER 8. CONCLUSIONS AND RECOMMENDATIONS	146

REFERENCES	151
APPENDICES	162
CURRICULUM VITAE	202

LIST OF TABLES

Table 2.1. Major sulfur compounds in transportation fuels (Song & Ma, 2006)	5
Table 2.2. Molecular diameters of some hydrocarbons and pore sizes of some zeolites.	29
Table 4.1. Self-diffusion coefficient of n-dodecane reported in the technical literature.	48
Table 4.2. Reported self diffusivity in the literature for some aromatic hydrocarbons. ..	50
Table 5.1. Mass Selective Detector parameters and settings.	86
Table 5.2. GC method and parameters.	88
Table 6.1. SEM-EDX analysis results in wt %. Reported values are averages of three runs with standard deviation of ± 2	94
Table 6.2. Acid properties of zeolite samples.	97
Table 6.3. Specific surface area SSA (m^2/g), pore volume PV (cm^3/g), and Median Pore Diameter (\AA).	101
Table 6.4. Hydrocarbon and sulfur products distribution from catalytic conversion of pure n-dodecane and benzothiophene / n-dodecane mixture at 450 °C, cat/oil = 5, and 7 seconds reaction time.	118
Table 7.1. Intrinsic kinetics parameters of the proposed kinetic model along with their 95% confidence intervals and standard deviations.	139
Table 7.2. Cross-correlation coefficients for the kinetic model optimized parameters .	141

LIST OF FIGURES

Figure 2.1. Relationship between the reactivity and the size of sulfur containing compounds (Song, 2003; Zhao, 2009).....	6
Figure 2.2. Mechanism of Benzothiophene HDS reactions (Adapa, 2008; Babich & Moulijn, 2003).	7
Figure 2.3. Reactions of BZT following the ODS process (Campos-Martin et al., 2004)	10
Figure 2.4. Thiophene conversion via ring opening (Jaimes et al., 2009)	17
Figure 2.5. Thiophene conversion via alkylation (Jaimes et al., 2009)	18
Figure 2.6. Schematic representation of Silanol, and Brønsted acid sites present in zeolites frameworks.	24
Figure 2.7. Formation of Lewis acid sites in the zeolite framework.	25
Figure 2.8. Shape selectivity of Zeolites (Hagen, 2006; Xiao, 1990; Zheng, 2002)	26
Figure 2.9. Schematic drawing of the silicalite pore structure (Smit et al., 1997).....	31
Figure 4.1. Different 2D views of a ZSM-5 supercell (8 unit cells) used in the current study with arrows indicating: a) The straight channels locations, b) The intersections of straight and zigzag channels, and c) The zigzag channels locations.	53
Figure 4.2. Self diffusivity of n-dodecane as a function of simulation time (molecule loading = 1/ u.c).	56
Figure 4.3. Self diffusivity of benzothiophene as a function of simulation time (molecule loading = 1 / u.c).	57
Figure 4.4. Self diffusivity of n-dodecane as a function of simulation temperature (molecule loading = 1 / u.c, and simulation time is 400 ps).	59
Figure 4.5. Self diffusivity of n-dodecane as a function of molecule loading per unit cell (Temperature is 723 K and simulation time is 400 ps).	60
Figure 4.6. Self diffusivity of benzothiophene as a function of simulation temperature (molecule loading = 1 / u.c, and simulation time is 400 ps).	62
Figure 4.7. Self diffusivity of benzothiophene as a function of molecule loading per unit cell (Temperature is 723 K and simulation time is 400 ps).	64

Figure 5.1. Schematic diagram of the CREC Riser Simulator with components at the time of assembly.	79
Figure 5.2. Schematic description of the CREC Riser Simulator, with associated valves, and accessories: (MFC: mass flow controller, 4PV: four port valve, 6PV: six port valve, V ₁ , V ₂ and V ₃ : auxiliary on-off valves, P: pressure, T: temperature).	80
Figure 5.3. Typical pressure profile in the CREC Riser Simulator.	85
Figure 6.1. XRD patterns for the catalyst samples: (A) matrix alone with incorporated fused alumina filler, (B) fresh H-ZSM5 (before calcinations), (C) H-ZSM5 after calcinations, and (D) catalyst pellets containing 30 wt % of H-ZSM5 and 50 wt % fused alumina filler.	93
Figure 6.2. NH ₃ -TPD spectra for: (a) the H-ZSM5 zeolite and (b) the catalyst pellets containing 30 wt % zeolite.	96
Figure 6.3. FTIR spectra of pyridine for: (A) catalyst pellets with 30 wt % H-ZSM5, (B) H-ZSM5 zeolites, (C) matrix, and (D) H-ZSM5 before pyridine adsorption.	98
Figure 6.4. Adsorption-desorption isotherms of nitrogen on: (a) H-ZSM5 zeolites, (b) matrix and (c) zeolite pellets.	100
Figure 6.5. Conversion of n-dodecane versus run number. Reaction conditions: 450 °C, cat/oil = 5, 7 seconds reaction time, and without catalyst regeneration in between runs.	104
Figure 6.6. Conversion of n-dodecane versus cycle number. Reaction conditions: 450 °C, cat/oil = 5, 7 seconds reaction time, and with catalyst regeneration in between runs. ...	105
Figure 6.7. Total conversion of benzothiophene as a function of reaction time. Reaction conditions: T = 350, 375, 400, 425, and 450 °C, cat/oil = 5. Feed composition is 6 wt % benzothiophene / 94 wt % n-dodecane. Error bars correspond to standard deviation of three repeats.	108
Figure 6.8. Conversion of benzothiophene in gas phase products as a function of reaction time. Reaction conditions: T = 350, 375, 400, 425, and 450 °C, cat/oil = 5. Feed composition is 6 wt % benzothiophene / 94 wt % n-dodecane. Error bars correspond to standard deviation of three repeats.	109
Figure 6.9. Conversion of benzothiophene as coke-on-catalyst as a function of reaction time. Reaction conditions: T = 350, 375, 400, 425, and 450 °C, cat/oil = 5. Feed	

composition is 6 wt % benzothiophene/94 wt % n-dodecane. Error bars correspond to standard deviation of three repeats.	110
Figure 6.10. Conversion of n-dodecane as a function of reaction time. Reaction conditions: T = 350, 375, 400, 425, and 450 °C, cat/oil = 5. Feed composition is 100 wt % n-dodecane. Error bars correspond to standard deviation for three repeats.	112
Figure 6.11. Conversion of n-dodecane as a function of reaction time. Reaction conditions: T = 350, 375, 400, 425, and 450 °C, cat/oil = 5. Feed composition is 6 wt % benzothiophene / 94 wt % n-dodecane. Error bars correspond to standard deviation for three repeats.	113
Figure 6.12. FID signal of hydrocarbon gas-phase products from 6 wt % benzothiophene / 94 wt % n-dodecane conversion and unconverted reactants at 450 °C, cat/oil = 5, and 7 seconds reaction time.	115
Figure 6.13. FID signal of sulfur gas phase products from 6 wt % benzothiophene / 94 wt % n-dodecane conversion at 450 °C, cat/oil = 5, and 7 seconds reaction time.	116
Figure 6.14. FPD signal showing unconverted benzothiophene and traces sulfur species from 6 wt % benzothiophene / 94 wt % n-dodecane conversion at 450 °C, cat/oil = 5, and 7 seconds reaction time.	117
Figure 6.15. Selectivity of benzothiophene as a function of reaction time. Reaction conditions: T = 350, 375, 400, 425, and 450 °C, cat/oil = 5. Feed composition is 6 wt % benzothiophene / 94 wt % n-dodecane.	121
Figure 6.16. Benzothiophene total conversion versus benzothiophene initial concentration. Reaction conditions: T = 450 °C, cat/oil = 5, and 7 seconds reaction time. Error bars correspond to standard deviation of three repeats.	122
Figure 6.17. n-Dodecane conversion versus its mass injected in the Riser Simulator. Reaction conditions: T = 450 °C, cat/oil = 5, and 7 seconds reaction time. Error bars correspond to standard deviation of three repeats.	123
Figure 7.1. Benzothiophene alkylation mechanism over H-ZSM5 zeolite catalyst.	127
Figure 7.2. Proposed reaction network for benzothiophene conversion.	128
Figure 7.3. Proposed reaction network for n-dodecane cracking.	129

Figure 7.4. Comparison between experimental and predicted reaction products yields as a function of reaction time at different reaction temperatures with: (a) Hydrocarbons, (b) Aromatics, (c) Sulfur species in diesel range, and (d) Sulfur in coke. 142

Figure 7.5. Parity plot showing the model prediction as opposed to the experimental data 143

LIST OF APPENDICES

Appendix A. MD Simulation Parameters	162
Appendix B. Assessment of Volume	168
Appendix C. Benzothiophene Calibration Curve	171
Appendix D. Mass Balance.....	175
Appendix E. Conversion and Products Distribution.....	182
Appendix F. Kinetic Modeling Parameters	198

NOMENCLATURE

Abbreviations

ABD	Average Bulk Density
API	American Petroleum Institute
APS	Average Particle Size
Ar	Aromatics
BET	Brunauer, Emmet, and Teller
BZT	Benzothiophene
cat/oil	catalyst to oil ratio
CI	Confidence interval
COMPASS	Condensed-Phase Optimized Molecular Potentials for Atomistic Simulation Studies
CREC	Chemical Reactor Engineering Center
d	d-spacing
DBT	Di-benzothiophene
DFT	Density Functional Theory
DRIFT	Diffuse Reflectance Infrared Spectroscopy
DOF	Degree of freedom
EDX	Energy Dispersive X-ray Spectroscopy
EFAL	Extra framework aluminium
EM	Ethyl-mercaptan
FCC	Fluid Catalytic Cracking

FID	Flame Ionized Detector
FPD	Flame Photometric Detector
FTIR	Fourier Transform Infrared Spectroscopy
GC	Gas chromatography
HC	Hydrocarbon
HDS	Hydrodesulfurization
HTP	High temperature peak
ICP	Inductively Coupled Plasma
LTP	Low temperature peak
MAT	Microactivity test unit
MD	Molecular dynamics
MFI	Mordenite framework inverted
MSD	Mass selective detector (Chapter 5 and 6)
MSD	Mean Square Displacement (Chapter 4)
MTG	Methanol to gasoline
nC ₈	n-Octane
n-C12 or C12	n-Dodecane
n-C16	n-Hexadecane
NHL	Nose-Hoover-Langevin
NVE	constant number of particles, volume, and energy
NVT	constant number of particles, volume, and temperature
ODS	Oxidative desulphurization
PFG NMR	Pulsed Field Gradient Nuclear Magnetic Resonance

PSD	Particle Size Distribution
PV	Pore volume
QENS	Quasi-Elastic Neutron Scattering
rpm	rotation per minute
RSH	Mercaptanes
RSSR	Disulfides
R ₂ S	Sulfides
SARS	Selective adsorption for removing sulfur
SC	Sulfur in coke
SD	Sulfur in diesel
SEM	Scanning Electron Microscopy
SG	Sulfur in gasoline
SSA	Specific Surface Area
SSM	Solid sample module
SSQ	Minimum sum of squares
SSW	Surface Science Western
STD	Standard deviation
STP	Standard Temperature Pressure
T	Reactor temperature
TCD	Thermal Conductivity Detector
Th	Thiophene
TOC	Total organic carbon
TPD	Temperature Programmed Desorption

TST	Transition State
u.c	unit cell
ULSD	Ultra Low Sulfur Diesel
USY	Ultra Stable Y zeolite
VB	Vacuum Box
VGO	Vacuum gas oil
XRD	X-ray diffraction
4PV and 6PV	four port valve and six port valve

Parameters

A_i	GC chromatogram area of species i
A_p	Area occupied by a single molecule
A_T	sum of all GC chromatogram areas
C	concentration
D_t	Transport diffusivity coefficient
D_s	Self diffusivity coefficient
E_D	Activation energy of diffusion
J	Flux
K_i	Adsorption constant of i
k_i	Kinetic constant of i
m_{after}	mass of feed syringe after injection
m_{before}	mass of feed syringe before injection
MW_i	Molecular weight of i

N	Avogadro's number
P_i	Partial pressure of i
P/P_0	Relative pressure
R	Universal gas constant
r_i	Reaction rate of i
S_{BZT}	Adsorption selectivity if benzothiophene
t	Time
V_A	Alcohol volume
V_{ads}	Volume adsorbed
V_m	Volume of monolayer
V_R	Reactor volume
V_T	Total volume
V_o	Molar volume
wt	Weight
W_{cat}	Weight of catalyst
W_{coke}	Total weight of coke formed
W_{hc}	Wight of hydrocarbons injected
$W_{i,conv}$	Total converted weight of species i
$W_{i,coke}$	Converted weight of species i in coke
$W_{i,initial}$	Initial weight of species i in feed mixture
W_P	Total weight of all products in gas phase
W_{hc}	Weight of hydrocarbon injected into the reactor
W_{sample}	Weight of catalyst sample used for TOC analysis

W_{TOC}	Weight of coke obtained from TOC analysis
X_i	Conversion of species i
$x_{i,\text{exp}}$	Mass fraction of component i obtained experimentally
$x_{i,\text{pred}}$	Mass fraction of component i predicted by the kinetic model
$y_{i,\text{feed}}$	Weight fraction of species i in feed mixture
ΔH_i	Heat of adsorption of i

Symbols

Ag	Silver
Al	Aluminium
Al_2O_3	Aluminium oxide
Au	Gold
Ce	Cerium
CH_4	Methane
C_2H_4	Ethane
Co	Cobalt
CoO	Cobalt oxide
CO_2	Carbon Dioxide
Cr	Chromium
Cu	Copper
$\text{C}_8\text{H}_8\text{S}$	Benzothiophene
Fe	Iron
HCL	Hydrochloric acid

He	Helium
HNO ₃	Nitric acid
H ₂	Hydrogen
H ₂ O ₂	Hydrogen peroxide
H ₂ S	Hydrogen sulfide
Mo	Molybdenum
MoO	Molybdenum oxide
Na	Sodium
Na ₂ O	Sodium oxide
NH ₃	Ammonia
NH ₄ ⁺	Ammonium
Ni	Nickel
N ₂	Nitrogen
O ₃	Ozone
Pt	Platinum
Si	Silicon
SiO ₂	Silicon oxide
So _x	sulfur oxides
Zn	Zinc

Units

Å	Angstrom
atm	Atmospheric

°C	degrees Celsius
cc or cm ³	cubic centimeters
fs	femtoseconds (10 ⁻¹⁵ s)
g	gram
h	hour
K	degrees Kelvin
Kg	kilogram
kV	kilo-Volt
m, mm, and μm	meter, millimeter, and micrometer
m ³ and m ²	cubic meters and square meters
mA	milli-ampere
mg	milligram
mL	milliliter
min	minutes
MPA	mega pascal
nm	nanometer
μm	micrometer or micron
ppmw	part per million per weight
ps	picoseconds (10 ⁻¹² s)
psia	pounds per square inch absolute
psig	pounds per square inch gauge
s	seconds

Greek symbols

σ_m	Lennard-Jones length constant
σ_o	van der Waals diameter
θ	Diffraction angle

CHAPTER 1

INTRODUCTION

New environmental legislations mandate a very low or near zero sulfur content in transportation fuels e.g. gasoline and diesel. On the other hand, crude oils nowadays, which are the sources for these fuels, are getting tougher to process in terms of quality (Song & Ma, 2003; Stanislaus et al., 2010).

In particular, high sulfur levels in these crude oils will require more severe operating conditions using the existing desulfurization technologies in order to comply with the environmental regulations. For example, high operating temperatures and large hydrogen consumption will limit the use of the classical hydrodesulfurization (HDS) process. In addition, this process is not very efficient when treating sterically hindered sulfur compounds such as benzothiophene and dibenzothiophene (Ali et al., 2006; Campos-Martin et al., 2004; Paniv et al., 2006). On this basis, there is a necessity for a viable desulfurization technology by which refiners meet the fuels market specifications and simultaneously keep their economical profits.

As a result, zeolites have emerged as a potential catalyst for a desulfurization process eliminating the use of hydrogen (de Lasa et al., 2006). The acidity of these materials as well as their shape selectivity qualifies them for the purpose of these processes. In this respect, there has been intensive research on the conversion of middle distillate (gasoline and diesel) sulfur containing compounds. These studies considered zeolite based catalysts and mild operating conditions with temperatures (350-450 °C) and pressure (1 atm). To be specific, a H-ZSM5 zeolite was tested for the removal of methyl mercaptan and

thiophene sulfur species from hydrocarbons mixtures (de Lasa et al., 2006; Jaimes et al., 2011; Jaimes et al., 2009; Jaimes et al., 2008; Jaimes & de Lasa, 2009; Yu et al., 1999). In general, the H-ZSM5 zeolite has been found to selectively remove sulfur compounds utilizing the hydrogen donor component (e.g. paraffin and olefin) that coexists in the reactants mixture.

The aim of the current research is to consider H-ZSM5 zeolites for the removal of sulfur containing compounds in the light diesel fuel fraction. In order to demonstrate the value of this approach, benzothiophene conversion over a H-ZSM5 based catalyst is investigated. In this respect, the major contributions of this study are the following:

- i. The development of a theoretical study based on Molecular Dynamics (MD) simulations for the self diffusion of benzothiophene and diesel fraction model compounds (n-dodecane) in ZSM-5 zeolites.
- ii. The development of fluidizable H-ZSM5 catalyst particles for a benzothiophene/n-dodecane mixture catalytic reaction.
- iii. The establishment of the stability and reactivity of the prepared H-ZSM5 catalyst in a CREC Riser Simulator under mild conditions: temperatures (350-450 °C), at around atmospheric pressure, catalyst to oil ratio of 5, and short reaction times.
- iv. The development of a kinetic model describing the conversion of benzothiophene over a H-ZSM5 zeolite.

To address these issues, this dissertation includes eight Chapters with the following content:

- Chapter 1 provides a brief introduction about the importance of a new desulfurization process for middle distillates fuels.

- Chapter 2 summarizes the recent literature which examines the conversion of benzothiophene sulfur species. In addition, it includes a description of zeolite properties and applications with a focus on the subject of ZSM-5 zeolites.
- Chapter 3 highlights the main objectives of the current research.
- Chapter 4 describes the theoretical part of this research which is the Molecular Dynamics (MD) Simulations study. It includes the methodology as well as the main results obtained.
- Chapter 5 describes the experimental methods of this thesis, including catalyst preparation, characterization, and testing.
- Chapter 6 reports the experimental results from catalyst characterization and catalytic runs.
- Chapter 7 describes the kinetic modeling development and the kinetic modeling results.
- Chapter 8 provides the dissertation conclusions and recommendations for future work.

CHAPTER 2

LITERATURE REVIEW

2.1 Introduction

Sulfur content, in addition to API gravity, is a major factor in determining the crude oil barrel value. Total sulfur in crude oils can vary between 0.05 and 6 weight percent depending on the type and source of crude oil. On this basis, crude oils can be classified into sweet crudes with less than 0.5 weight percent sulfur, and sour crudes with more than 1.5 weight percent sulfur (Fahim et al., 2010; Gary & Handwerk, 2001).

Sulfur is undesirable component in oil refining, as it can cause several corrosion problems in pipelines, pumps, and other refining equipments. Furthermore, sulfur species are responsible for catalyst deactivation in the downstream refining processes.

Nowadays, environmental regulations are a strong motivator for sulfur reduction in transportation fuels. Sulfur is the main cause for sulfur oxide (SO_x) emissions resulting from the combustion of transportation fuels (Ali et al., 2006; Brunet et al., 2005; Song, 2003).

2.2 Sulfur Compounds in Transportation Fuels

About 75-80 % of the total refining products form gasoline, diesel and non-transportation fuels. As a consequence, sulfur becomes a direct issue when hydrotreating these fuels (Babich & Moulijn, 2003). Table 2.1 reports the common types of sulfur containing compounds in transportation fuels.

Table 2.1. Major sulfur compounds in transportation fuels (Song & Ma, 2006)

Transportation fuel type	Sulfur compounds
Gasoline range, light naphtha, and FCC naphtha	Mercaptanes (RSH), Sulfides (R ₂ S), Disulfides (RSSR), Thiophene and alkylated-thiophenes, and Benzothiophene
Jet Fuel range, heavy naphtha, and middle distillate	Benzothiophene (BZT) and its alkylated derivatives
Diesel Fuel range, middle distillate, and light cycle oil	Alkylated-benzothiophenes, Dibenzothiophene (DBT) and alkylated-dibenzothiophenes

2.3 Reactivity of Sulfur Compounds

Figure 2.1 reports a qualitative description of the reactivities of sulfur compounds as a function of their molecular size and side group substitution. This figure covers the gasoline, jet fuel and diesel fuel ranges. It can be observed that reactivities of the 1- to 3-ring sulfur compounds decrease in the following reactivity order: thiophene > benzothiophene > dibenzothiophene (Song, 2003; Zhao, 2009).

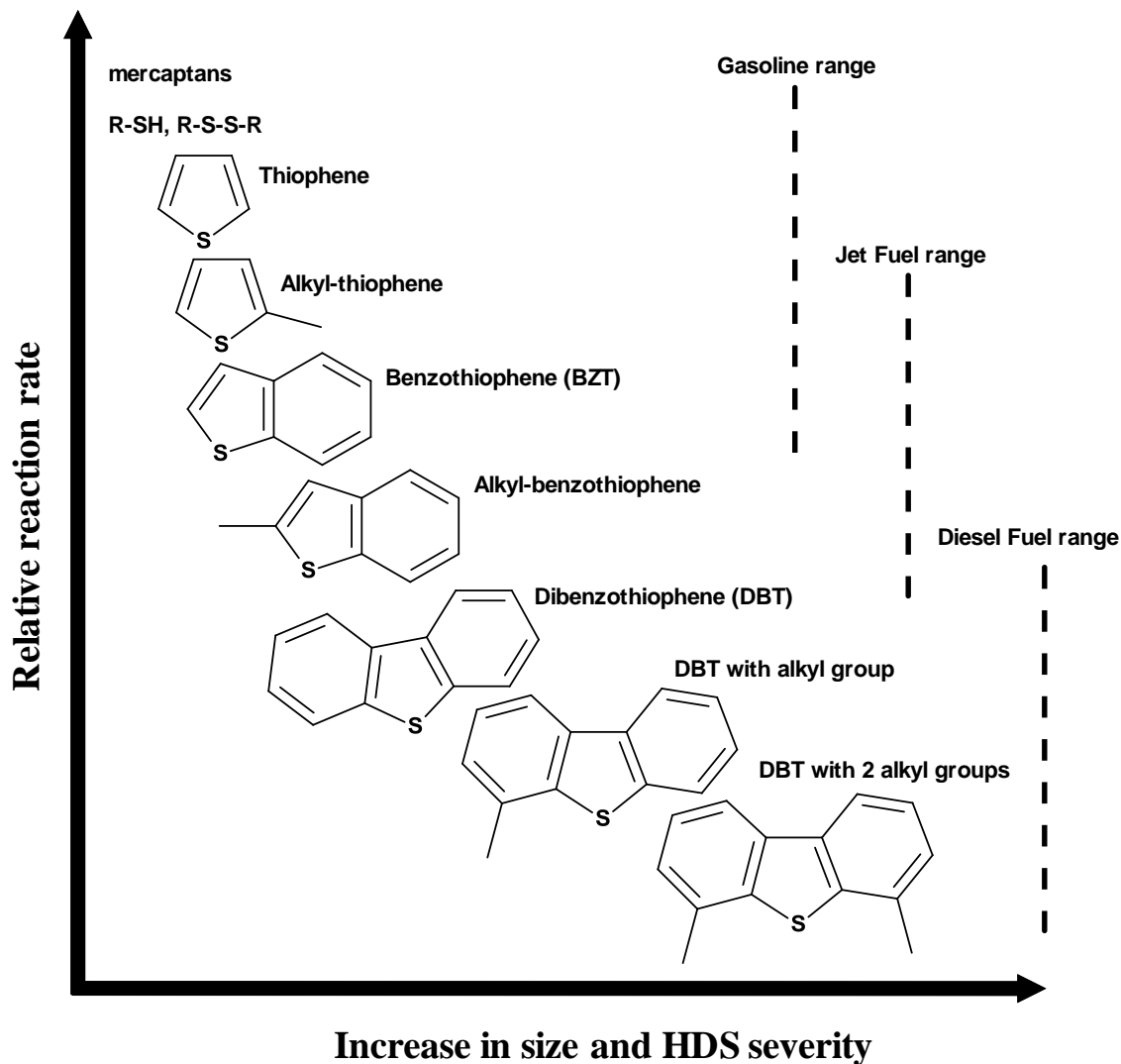


Figure 2.1. Relationship between the reactivity and the size of sulfur containing compounds (Song, 2003; Zhao, 2009)

2.4 Benzothiophene

Benzothiophene (BZT) is one of the most refractory sulfur species in transportation fuels. It can be found in heavy gasoline range, jet fuel (kerosene) and light diesel range. BZT has a molecular size of 6 Å as compared to the 5.3 Å of thiophene and the 8 Å of dibenzothiophene, as well as a 220-221°C boiling point (Contreras et al., 2008).

2.4.1 Methods for Benzothiophene Removal from Transportation Fuels

In general, there are two approaches used to reduce sulfur content in petroleum refining feedstocks: conventional hydrodesulfurization and desulfurization processes without the requirement for the use of hydrogen. These desulfurization processes include: oxidative desulfurization (ODS), biodesulfurization, desulfurization using zeolites, and adsorption methods (Ali et al., 2006; Jaimes et al., 2008; Song, 2003).

2.4.1.1 Hydrodesulfurization (HDS)

HDS is a catalytic process that converts organic sulfur to hydrogen sulfide by reacting crude oil fractions with hydrogen. Typical pressures used are between 1 and 20 MPa and temperatures are between 290 and 455 °C. Selected pressures and temperatures depend upon the feed type and level of desulfurization required (Fahim et al., 2010; Gary & Handwerk, 2001). The main reactions involved in HDS for benzothiophene sulfur compounds are reported in Figure 2.2.

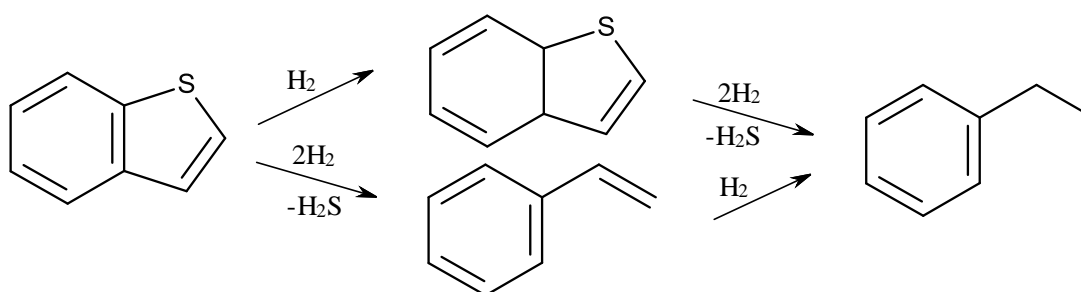


Figure 2.2. Mechanism of Benzothiophene HDS reactions (Adapa, 2008; Babich & Moulijn, 2003).

Daly (1978) investigated the HDS of benzothiophene over a $\text{CoO-MoO}_3\text{-Al}_2\text{O}_3$ catalyst. A stirred mini batch reactor operating at 200-400 °C, and 1250 psig was used in this study. It was concluded that benzothiophene HDS proceeds via two separate mechanisms: (i) initial hydrogenation of the thiophene double bond followed by hydrodesulfurization, and (ii) hydrodesulfurization with the formation of unsaturated hydrocarbons followed by hydrogenation. Both routes are of pseudo-first order in benzothiophene, and produced the same final product, ethylbenzene.

Using a sulfided $\text{CoO-MoO}_3\text{-}\gamma\text{Al}_2\text{O}_3$, Kilanowski et al. (1978) studied the HDS of thiophene, benzothiophene, and dibenzothiophene. Experiments were carried out in a pulse microreactor operating at 350-450 °C and atmospheric pressure. Results demonstrated that the reactivities of these sulfur containing compounds are about the same.

Taniguchi et al. (1999) investigated the HDS of benzothiophene over zeolites supported catalysts prepared from Mo and Mo-Ni sulfide clusters. A flow-type fixed bed reactor operating at 350 °C and 3 MPa was used for reactivity tests. One important conclusion from this study was the occurrence of benzothiophene alkylation with alkenes derived from the n-decane cracking, which was used as a co-reactant.

Wang & Prins (2008) studied the hydrodesulfurization of benzothiophene and dihydrobenzothiophene (dihydro-BZT) over a $\text{Mo}/\gamma\text{Al}_2\text{O}_3$ catalyst, in the absence and presence of H_2S . A fixed bed reactor operating at 5 MPa and 280-300 °C was used to carry out the catalytic reactions. Benzothiophene was found to react by hydrogenation to

dihydro-BZT and by hydrogenolysis to ethylbenzene. However, when present, H₂S inhibited both reactions.

Recently, Ahmed (2011) studied the HDS of benzothiophene and dibenzothiophene over a prepared phosphorus modified CoMo/Al₂O₃ catalyst. An autoclave batch reactor operating at 300-350 °C and 900 psig hydrogen pressure was used in this research. It was found that the rate of benzothiophene HDS was 10 times higher than dibenzothiophene at 300 °C and decreases up to 3 times more at 350 °C.

2.4.1.2 Oxidative Desulfurization (ODS)

Oxidative desulfurization (ODS) has been given much interest as an alternative technology for deep desulfurization. The ODS is basically a two-stage process. Oxidation occurs first, followed by liquid extraction. In the ODS process, the sulfur-containing compounds are oxidized using appropriate oxidants to convert these compounds to their corresponding sulfoxides and sulfones. These species are preferentially extracted from light oil due to their increased relative polarity. Any unused oxidant that remains in the light oil can be removed by water washing and extraction. The oxidized compounds can be extracted from the light oil by using a non-miscible solvent. Depending on the solvents used for extraction, the oxidized compounds and solvent are separated from the light oil by gravity separation or centrifugation. The light oil is water washed to recover any traces of dissolved extraction solvent and polished using other methods, such as absorption using silica gel and aluminum oxide. The solvent is separated from the mixture of solvent and oxidized compounds by a simple distillation procedure for

recycling and re-use. By using this process, a high sulfur removal is achieved with minimum impact on the fuel quality (Al-malki, 2004).

Many oxidants have been investigated which include peroxy organic acids, catalyzed hydroperoxides, and inorganic oxidants such as inorganic peroxy acids, peroxy salts and O_3 . The greatest advantages of the ODS process are low reaction temperature and pressure, and removing the need for expensive hydrogen that is used in the conventional HDS process. Another feature of ODS is that the refractory sulfur compounds such as benzothiophene are easily converted by oxidation (Al-malki, 2004; Ali et al., 2006).

Recently, ODS of middle distillate fuels using H_2O_2 plus formic acid as an oxidant, activated carbon as a reaction enhancer, and power ultrasound for phase dispersion was studied by Gonzalez et al. (2012). It was concluded that the ODS performance increases with (1) decreasing pH, (2) increasing reaction temperature, and (3) increasing the ultrasound power. A proposed mechanism for BZT removal using ODS is shown in Figure 2.3.

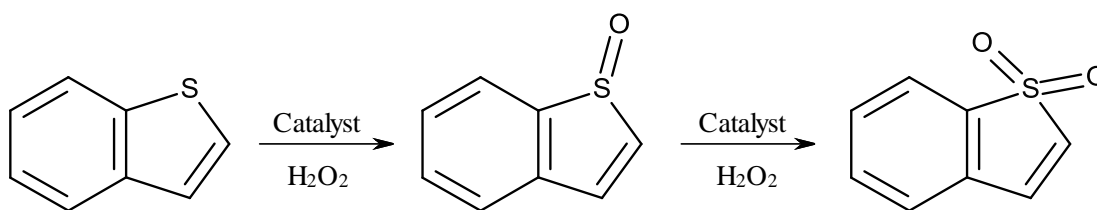


Figure 2.3. Reactions of BZT following the ODS process (Campos-Martin et al., 2004)

2.4.1.3 Biodesulfurization

One of the alternative options to remove sulfur from fossil fuels is by biological methods. Microorganisms require sulfur for their growth and biological activities. Some microorganisms can consume the sulfur in thiophenic compounds such as BZT and DBT and as a result reduce the sulfur content in fuel. Desulfurization by microorganisms is carried out at mild temperature and pressure conditions; therefore, it is considered as an energy-saving process when compared to conventional HDS (Soleimani et al., 2007).

2.4.1.4 Adsorption Methods

Song (2003) described a new process called selective adsorption for removing sulfur (SARS) for deep desulfurization of liquid hydrocarbon fuels (diesel, gasoline, and jet fuels). In this process which takes place at an ambient temperature and in H_2 free conditions, the refractory sulfur compounds are selectively adsorbed onto the surface of the solid adsorbent leaving other hydrocarbon species unchanged. The adsorbent used was prepared from transition metal oxides supported on alumina. Another adsorptive method for sulfur compound removal using carbon adsorbents was reported by Sakanishi et al. (2003). Moreover, Wang et al. (2009) reported a new approach for jet fuel desulfurization. Their technique was based on a pervaporation process with subsequent adsorption. It was shown that this method can reduce the sulfur content of different jet fuels from 1675 ppmw to 10 ppmw.

2.4.1.5 Desulfurization Using Zeolites

Nowadays, zeolites are receiving more attention for sulfur removal from transportation fuels. Zeolites eliminate the need for use of hydrogen in the process. In

addition, zeolites display unique hydrogen transfer properties allowing for catalytic desulfurization. In particular, shape selectivity can play a major role in determining the product selectivity (Jaimes et al., 2008). Zeolite shape selectivity is the result of (a) the difference in diffusivities of reactants and products; (b) the difference in adsorption of reactants in zeolite cavities of different sizes and shapes; and (c) transition state selectivity (Rozanska & Van Santen, 2003). There has been significant research performed, investigating benzothiophene conversion using zeolites. In general, benzothiophene conversion studies using zeolites can be divided into two main categories: (a) transformation studies, and (b) adsorption studies.

2.4.1.5.1 Transformation Studies

Valla et al. (2006) studied the mechanism and kinetics of thiophene and benzothiophene catalytic cracking. A commercial FCC catalyst and a microactivity test unit (MAT) operating at 560 °C were used in the experiments. It was concluded that benzothiophene is more reactive than thiophene. Although desulfurization reactions of benzothiophene occurred almost to the same extent as those of thiophene, alkylation reactions were strongly promoted with alkylated benzothiophenes being produced. Moreover, using a commercial FCC catalyst and gas oil, Valla et al. (2007) investigated the cracking of sulfur compounds under FCC conditions. It was shown that benzothiophene desulfurization to H₂S is not feasible and that benzothiophene mainly undergoes alkylation producing C₁-C₃-benzothiophenes.

Boita et al. (2006) studied the conversion of thiophenic compounds over acidic zeolites. Namely, the transformations of a) 2-methyl-Th, b) 3-methyl-Th, c) 2,3-

dimethyl-Th, d) 2,5-dimethyl-Th, e) 2-methyl-BZT, and f) 3-methyl-BZT over HY, H β , H-ZSM5 and H-mordenite (HMOR) zeolites were investigated. All catalytic runs were performed in a fixed bed reactor operating at 350 °C and atmospheric pressure. In the presence of HY zeolites, all the reactants underwent both isomerization and disproportionation in various proportions depending on their molecular structures. H-ZSM5 and H β were more active and more selective than HY for isomerization. One should notice that while HMOR was also selective for isomerization, it deactivated at a higher rate. Similar results were found by Richard et al. (2007) using HY zeolite.

Contreras et al. (2008) have studied the transformation of (a) thiophene, (b) benzothiophene, and (c) dibenzothiophene over Pt loaded HMF1, HMOR, and HFAU zeolites. Benzothiophene conversion was the highest on Pt/HMF1 while compared to thiophene and dibenzothiophene. The conversion increased in the case of Pt/HMOR or Pt/HFAU. In general, conversion of benzothiophene increased with zeolite pore size in the following order: Pt/HMF1 < Pt/HMOR < Pt/HFAU.

Recently, Dupuy et al. (2012) investigated the transformation of benzothiophene in the presence of 2-methyl-1-pentene over acidic zeolites. Namely, HBEA, HMCM-22, and HY zeolites having similar Brønsted acidities were used in this study. The catalytic runs were performed in a fixed bed reactor operating at 85 °C and atmospheric pressure. Benzothiophene underwent only alkylation over these zeolites. Moreover, HY showed the most active and stable zeolite in benzothiophene conversion. HBEA and HMCM-22 were found to have low initial activity and poor stability due to diffusional limitations and fast deactivation of active acid sites. Benzothiophene was transformed predominantly into monoalkylated products.

2.4.1.5.2 Adsorption Studies of Benzothiophene on Zeolites

Xue et al., (2005) studied adsorption of thiophene and benzothiophene in a model solution of gasoline (heptane with 1 wt% toluene and 5 ppmw thiophene or benzothiophen (BZT). This study was conducted at 80 °C using a metal-ion-exchanged Y-zeolites. The metal-ion-exchanged Y-zeolites showed selective adsorption properties for thiophene and benzothiophene under low-sulfur concentration (5 ppmw) conditions. The sulfur uptake increased in the order: CuY-zeolite (Na) < AgY-zeolite (Na) < CeY-zeolite (Na) for both sulfur compounds. The sulfur uptakes are strongly dependent on the amount of metal loading in the Y-zeolite. The uptake of thiophene was faster than that of BZT, which may be due to the smaller molecular size of thiophene as compared to that of BZT.

Another adsorption study using an ion-exchanged Y-zeolite at room temperature was reported by Bhandari et al. (2006). This study was conducted using a model diesel containing the three major sulfur compounds: thiophene, BZT, and DBT, and a commercial diesel fuel. The ion-exchanged Y-zeolite included Ni-Y, Cu-Y, Fe-Y, and Zn-Y. A very high sulfur removal capacity was observed for Ni-Y and Cu-Y. However, it was found that the main issue of using such ion-exchanged zeolites was the difficulty of the regeneration process.

Jiang & Ng (2006) investigated the adsorption of benzothiophene on a Y-zeolite using infrared spectroscopy and flow calorimetry. In addition, NaY and transition metal exchanged zeolites namely Cu and Ni Y zeolites were tested. Sulfur uptake decreased in the following order: CuY > NiY > NaY ~ USY. It was concluded that the transition metal

ion-exchanged zeolites exhibit excellent properties for sulfur adsorption. Moreover, the acidity of the zeolites is not advantageous for sulfur removal due to the strong adsorption and decomposition of the adsorbed species.

Sotelo et al. (2007) studied the adsorption of benzothiophene diluted in cyclohexane over agglomerated zeolites with a faujasite structure at 298 K. As a principal conclusion, it can be stated that adsorbents with medium basicity present best performance in fuel desulfurization due to their affinity with sulfur compounds (BZT), although diffusion problems should be taken into account. In spite of this, one has to be aware that regeneration of ion-exchanged zeolites require high desorption temperatures that may promote deactivation.

2.5 H-ZSM5 Zeolite as A Desulfurization Catalyst

Yu et al. (1999) studied thiophene desulfurization using (a) H-ZSM5, (b) Zn on H-ZSM5, and (c) Co on H-ZSM5. A pure thiophene and a thiophene/propane mixture were investigated in a micro-flow reactor at 500 °C. It was reported that these zeolites catalyze thiophene desulfurization with high H₂S selectivity using propane as the exclusive hydrogen source. Desulfurization rates and selectivities were much higher when H₂ was present during propane reactions. Zn⁺² and Co⁺² cations at exchanged sites increased desulfurization rates. This study showed that alkane dehydrogenation can be coupled with thiophene hydrogenation on surfaces in order to increase thiophene desulfurization and propane dehydrogenation rates simultaneously. Later studies were developed by Yu et al. (2003) using paraffins (propane, n-hexane, n-decane), and hydrogen as co-reactants in the desulfurization of thiophene catalyzed by H-ZSM5 at 673 K. Thiophene desulfurization

rates augmented with increasing alkane chain size. This suggests that the availability of hydrogen-rich intermediates rises with increasing alkane reactivity. Desulfurization rates with n-alkane co-reactants were significantly higher than those achieved with hydrogen. Sulfur is predominately removed as hydrogen sulfide ($> 80\%$ S-selectivity) in the presence of alkane co-reactants. However, much lower hydrogen sulfide selectivities were obtained when hydrogen was used and when thiophene decomposed in the absence of any co-reactants.

de Lasa et al. (2006) evaluated desulfurization (de-hydrosulfidation) reactions of ethyl mercaptan (EM) dissolved in n-octane (nC_8) on a H-ZSM5 based catalyst. A mini-fluidized bed CREC Riser Simulator reactor (de Lasa, 1992) was used during this study. It was found that there is a strong competition for the acid sites of the H-ZSM5 catalyst promoting both, de-hydrosulfidation and catalytic cracking. It appears that given the 10 to 20 time greater phase concentrations between nC_8 and EM, there should be either a bigger adsorption affinity of EM versus nC_8 or alternatively a much faster intrinsic rate of EM de-hydrosulfidation versus the one for the nC_8 cracking rate. With respect to the product distribution, the results obtained by de Lasa et al. (2006) showed that catalytic runs with a mixture of EM and nC_8 were richer in trans-butene compared with pure nC_8 runs. This indicates that EM conversion promotes the formation of trans-butene via inter-molecular dehydrosulfidation reaction. Furthermore, the amounts of ethene were also higher for the catalytic runs using mixtures of EM and nC_8 versus the ones using pure nC_8 . This was also considered as a good indication for the formation of ethene via intra-molecular dehydrosulfidation reaction.

Jaimes et al. (2009, 2011), and Jaimes & de Lasa (2009) evaluated the catalytic conversion of (a) thiophene, (b) thiophene in an n-octane mixture and (c) thiophene in a 1-octene mixture using a commercial FCC catalyst based on a H-ZSM5 zeolite. Catalytic experiments were carried out in the CREC Riser Simulator operating under mild conditions (450 °C and 2 atm), 20 s reaction time and cat/oil ratio of 5 using H-ZSM5 zeolite dispersed in a silica matrix supplied by Albemarle Catalyst Company. Results showed a higher thiophene conversion over n-octane and 1-octene. It was shown that thiophene conversion proceeds via ring opening as shown in Figure 2.4.

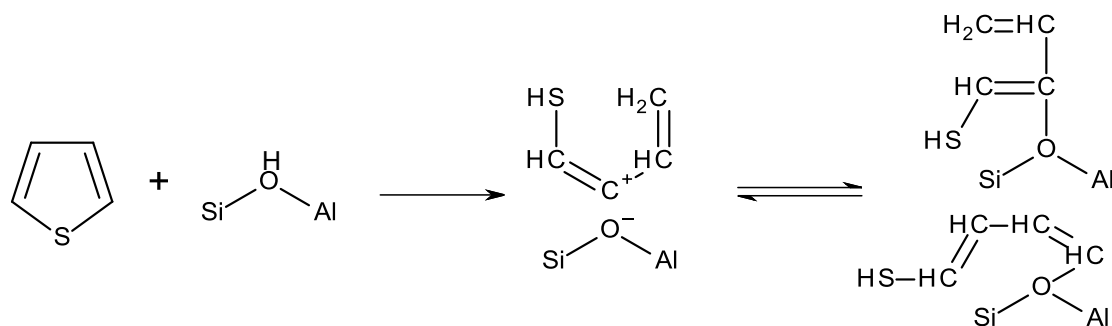


Figure 2.4. Thiophene conversion via ring opening (Jaimes et al., 2009)

In addition, thiophene can be converted via alkylation yielding H₂S, alkyl thiophenes, benzothiophene, and coke, with no measurable thiophene saturation or dimerization reactions observed. Figure 2.5 reports the alkylation of thiophene via (a) thiophene protonation and reaction of the carbenium ion formed with an olefin to produce a linear alkyl-thiophene and (b) protonation of the olefin and reaction with a free thiophene molecule, leading to a ramified alkyl-thiophene.

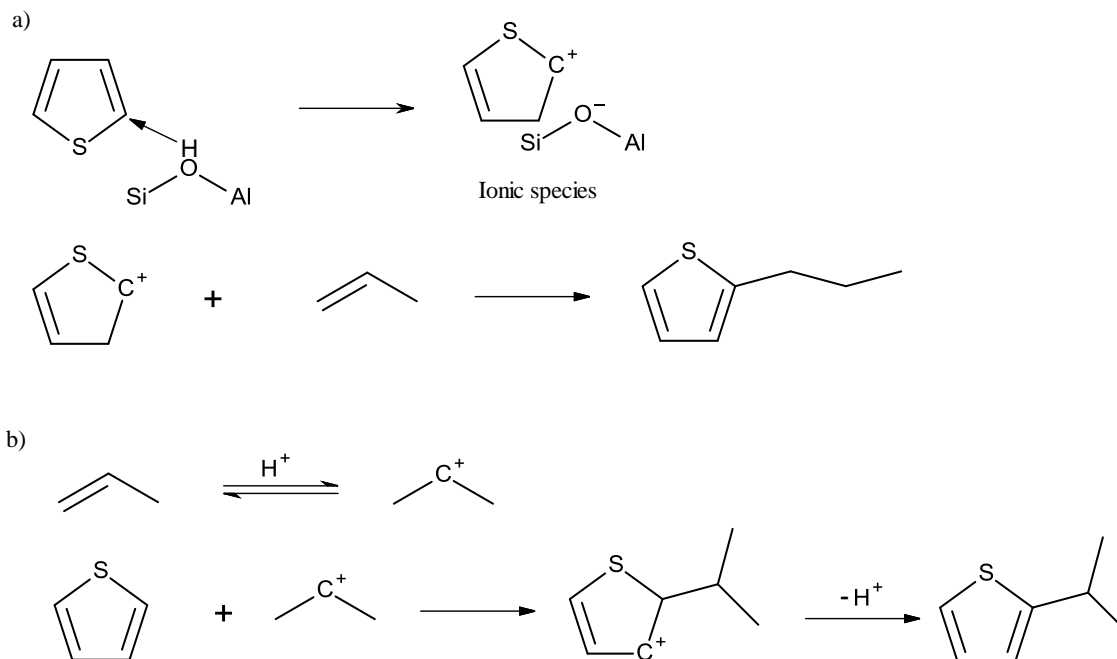


Figure 2.5. Thiophene conversion via alkylation (Jaimes et al., 2009)

On the basis of the above results, it was concluded that gasoline components can play a key role as hydrogen donors for thiophene ring opening as well as co-reactants for alkylation. These observations are in agreement with previous thermodynamic analyses by Jaimes et al. (2009).

2.6 Kinetics of Benzothiophene Reactions

Kilanowski & Gates (1980) studied the kinetics of benzothiophene HDS over a Co-Mo/ Al_2O_3 catalyst in a flow microreactor. Five different rate equations, based on Langmuir-Hinshelwood formulations, were proposed to fit the experimental data using nonlinear least-square regression. Equation (2.1) was found to give the best fit for their data:

$$r = \frac{kP_{\text{BZT}}P_{\text{H}_2}}{(1 + K_{\text{BZT}}P_{\text{BZT}} + K_{\text{H}_2\text{S}}P_{\text{H}_2\text{S}})^2} \quad (2.1)$$

where P represents the partial pressure, K is the adsorption constant, and k is a constant lumping the kinetic constant, BZT adsorption constant, and H₂ adsorption constant. These authors concluded that there is a competitive adsorption of BZT and H₂S on one type of catalytic site as well as non-competitive adsorption of H₂ on another kind of site.

In a very detailed review on the kinetics of sulfur containing compound under hydrodesulfurization (HDS) conditions, Vrinat (1983) reported different rate expressions for thiophene, benzothiophene, and dibenzothiophene. It was concluded that kinetics based on Langmuir-Hinshelwood rate equations provide important information about catalytic sites and reaction mechanisms. This is due to the fact that the HDS reaction is taking place between adsorbed sulfur species and adsorbed hydrogen, with this surface reaction being the rate limiting step. In addition, these models can also account for the inhibiting effect of hydrogen sulfide.

Ho & Sobel (1991) studied the kinetics of dibenzothiophene HDS. A Langmuir-Hinshelwood kinetic model was found to correlate the rate data. The proposed model assumes the following: (i) The adsorption of dibenzothiophene and hydrogen involves two different types of catalytic sites, (ii) The surface reaction is the rate limiting step, and (iii) The reaction products compete with dibenzothiophene for catalytic sites. Following the same principle, Laredo et al. (2001, 2003) proposed a Langmuir-Hinshelwood model to study the kinetics of nitrogen compounds inhibition on dibenzothiophene HDS.

Valla et al., (2006) investigated the kinetics of thiophene and benzothiophene (dissolved in n-C16) catalytic cracking in a fixed bed reactor using a commercial FCC catalyst (Y-zeolite). A three lump kinetic model involving sulfur species, short alkylated sulfur species, and H₂S plus sulfur in coke, was proposed to represent the thiophene and benzothiophene experimental data. The kinetics of sulfur containing compounds was assumed to be of first order displaying a relatively simple power law rate equation. The same kinetics was assumed for n-C16 cracking, however, with a four lump model.

Jaimes & de Lasa, (2009) studied the kinetics of thiophene catalytic conversion over a H-ZSM5 zeolite in the CREC Riser Simulator. The lumped kinetic model considers a Langmuir-Hinshelwood rate expression for thiophene conversion with all constants of adsorption and kinetics (equation 2.2). The lumps include H₂S, sulfur in gasoline range (SG), aromatics (Ar), and sulfur in coke (SC). It was found that the thiophene overall rate suggests a second order reaction at a low thiophene concentration and a first order reaction at a higher thiophene concentration. However, a simple first order rate equation was used to model the solvent (n-octane or and 1-octene) catalytic cracking. The products from n-octane and 1-octene were lumped into aromatics and non-aromatics groups. The proposed model was found adequate to represent the experimental data obtained.

$$r_{Th} = \frac{k_{H_2S} K_{Th} P_{Th}^2}{1 + K_{Th} P_{Th}} + \frac{k_{Ar} K_{Th} P_{Th}^2}{(1 + K_{Th} P_{Th})^2} + \frac{(k_{SG} + k_{SC}) K_{Th} P_{Th}}{1 + K_{Th} P_{Th}} \quad (2.2)$$

where k_i is the kinetic constant of i , K_{Th} is the adsorption constant of thiophene, and P_{Th} is the partial pressure of thiophene.

Recently, Stanislaus et al. (2010) published a comprehensive review on the recent advances of ultra low sulfur diesel (ULSD) production. As part of this work, the kinetics of dibenzothiophene was reviewed in the literature. It was shown that Langmuir-Hinshelwood type mechanistic kinetic equations were used widely by many researchers. The advantage of using this type of kinetic is that it allows for the accounting of competitive and non-competitive adsorption.

2.7 Zeolites Catalysts

Zeolites are high crystalline aluminosilicate materials with a microporous structure formed of alumina [AlO_4^-] and silica [SiO_4] tetrahedra. The zeolite pores and cages have molecular dimensions which make it possible to discriminate between molecules of different sizes. As a result, zeolites are also known as molecular sieves. The zeolite unit cell formula is usually reported as $\text{M}_j/\text{n}(\text{AlO}_2)_j(\text{SiO}_2)_y \cdot z\text{H}_2\text{O}$, where M represents the exchangeable cations and j, y, z, and n are integers. Zeolites are classified according to their pore sizes which depend on the number of oxygen atoms forming the zeolite ring into: (i) 8-member rings (small pore zeolite), (ii) 10-member rings (medium pore zeolite), and (iii) 12-member oxygen rings (large pore zeolite). In addition, zeolites can be classified into three groups based on Si/Al atomic ratio or by the molar ratio M ($\text{M} = \text{SiO}_2/\text{Al}_2\text{O}_3$) in their frameworks: (i) Low-silica or aluminium rich zeolites ($\text{Si}/\text{Al} \approx 1$), for example, zeolites A and X, (ii) Intermediate silica zeolites (Si/Al between 2 and 5), for example, zeolite Y, mordenite, zeolite L, natural zeolites, and (iii) High silica or silicalite zeolites ($\text{Si}/\text{Al} \geq 10$), for example zeolite beta, and ZSM-5 (Hagen, 2006; Auerbach et al., 2003; Satterfield, 1980).

Approximately 40 natural zeolites have been found and more than 150 have been synthesized. In industry, zeolites are applied in three major fields: (1) detergents (type A zeolite), (2) adsorbents and desiccants (type A and X zeolite), and (3) catalysts (especially the type Y and ZSM-5 zeolites) which cover about 50% of the world market for synthetic zeolites (Hagen, 2006; Zheng, 2002; Satterfield, 1980). As catalysts, zeolites have shown to be an essential element for the oil refining industry since their first use early sixties. For example, Fluid Catalytic Cracking (FCC) catalysts account for more than 95% of the world consumption of Y-type zeolites (Bogdanov et al., 2009; Marcilly, 2001). The MFI-type zeolite and especially the ZSM-5 is the second most used catalyst with main applications in catalytic cracking, alkylation of aromatics, xylene isomerization and catalytic dewaxing (Bogdanov et al., 2009).

2.8 Zeolite Properties

2.8.1 Acidity

In principle, the acid strength and acid type are the key properties of zeolites which play a critical role in both the activity and selectivity of the zeolites (Zheng, 2002). Recently, Katada et al. (2010) have studied the catalytic cracking activity of n-octane and n-hexane versus the acidity of different zeolite types. They found that the acidity is essential to control the cracking activities in zeolites. In addition, Borm et al. (2010) confirmed the same findings in their studies of 2,2,4-trimethylpentane catalytic cracking using different zeolites. It was concluded that within one framework type, cracking activity is controlled by the acid properties of zeolites, while selectivity is governed by

the framework topology. Typically, the acid strength of a zeolite is mainly dependent on the Si/Al ratio (Hagen, 2006; Zheng, 2002).

When Si^{+4} is replaced by Al^{+3} in the zeolite framework, the negative AlO_4^- building block has to be compensated by a counter ion. Brønsted acidity (H^+ donator) can be introduced by using protons as compensation ions, thus making the material a solid acid. The concentration of Brønsted sites is, therefore, directly related to the number of framework Al atoms per unit cell. Since aluminum carries a lower charge than the silicon atoms, the electro-negativity of the material is strongly dependent on the ratio between silicon and aluminum atoms in the framework. A higher amount of silicon atoms in the framework causes a strengthening of the Brønsted acidic OH bond and, with it, lower deprotonation energy (higher acid strength). As a consequence, the number of Brønsted acid sites decreases (Woltz, 2005; Gauw, 2002; Govind et al., 2002).

The strongest Brønsted acid sites can be obtained upon completely isolating Al in the framework due to the higher electro-negativity of Si compared to Al. If the Si/Al ratio is higher than 10, the strength of the acid sites remains almost constant (Hagen, 2006; Zheng, 2002). The Si/Al ratio at which the acidity reaches its maximum, is a function of zeolite type (Gauw, 2002). Zeolites in protonic or H form are solid acids. Their acid strength can be varied over a wide range by modification of the zeolites, for example by ion exchange, partial dealumination, and isomorphic substitution of the framework Al and Si atoms. Brønsted acid centers are generally the catalytically active sites of H-zeolites. The highest proton-donor strengths are exhibited by zeolites with the lowest concentration of AlO_4^- tetrahedral such as H-ZSM5 and ultrastable HY zeolites (USY). These are super acids, which at high temperatures (500 °C) can even protonate n-alkanes

(Woltz, 2005). In addition, it was found that the acid strength depends on the number of Al atoms that are adjacent to a silanol group (Si-O-H). Since Al distribution is nonuniform, a wide range of acid strengths can be obtained (Hagen, 2006). Figure 2.6 shows that both Brønsted acid sites and Silanol that are present in zeolite framework.

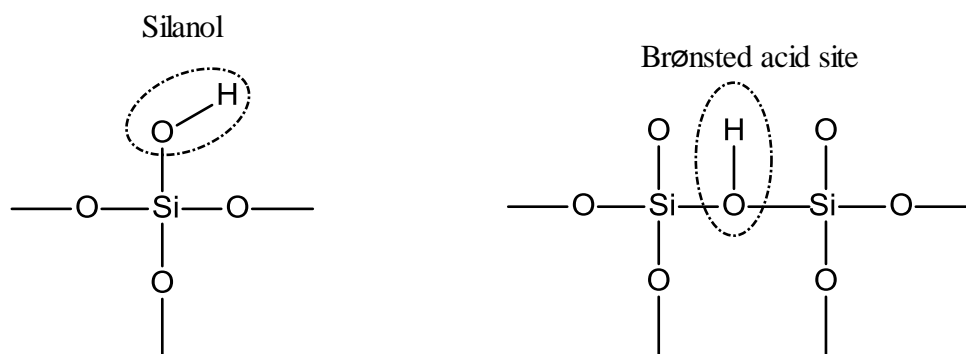


Figure 2.6. Schematic representation of Silanol, and Brønsted acid sites present in zeolites frameworks.

Zeolites are not thermodynamically stable materials. High temperature, concentrated mineral acids and alkalines or steam can destroy the structure of the zeolite causing the aluminum atoms to leave the framework. These extra framework aluminum (EFAL) sites feature Lewis acidic character (electron acceptor) (Borm et al., 2010; Woltz, 2005). When an H-zeolite is heated to a high temperature, water is driven off and coordinated unsaturated Al^{+3} ions are formed. These are Lewis acids as shown in Figure 2.7 (Hagen, 2006; Satterfield, 1980).

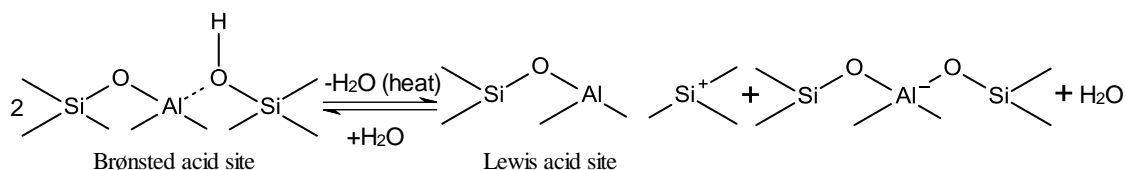


Figure 2.7. Formation of Lewis acid sites in the zeolite framework.

2.8.2 Shape Selectivity

The pore size and shape in zeolites may affect the selectivity of a reaction in two ways: (i) Reactant selectivity, and (ii) Product selectivity. Reactant selectivity takes place when the zeolite pores admit only certain smaller molecules and excludes larger molecules. Hence, in a mixture, effectively only the smaller molecules react. Product selectivity occurs when bulkier product molecules cannot diffuse out, and if formed, they are converted to smaller molecules or to carbonaceous deposits within the pores. These eventually may cause zeolite pore blockage. For shape selectivity to occur, essentially all the active catalytic sites must be located inside the zeolite pores. The external area of zeolite crystals is only 1 percent of the total area, but if diffusion limitations are significant, it may become necessary to poison or inactivate the external sites so they do not contribute excessively to the reaction. Some zeolites having suitable pore sizes are not stable under reaction conditions. With some metal-loaded zeolites, metal may migrate out of the pores with time, thus destroying this type of catalyst selectivity (Satterfield, 1980).

Another form of shape selectivity depends on the fact that chemical reactions often proceed via intermediates. Owing to the pore system, only those intermediates that have a geometrical fit to the zeolite cavities can be formed during catalysis. This type of shape

selectivity is called restricted transition state selectivity. In practice, it is often difficult to distinguish restricted transition state selectivity from product selectivity (Hagen, 2006; Xiao, 1990; Zheng, 2002).

In general, zeolite shape selectivity is the result of: (a) the difference in diffusivities of reactants and products; (b) the difference in the adsorption of reactants in zeolitic cavities of different sizes and shapes; and (c) transition state selectivity (Rozanska & Van Santen, 2003).

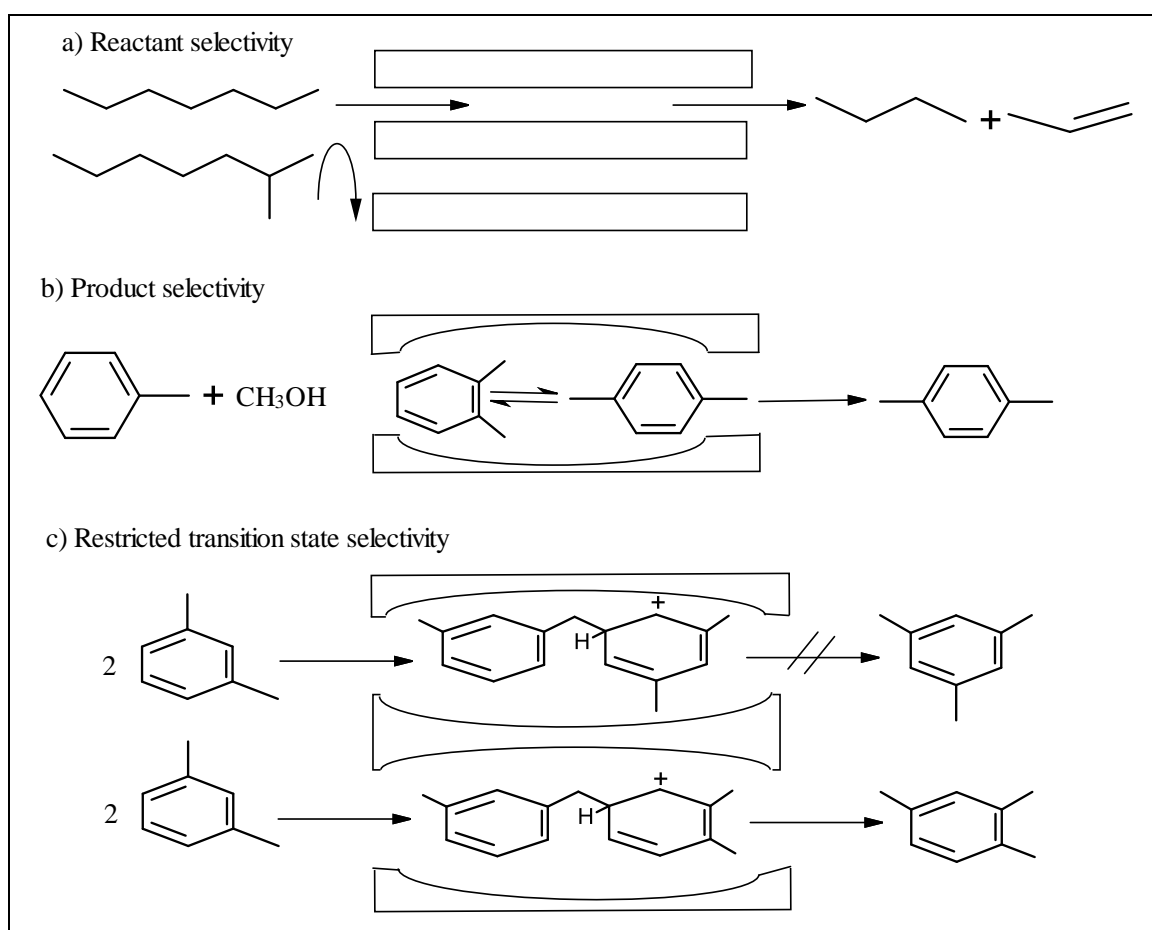


Figure 2.8. Shape selectivity of Zeolites (Hagen, 2006; Xiao, 1990; Zheng, 2002)

Shape selectivity can be assumed to be independent of the Si/Al ratio. Al content in the zeolites does not modify their structural dimensions (Uguina et al., 2006). Figure 2.8 shows the three types of shape selectivity in zeolite.

2.9 Pore Size and Molecular Diameters

Pore size and molecular diameter, are aspects of considerable importance given that whether the reacting molecules have free access to the zeolite inner network, and whether product molecules can readily escape towards the outer zeolite surface under a particular set of reaction conditions. This is a major issue given the very small pore sizes in zeolites.

In this respect, only limited evidence is available. The minimum pore size is usually assigned on the basis of crystallographic measurements. However, it is affected by the nature of the cations present and by heat treatments performed. Many materials also incorporate stacking faults, impurities, or deformations of various kinds that restrict channels, or they may have been treated in various ways to open up channels. A more useful characterization in practice, especially on a relative scale, stems from measurements with fluids consisting of molecules of progressively increasing size to determine which are absorbed into the pores and which are not, under a specified set of conditions (Satterfield, 1980).

The free diameter of a zeolite channel can be calculated from the structural model of the oxygen rings forming the channel openings, by assuming a diameter for the oxygen atoms. This method gives the most quoted zeolite pore sizes: 2.8 Å for 6-membered

rings, 4.2 Å for 8-membered rings, 5.7 Å for 10-membered rings, and 7 to 7.4 Å for 12-membered rings. In these calculations, a radius of 1.4 Å for oxygen atoms was used.

The channel size of a zeolite can also be characterized by the occlusion of guest molecules. The so-called effective diameter of the zeolite channel is determined experimentally by subjecting a zeolite to guest molecules with different kinetic diameters. For the case where the molecular diameter of diffusing molecule is close to, but still smaller than the zeolite channel diameter, molecules might experience a net attraction force when passing through channels. If the molecular diameter is slightly larger than the zeolite channel diameter, molecules might experience a net repulsive force instead. If the molecular diameter is much larger than channel diameter, molecules can no longer enter the zeolite due to the strong repulsive force from the channels. For the unobstructed 8-, 10-, and 12-membered ring zeolites, the effective sizes are approximately 4.5, 6, and 8.5 Å, respectively (Xiao, 1990).

In the study of a guest molecule in a zeolite channel, the molecular diameter is often characterized by either the minimum kinetic diameter of the molecule or the Lennard-Jones length constant σ_m or its corresponding van der Waals diameter σ_o . The minimum kinetic diameter can be calculated from the minimum equilibrium cross-sectional diameter, and is often used to characterize how difficult it is for a molecule to penetrate through a zeolite channel. The Lennard-Jones length constant can be determined either from transport properties (viscosity, and thermal conductivity) or from detailed measurements of the deviations from the ideal gas law. This method gives a spherical representation of a molecule. However, molecules should not be viewed as rigid spheres nor should zeolite channels be viewed as rigid walls (Xiao, 1990). Molecules are not rigid

objects and their kinetic diameter gives only a rough estimate of the molecular size (Hagen, 2006). Neither zeolite channels nor molecular diameters can be described by a well defined number. The vibration of the crystal lattice and the possible distortions of both molecule and zeolite make it even more difficult to assess the true diameter of either molecule or zeolite pores (Xiao, 1990).

Examples of molecular diameters of some hydrocarbons with zeolite pore sizes are given in Table 2.2. However, the reported values for the molecular diameter differ in different sources based on the method by which this property was calculated (Ainscough & Dollimore, 1987). In addition, the available information for C5-C8 paraffins is very scarce and a few data were found in the literature (Jimenez-Cruz & Laredo, 2004).

Table 2.2. Molecular diameters of some hydrocarbons and pore sizes of some zeolites

Hydrocarbon	Molecular Diameter (nm)	Zeolite	Pore Size (nm)
n-butane	0.43	Y-zeolite	0.74
n-Pentane and higher n-paraffins	0.49	ZSM-5	0.54×0.55 0.51×0.55
Iso-butane	0.56	Mordenite	0.67-0.70
Benzene	0.53	NaX	0.74

It is generally accepted for systems with a λ ratio (ratio of molecular diameter to channel diameter) significantly above unity that the molecular sieve effect is the controlling separation mechanism (Uguina et al., 2006; Xiao & Wei, 1992).

2.10 ZSM-5 Zeolite

The first application of ZSM-5 in catalytic cracking was performed around 1983 and aimed to increase the quality of the gasoline octane number. This increase was obtained at the expense of the amount of gasoline and was accompanied by an increase in the yield of light olefins (olefins with a carbon number of five and lower). ZSM-5 is a typical FCC additive due to its acidity, shape selectivity, and coke resistance (Hollander, 2000). ZSM-5 is one of the most important zeolites used in petrochemical industry. For example, middle porous ZSM-5 zeolite showed marked advantages in terms of selectivity and coke resistance for toluene alkylation with methanol, toluene disproportionation and o-xylene isomerization to produce p-xylene (Zheng, 2002). Silicalite and ZSM-5 are the most widely used zeolites for membranes (Jia & Murad, 2005). ZSM-5 zeolites are the aluminum-containing members of the MFI family, while silicalites are the members composed entirely of SiO_4 tetrahedra (Liu et al., 2004). In general, ZSM-5 is classified as a high silica zeolite with a silica to alumina ratio typically above 10. ZSM-5 with a Si/Al ratio above 500 is sometimes referred to as silicalite (Auerbach et al., 2003; Govind et al., 2002).

The structure of a ZSM-5 zeolite has a 10-membered oxygen ring and two types of channel as follows: elliptical straight channels with major and minor axes of 0.53×0.56 nm cross linked with elliptical (near circular) sinusoidal channels of 0.51×0.55 nm. These two different channels are perpendicular to each other and generate intersections with diameters of 8.9 \AA or 9 \AA (Liu et al., 2004; Xiao, 1990; Zheng, 2002). The pore structure of the ZSM-5 is shown in Figure 2.9.

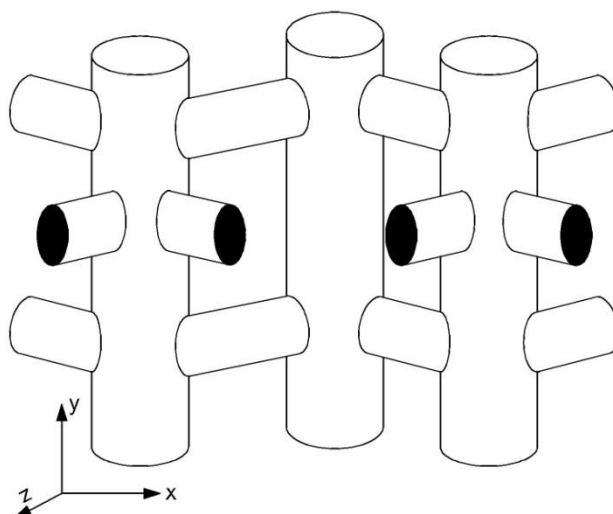


Figure 2.9. Schematic drawing of the silicalite pore structure (Smit et al., 1997)

The catalytic active centers in ZSM-5 are typically Brønsted acid sites. They are located in channels or channel intersections. As a result, for a reaction to take place, reactants must have access to these sites, and products must be able to diffuse out. This issue is of particular importance in ZSM-5 zeolites because the diameters of the channels and channels intersections are comparable to the kinetic diameters of the reactants and products (Trout et al., 1997).

At ambient temperature, ZSM-5 adsorbs molecules as large as benzene (kinetic diameter of 5.85 Å) but rejects molecules larger than 6 Å, such as neopentane (kinetic diameter of 6.2 Å) (Flanigen et al., 1978; Nicholas et al., 1993). Normal paraffin molecules such as n-hexane, rapidly diffuse into silicalite and are packed in the channels at a higher density due to their small diameter and elastic configuration. Benzene and its substitutes with one or two alkyl groups on the same axis (ethylbenzene and p-xylene) also can diffuse into silicalites easily. Molecules with diameters larger than the size of the channels but with a somewhat elastic methyl group (m-xylene and o-xylene) still can be

adsorbed at moderate rates. They are probably placed at the intersections of the channels, thus being packed at a low density. A cyclohexane molecule has a kinetic diameter only slightly larger than the channel, but its rigid configuration causes the diffusion to be very slow at room temperature. However, at a higher temperature, the diffusion rate becomes substantial and the adsorption capacity is comparable with that of benzene (Wu et al., 1983).

The small pore size of ZSM-5 restricts the entry of large hydrocarbons and enables a higher interaction with the reaction intermediate. Only linear and mono-branched hydrocarbons can easily enter the pores of ZSM-5 (Hollander, 2000). The upper critical molecular diameter required for chemical species to evolve in ZSM-5 zeolites is 6.6 Å (0.66 nm) or smaller. This critical diameter corresponds to durene (tetra-methylbenzene). Durene is the molecule with the largest critical diameter diffusing out of a ZSM-5 zeolite during methanol conversion (Ravella et al., 1987). The efficiency of ZSM-5 in converting normal hydrocarbons decreases with increasing the number of carbon atoms due to the difficulty of long chains to diffuse inside tiny zeolite pores (Al-Baghli & Al-Khattaf, 2005).

ZSM-5 zeolites in protonic form (HZSM-5 or H-ZSM5) have been extensively used in acid catalyzed reaction in the chemical and petrochemical industry. Typical industrial catalytic processes using H-ZSM5 zeolites include cracking of waxy components, and the conversion of methanol to gasoline (MTG) (Hagen, 2006). Recent research using H-ZSM5 as a desulfurization catalyst for FCC gasoline under mild conditions of pressure and temperatures showed promising results regarding the shape selectivity of H-ZSM5

towards sulfur species conversion (Jaimes et al., 2011; Jaimes & de Lasa, 2009; de Lasa et al., 2006; Yu et al., 2003).

The protonic form of ZSM-5 zeolites can be typically obtained from as-synthesis zeolites by following steps: (i) calcination of as-synthesis ZSM-5 zeolites to decompose the organic amine template, (ii) ion exchange of ZSM-5 zeolite in sodium form with NH_4NO_3 solution to give NH_4^+ form, and (iii) subsequent calcination of the NH_4^+ ZSM-5 zeolite forms ammonia, which evolves from the zeolite framework, leaving a H-ZSM5 zeolite (Zheng, 2002).

2.11 Conclusions

The present chapter provides a detailed review of literature on benzothiophene sulfur species conversion studies. In addition, it provides the background to justify the goals and objectives set for this PhD dissertation using H-ZSM5 zeolite as a catalyst for benzothiophene conversion aiming to light diesel cut desulfurization. This chapter also provides a detailed review of literature on zeolites properties and applications. To be more specific, this chapter gives the background on the H-ZSM5 zeolite which is the catalyst used in present PhD dissertation.

In summary, these are the main points considered in this chapter:

- Existing desulfurization technologies of middle distillates cannot cope with the mandated environmental legislations of ultra low sulfur transportation fuels. For example, the classical HDS process will require more hydrogen consumption and high operating temperatures with this being an area of concern for the economics of VGO refining.

- There is, as a result, a need for a new fuel desulfurization process using zeolites as catalysts due to their unique properties and allowing desulfurization without the use of hydrogen.
- Zeolites possess special properties which make them adequate for different applications. Petroleum refining remains a main area for zeolites as catalysts.
- Zeolite acidity remains the activity property which is a key function for acid catalyzed chemical reactions. Acidity of zeolites is a result of Brønsted and Lewis acid sites present in the zeolite structure. Silica to Alumina ratio plays a crucial role in determining zeolite acidity.
- Zeolite shape selectivity is a property that allows discrimination between different reactant molecules, transition products, and final reaction products. Shape selectivity is a result of zeolite channel dimensions and pore sizes.
- ZSM-5 is a high silica zeolite ($\text{Si}/\text{Al} \geq 10$) containing a two system of channels: straight and zigzag channels. ZSM-5 in its protonic form (H-ZSM5) has a wide range of applications. For the objectives of the current research, H-ZSM5 was found to be a very active catalyst for the conversion of sulfur containing compounds in the middle distillate fuel boiling range (180 °C – 370 °C).
- Recent studies showed that the H-ZSM5 zeolite can convert sulfur species contained in middle distillate fractions in a fluidized bed reactor. The suitability and promise of the H-ZSM5 zeolite for desulfurization has been proven using model sulfur containing species. However, there is also the non-selective cracking of co-reactant species (e.g. paraffin) that is used to simulate the middle distillate fuel cut needs. This problem requires further study given that if dominant, it can

reduce fuel quality. Nonetheless, this negative factor can be minimized, as shown in the present study by manufacturing zeolite catalyst particles with an inert catalyst matrix.

CHAPTER 3

SCOPE OF RESEARCH

The aim of this research is to investigate the H-ZSM5 zeolite as a potential catalyst for light diesel fuel range desulfurization. In particular, benzothiophene conversion over an H-ZSM5 based catalyst is studied.

The specific objectives of this dissertation are as follows:

Objective 1: To perform a theoretical study using Molecular Dynamics (MD) simulation for n-dodecane (n-C12) and benzothiophene self diffusion into a ZSM-5 catalyst.

Objective 2: To prepare H-ZSM5 zeolite pellets using an inert silica-alumina matrix.

Objective 3: To characterize the prepared zeolite catalyst using advanced materials characterization techniques in order to study:

- (i) Physical properties of the prepared catalyst such as surface area and particle size
- (ii) Mechanical properties such as bulk density
- (iii) Chemical properties such as acidity and chemical composition
- (iv) Structural properties such as crystallinity

Objective 4: To conduct catalytic runs using the prepared catalyst in the fluidized bed CREC Riser Simulator reactor using benzothiophene and n-dodecane as sulfur containing compounds and light diesel cut model chemical species. This specific objective includes the following activities:

- (i) Evaluating the overall conversion of both benzothiophene and n-dodecane model compounds
- (ii) Determining the product distribution for the reaction
- (iii) Determining the desulfurization selectivity based on benzothiophene conversion reaction
- (iv) Characterizing the coked catalyst sample in terms of coke formation and sulfur content

Objective 5: To establish a heterogeneous kinetic model for benzothiophene conversion over a H-ZSM5 catalyst where the following activities are considered:

- (i) Proposing a reaction network based on the distribution of products observed
- (ii) Establishing the appropriate reaction rate expressions (differential equations) with their intrinsic kinetic and adsorption parameters
- (iii) Evaluating the kinetic model parameters including the following: intrinsic kinetic constants, adsorption constants, heat of adsorption, and activation energies

CHAPTER 4

MOLECULAR DYNAMICS SIMULATION

4.1 Introduction

Heterogeneous catalytic processes necessarily proceed via at least the following five steps: (1) Diffusion of the reactants towards the catalyst surface, (2) Adsorption of the reactants on the catalyst active sites, (3) Chemical reaction at the active sites, (4) Desorption of the products from the active sites, and (5) Diffusion of the products away from the catalyst surface. In principle, any of the above mentioned five steps can be the rate determining step of the reaction. Therefore, it is crucial to understand the catalytic cycle process completely, considering the diffusion and adsorption steps. However, in zeolitic processes, the catalytic reaction takes place mainly inside the zeolite pores. Hence, it is important to characterize the diffusion of the reacting molecules in order to understand the phenomenon of shape selectivity (Lins & Nascimento, 1997; Smit et al., 1997).

4.2 Diffusion in Zeolites

Transport of species in porous materials can take place by one or more of the three following mechanisms: (a) bulk or molecular diffusion, (b) Knudsen diffusion, and (c) configurational diffusion. When the average free distance (mean free path) of molecules is smaller than the pore diameter of the porous materials, collision between molecules is dominant and the molecules transport takes place by molecular diffusion. If the mean free path of evolving molecules is larger than the diameter of pores, collision between

molecules and the wall of the channels is dominant and the diffusion follows Knudsen diffusion. On the other hand, when the diameter of diffusing molecules is comparable to that of the channels of the porous materials, transport happens following configurational diffusion (Al-Khattaf, 2001; Xiao & Wei, 1992a).

Diffusion in zeolites belongs to the configurational regime because the molecular diameter is comparable to the zeolite channel diameter. Configurational molecule transport displays energies of activation much larger than Knudsen and molecular diffusion. This regime involves very small diffusivity coefficients, typically in the order of 10^{-10} to 10^{-12} $\text{cm}^2 \text{s}^{-1}$. In addition, there is a strong dependence of these coefficients on the size and shape of the evolving molecules. In this respect, one can notice that diffusivity of hydrocarbon molecules is increased markedly with decreasing molecular size (Zheng, 2002; Al-Khattaf, 2001; Xiao & Wei, 1992a, 1992b; Satterfield, 1980).

4.2.1 Self Diffusivity and Transport Diffusivity

Diffusivities which are measured under the influence of concentration gradients, i.e. under non-equilibrium conditions, are generally referred to as transport diffusivities. The transport diffusivity measures the evolution of local concentration gradients. This parameter can be defined as a proportionality constant relating the flux of molecules to a driving force or the concentration gradient according to Fick's first law as:

$$J = -D_t \left(\frac{\partial C}{\partial X} \right) \quad (4.1)$$

in which C is the concentration, X is the spatial coordinate, and D_t is the transport coefficient. Transport properties can be determined by macroscopic methods like

gravimetry, volumetry, chromatography, or frequency response techniques. By contrast, self-diffusivity is obtained by following the motion of tagged molecules and measuring the mean square displacement (MSD) versus time. Then, self-diffusivity (D_s) can be calculated from the slope of the MSD versus time (t) curve using the Einstein's equation (in three dimensions) as:

$$\text{MSD} = 6 D_s t \quad (4.2)$$

Self-diffusivity is frequently called tracer diffusivity. It can be measured under equilibrium conditions by microscopic techniques, for example quasi elastic neutron scattering (QENS) and pulsed-field gradient (PFG) NMR, or by using molecular dynamics simulations.

4.2.2 Factors Influencing the Diffusivity

4.2.2.1 Adsorbate Concentration

In zeolites, the diffusivity of the adsorbates can be strongly dependent on the concentration of gas phase species. As the diffusion of species in zeolites takes place in channels, where it is difficult or essentially impossible for molecules to pass each other, encounters between different molecules have a much more pronounced influence on mobility (Schuring, 2002).

Zheng (2002) reported that diffusivity is sometimes dependent on the concentration of the sorbate. For example, regarding the transport of aromatic molecules in ZSM-5 zeolites, the dependence of the diffusivity on the molecule loading is still under controversy. Some researchers have observed a markedly increased benzene diffusivity

with the increase of molecule loading while others claimed an independence of the diffusivity of benzene in silicalite on benzene concentration. On the other hand, some observed a decreased dependence of the diffusivities of aromatic molecules from the species concentration. According to Kärger & Pfeifer (1987), there are five different types of self-diffusivity dependence on concentration (using NMR measurements). These different dependencies can be attributed to differences in the interactions between the framework atoms and the diffusing molecules. However, the prediction of the concentration dependence in different systems remains difficult, and further investigation on this dependence remains of interest (Schuring, 2002).

4.2.2.2 Temperature

It appears that diffusivities are highly temperature dependent and display an Arrhenius behavior (Tepper, 2001) . On this basis, configurational diffusion in zeolites can be modeled as an activated process, as described by an Eyring equation (Xiao & Wei, 1992):

$$D = D_0 \exp\left(-\frac{E_D}{RT}\right) \quad (4.3)$$

where D is the diffusion coefficient, D_0 is the a pre-exponential factor, E_D is the apparent activation energy of diffusion, R is the universal gas constant, and T is the temperature.

It is worth noting that the apparent activation energy for configurational diffusion is much greater than that for bulk or Knudsen transport. Generally, the smaller the diffusion coefficient, the higher the activation energy (Schuring, 2002; Al-Khattaf, 2001).

4.2.2.3 Zeolite Crystal Size

Regarding the modeling of configurational molecular transport in zeolite crystals, it was noticed that this could be in principle affected by crystallite size. In this respect, experiments at the same conditions showed no effect of crystallite size on diffusivity coefficients. For example, experiments using n-butane, n-decane, and C7-C16 linear paraffins in zeolite 5 A, showed no influence of crystallite size on the diffusivity coefficient (Al-Khattaf, 2001). Due to the surface barrier, a low diffusion coefficient can be observed in zeolites with small crystallites while compared to the zeolites with large crystallites (Zheng, 2002).

4.2.2.4 Si/Al Ratio

Nicholas et al. (1993) found experimentally that the methane transport in ZSM-5 is not affected by Si/Al ratio. Lins & Nascimento (1997) in their MD simulations of light hydrocarbon evolving in ZSM-5 reported that the diffusion constants seem to be very insensitive to the Si/Al ratio. The role of the zeolite Si/Al ratio on hydrocarbon diffusivity coefficients was investigated using a ZSM-5 zeolite. Results suggest that the Si/Al ratio has a limited influence on the hydrocarbon diffusivity coefficients. It was reported that benzene diffusivity in ZSM-5 is virtually independent of the framework composition (Al-Khattaf, 2001). On the other hand, Bhide et al. (1999) and Zheng (2002) reported that the change in Si/Al ratio and ion exchange degree can influence molecular transport.

4.3 Methods for Determining the Diffusion in Zeolites

In general, the experimental techniques for measuring diffusion in zeolites can be classified into two main categories: macroscopic and microscopic methods. Macroscopic

techniques typically use a bed of zeolite crystals or a zeolite membrane, and measure the response to a change of the adsorbate concentration in the surrounding gas phase. The interpretation of the response is mostly based on a description of the diffusion via Fick's law. As these experiments measure the response to a concentration change, these methods usually measure the transport diffusivity. Some macroscopic techniques can also be used to measure self-diffusion by making use of labelled molecules. Macroscopic techniques include: i) Uptake methods, ii) Membrane permeation, and iii) Chromatographic methods. Microscopic techniques, on the other hand, are capable of measuring the mobility of adsorbates in a much shorter time and length scale than the previous mentioned macroscopic techniques. Microscopic techniques can, in principle, measure the propagation of molecules through a single zeolite crystal, and can directly probe the underlying microscopic mechanisms of diffusion. Microscopic methods include: i) Pulsed Field Gradient Nuclear Magnetic Resonance (PFG NMR), ii) other NMR methods, iii) Quasi-Elastic Neutron Scattering (QENS), and iv) Interference Microscopy. In contrast, theoretical methods form a valuable addition to the available experimental techniques. These methods encompass: i) Molecular Dynamics (MD) simulation, ii) Monte Carlo simulation and iii) Transition State (TST) method (Schuring, 2002).

4.3.1 Molecular Dynamics (MD) Simulation

Since their first appearance, Molecular Dynamics simulations have become a standard tool in computational chemistry. MD simulations have been used extensively to study the diffusion of hydrocarbons in different zeolitic structures. This method showed to be a better alternative for visualizing the diffusion process than other approaches, as they simulate the motion of the diffusing molecules inside the pores. In addition, they allowed

assessing the self-diffusion coefficients in the host pores (Catlow et al., 1991; Szczygieł & Szyja, 2005).

4.3.1.1 Molecular Dynamics Studies of Hydrocarbons Diffusion in ZSM-5

Diffusion of short n-alkanes and alkenes (C1-C7) in silicalite and ZSM-5 was extensively studied using MD simulations by many authors. Catlow et al. (1991) reported the diffusion of methane (CH₄) and ethene (C₂H₄) in silicalite. They used a (20.07 Å × 19.92 Å × 26.84 Å) box containing 576 framework atoms to represent the zeolite structure which was considered as a flexible framework. A trajectory (simulation time) of 30 ps was used at 300 K and 600 K with one molecule per simulation box to calculate the diffusion coefficients. In addition, a long simulation of 120 ps was performed for two methane molecules at 600 K. The results showed that the diffusion coefficient is higher in the run containing two methane molecules than that in which only one molecule was included.

Nicholas et al. (1993) used MD simulations to study the diffusion of propane and methane in silicalite. In their work, they used a (60.132 Å × 59.754 Å × 40.185 Å) or (3 × 3 × 3) arrangement of ZSM-5 unit cells containing 7776 framework atoms. The zeolite atoms were held fixed in the framework while guest molecules are transported. The MD runs were performed at 300 K with a trajectory of 60 ps and a load of 4 molecules per unit cell after they were equilibrated for 40 ps. Furthermore, they studied the effect of concentration or molecules loading on the diffusion rate by applying six different loadings of methane in silicalite. The results showed that the diffusion coefficient decreases as the molecule loading increases.

Dumont & Bougeard (1995) studied the diffusion of methane, ethane, propane, ethene, and ethylene in silicalite. Two unit cells of orthorhombic silicalite of *pnma* space group and cell parameters of $20.07 \text{ \AA} \times 19.92 \text{ \AA} \times 26.84 \text{ \AA}$ were used to represent the MD box. Furthermore, a trajectory of 42 ps and a load of 4 molecules per unit cell were used at 300 K in all MD runs. One important result of their research is that the influence of molecular flexibility on the calculated diffusion coefficient is not obvious. In addition, the influence of adsorption on the molecular geometry, which in this case is a purely siliceous framework geometry without cations, is not very significant.

Hernandez & Catlow (1995) performed MD simulations for n-butane and n-hexane diffusion in silicalite to study the effect of temperature and molecules loading. In their simulations, a rigid framework to represent the silicalite structure was used. It was concluded that temperature has a stronger effect than variations in the loading.

Lins & Nascimento (1997) performed molecular dynamics simulations to study the diffusion of methane, ethane, propane, and i-butane in the ZSM-5 pores. In their study, the ZSM-5 zeolite was represented using a cluster containing four unit cells or 1152 atoms superimposed along c-axis to give cell parameters of $20.076 \text{ \AA} \times 19.926 \text{ \AA} \times 13.401 \text{ \AA}$. In all experiments, a load of two molecules per unit cell was considered with the zeolite structure held rigid and the temperature kept constant at 300 K. Long trajectories (up to 120 ps) were chosen to perform the simulations. Results obtained were consistent with expected trends based on molecular shapes of these molecules. Diffusion of ethene (C_2H_4) into MFI (silicalite) and H-ZSM5 was studied by Jianfen et al. (1999) using Biosym molecular dynamics simulation software. The diffusion of 16 ethene molecules was carried out in two unit cells of MFI. In their simulation, framework atoms

were held fixed at their crystallographic positions, while guest molecules were treated as totally flexible. A trajectory of 213.84 ps was performed for both orthorhombic and monoclinic MFI while a trajectory of 377.68 ps was used in the case of H-ZSM5. In both cases, the first 50 ps is considered as an equilibration step. The simulation results showed that molecules prefer locations at the centers of channel intersections, especially those near Al substitutions.

Hussain & Titiloye (2005) studied the transport and adsorption of mixed hydrocarbon components in silicalite using MD simulation. In their work, the self-diffusion coefficients of methane, ethane, and propane were calculated at different loadings (2, 4, 8, and 12 molecules) and at different temperatures (300 K and 400 K). In general, the simulation results showed a decrease in diffusivity with increasing molecule loading. Furthermore, the diffusion coefficient increases with temperature increase. For binary mixtures of hydrocarbons, the simulation results showed a higher molecular transport for the molecules with smaller size. For example, in the methane-ethane mixture, methane diffuses faster than ethane. In the ternary mixture however, the temperature had an effect on diffusivity, with methane diffusing faster at 300 K while ethane displaying the highest diffusion coefficient at 400 K.

Krishna & Van Baten (2008) investigated the diffusion of branched isoparaffins and cyclic hydrocarbons mixtures in MFI zeolites using MD simulations. The results showed that branched and cyclic hydrocarbons such as isobutane, 2-methylpentane, 3-methylpentane, 2,2-dimethyl-butane, and benzene are preferentially adsorbed at the intersections of the channels of MFI zeolites. In addition, as the loading of cyclic and branched hydrocarbons is progressively increased to four molecules per unit cell, the

transport of the more mobile linear n-alkane is reduced nearly to zero. The reduction in alkane diffusivity was found to be quantitatively similar irrespective of the branched/cyclic hydrocarbon and attributed to intersection blocking. Intersection blocking in MFI has consequences in catalysis; it is often observed experimentally that the addition of small amounts of branched hydrocarbons reduces the reactivity of linear hydrocarbons significantly.

However, only a few studies have considered long n-alkane transport in silicalite. For example, n-dodecane (n-C12) self-diffusion in silicalite was studied by Runnebaum & Maginn (1997) using Molecular Dynamics simulation. The results showed an increase in the self-diffusion coefficient with temperature. Jobic (2000) found the same temperature effect on n-dodecane transport in ZSM-5 zeolites using quasi-elastic neutron scattering (QENS). Self-diffusion coefficients obtained by QENS were two orders of magnitude smaller when compared to MD simulations. Table 4.1 compares the self-diffusivity coefficients reported in the literature for n-dodecane obtained with both MD simulation and QENS.

Jobic & Theodorou (2006) studied the self-diffusivity of long n-alkanes (C8-C16) in silicalite and Na-ZSM5 using QENS at 300 K. It was found that the self-diffusion coefficient was always higher in silicalite than in Na-ZSM5. For example, n-dodecane self-diffusivity was reported to be 5.3 times higher in silicalite than in Na-ZSM5. This observation was attributed to the presence of Na counter ions, which are expected to slow down n-alkane diffusion in MFI zeolites.

Diffusion of n-alkanes (C2-C14) in silicalite and Na-ZSM5 was investigated by Jobic et al. (2006) using PFG NMR and QENS. Both results were in good agreement with the general trend, showing a decrease in self-diffusivity as the chain length of n-alkanes increases. However, the diffusivities measured by PFG NMR were up to one order of magnitude lower than the diffusivities determined by QENS technique. This difference was explained as the result of internal diffusion barriers in MFI-type zeolites. Since PFG NMR typically monitors molecular displacement in a micrometer scale, the estimated diffusivities are affected by these transport resistances only. However, this is of no relevance for QENS where much shorter displacements are recorded. A comprehensive review considering n-alkane diffusion in zeolites can be found in Jobic & Theodorou (2007).

Table 4.1. Self-diffusion coefficient of n-dodecane reported in the technical literature.

Reference	Method	Temperature (K)	Diffusion coefficient
(Runnebaum & Maginn, 1997) $D_s \times 10^5$ (cm ² /s)	MD	300	3.79
	simulation	350	3.82
	Silicalite	400	4.03
(Jobic, 2000) $D_s \times 10^7$ (cm ² /s)	QENS	300	1.6
	ZSM-5	350	3
		400	5

Diffusion of aromatic hydrocarbons namely benzene, toluene, ethylbenzene, m-xylene, and o-xylene in H-ZSM5, H-Beta and H-MCM-22 was investigated experimentally using FTIR Spectrometry by Roque-Malherbe et al. (1995). The diffusivity coefficient was measured at different temperatures. In all cases, the diffusion

coefficient was found to increase with temperature. Sastre et al. (1998) studied the self diffusivity of o- and p-xylene in a 10 and 12 member ring zeolite model using MD simulation. The study was performed employing a flexible zeolite framework at 500 K and 100 ps of simulation time. Different molecule loadings were investigated. In addition, FTIR spectrometry was also used to measure the diffusion coefficient experimentally. Results showed that p-xylene diffuses faster than o-xylene in the two zeolites channels. The self diffusivity coefficient was higher in the case of low loading compared to high loading. However, diffusion coefficients obtained experimentally were three orders of magnitude lower than those found using MD simulations. The reason for this discrepancy can be found in the fact that the uptake methods like FTIR do not measure the self diffusivity, which is the quantity obtained using MD simulation.

Diffusion of C7 hydrocarbons namely heptanes, 3-ethylpentane, methylcyclohexane, and toluene in microporous materials (γ -Al₂O₃, Faujasite, and ZSM-5) was considered using MD simulations by Szczygieł & Szyja (2005). Heptane was found to have the highest diffusivity in ZSM-5 while toluene has the lowest diffusion coefficient. These results were attributed to the flexibility of the heptane molecules as compared to the rigid ring structures of methylcyclohexane and toluene.

Song et al. (2002) studied the diffusion and adsorption of cyclic hydrocarbons, namely benzene, p-xylene, cyclohexane and 1,4-dimethylcyclohexane in silicalite using the Monte Carlo simulation. This study considered a rigid zeolite framework at different temperatures. One important conclusion from these computations is that saturated hydrocarbons diffuse much more slowly than their aromatic equivalents.

Using MD simulation, Rungsirisakun et al. (2006) studied benzene self-diffusion in siliceous ZSM5, FAU and MCM-22 zeolites. This study was performed at 300 K with different molecule loadings. It was found that the self-diffusion coefficient decreases as molecule loading increases.

Table 4.2 reports a comparison between the diffusion coefficient values found in literature for some aromatic hydrocarbons.

Table 4.2. Reported self diffusivity in the literature for some aromatic hydrocarbons.

Reference	Method	Benzene	Toluene	O-xylene	p-xylene
Roque-Malherbe et al. (1995) $D_s \times 10^9$ (cm ² /s)	FTIR, H-ZSM5, 300K	0.5	1	0.01	
Sastre et al. (1998) $D_s \times 10^6$ (cm ² /s)	MD simulation, ZSM-5, 500K			7.79	25.18
Szczygieł & Szyja (2005) $D_s \times 10^6$ (cm ² /s)	MD simulation, ZSM-5		0.326		
Rungsirisakun et al. (2006) $D_s \times 10^6$ (cm ² /s)	MD simulation, ZSM-5, 300K	1.65			

4.3.1.2 Flexibility of Zeolite Framework in MD Simulation

The use of a fixed or flexible zeolite framework in MD studies is a controversial topic in the open literature. For example, Leroy et al., (2004) compared the self-diffusion coefficients for a series of n-alkanes in silicalite, obtained by using rigid and flexible frameworks. This MD study showed that zeolite flexibility affects the adsorbate transport properties differently according to n-alkane length and loading. The self-diffusion was

enhanced using a flexible silicalite structure for the lowest loading and the shortest alkanes namely methane and n-butane. However, this effect was not observed for long chain alkanes, namely n-hexane and n-octane. A detailed review of the framework flexibility effect in MD simulations of zeolites can be found in Demontis & Suffritti (2009).

4.4 Methodology

The ZSM5 zeolite structure was represented by a siliceous MFI (silicalite) without Al substitution in the framework. A supercell containing eight ($2 \times 2 \times 2$) unit cells (2304 atoms) superimposed along the c axis was constructed, with unit cell parameters $a = 20.076 \text{ \AA}$, $b = 19.926 \text{ \AA}$ and $c = 13.401 \text{ \AA}$. This structure contains two interconnecting channel systems.

The straight channels run parallel to the b-axis (010) and present elliptical cross-sections with minor and major axes of 5.2 \AA and 5.8 \AA , respectively. The sinusoidal (zigzag) channels run along the a-axis (100) and present a more circular but still elliptical cross-section ($5.1 \text{ \AA} - 5.2 \text{ \AA}$) slightly smaller than the one of the straight channels. The intersection between these channels has a diameter of 9 \AA . Figure 4.1 shows the structure of the ZSM-5 supercell used throughout the current simulation work.

The interaction between the zeolite framework and the hydrocarbons was described by using a COMPASS (Condensed-Phase Optimized Molecular Potentials for Atomistic Simulation Studies) Forcefield (Bunte & Sun, 2000; McQuaid et al., 2004; Sun et al., 1998).

Before starting any Molecular Dynamic simulation, the zeolite structure and the hydrocarbon molecules were optimized and their energy minimized. Following this step, the n-dodecane or benzothiophene molecules were introduced inside the zeolite structure randomly. A load of 1 molecule per unit cell (8 molecules/supercell) was considered and the initial velocities were assigned according to a Maxwell-Boltzmann distribution corresponding to the required temperature.

The system was then thermalized for 25 ps (picosecond) using a canonical NVT ensemble, including a constant number of atoms, a constant system volume, and a constant system temperature. The NVT ensemble was coupled with a NHL (Nose-Hoover-Langevin) thermostat (Samoletov et al., 2007).

Using the data from NVT, Molecular Dynamics runs were performed within a microcanonical NVE ensemble having a constant number of atoms, a constant system volume, and a constant system energy or equivalent to adiabatic conditions. This was done at different temperatures with a fixed zeolite structure. The equations of motion were then integrated under these conditions using the Verlet algorithm (Verlet, 1967) with an integration time step of 1 fs (femtoseconds) which is small enough to ensure energy conservation.

More details regarding the above mentioned simulation procedure and parameters are given in Appendix A of this thesis.

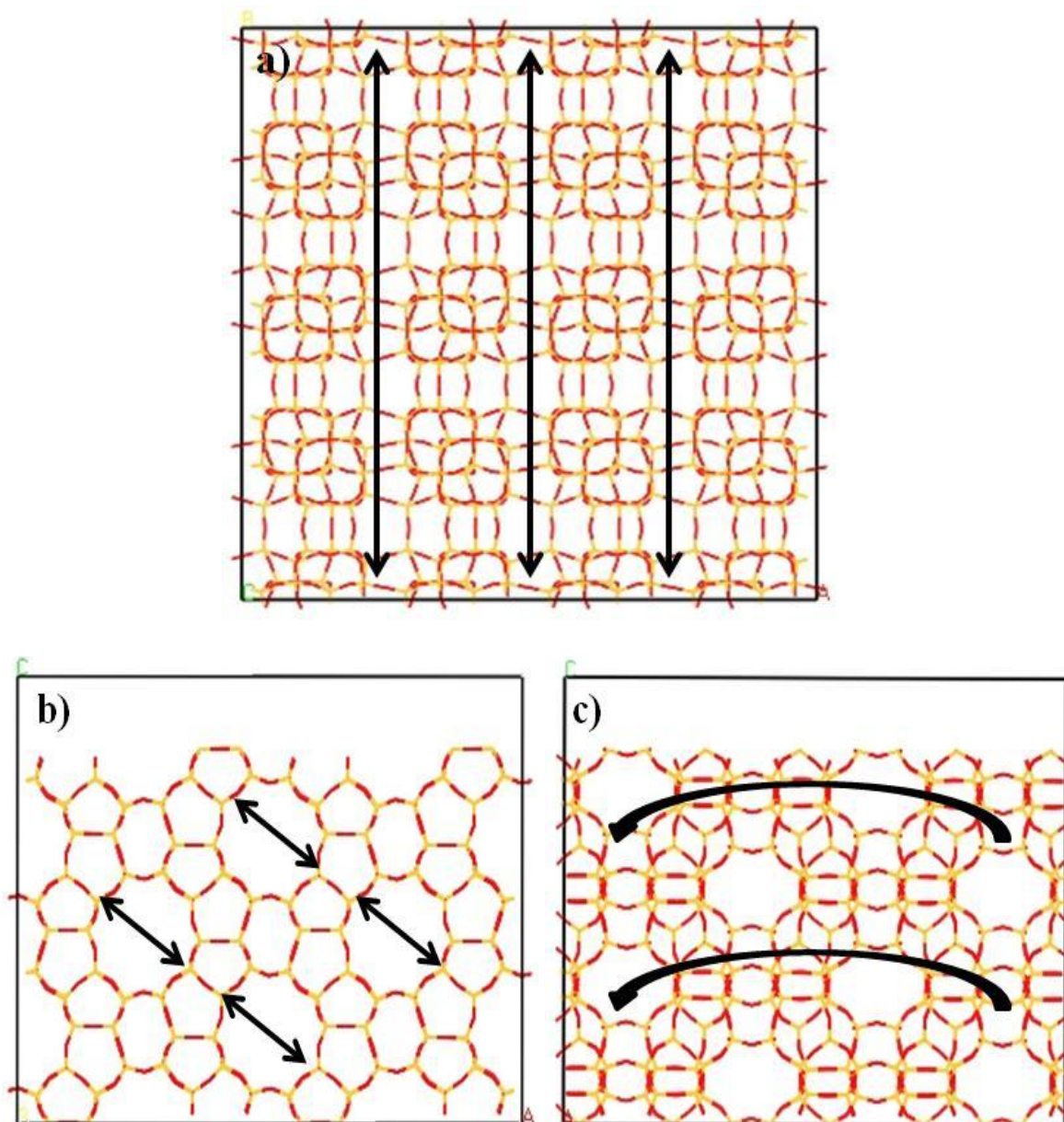


Figure 4.1. Different 2D views of a ZSM-5 supercell (8 unit cells) used in the current study with arrows indicating: a) The straight channels locations, b) The intersections of straight and zigzag channels, and c) The zigzag channels locations.

As a result of the above described simulation procedure, one can define an average mean square displacement (MSD) for all moving particles. This was obtained from the coordinate data stored in the trajectory files as follows:

$$\text{MSD} = (\Delta R(t))^2 = \sum_i \left\langle | \mathbf{r}_i(0) - \mathbf{r}_i(t) |^2 \right\rangle \quad (4.4)$$

where \mathbf{r}_i represents the coordinates of molecule i and, t is the simulation time in picoseconds (ps).

Given the calculated MSD, a self-diffusion coefficient D_s , was then extracted using Einstein's relation as in equation (4.5):

$$D_s = \frac{1}{6t} \left\langle (\Delta R(t))^2 \right\rangle \quad (4.5)$$

Consequently, one can deduce that:

$$D_s = \frac{a}{6} \quad (4.6)$$

where a , is the slope of the linear least square fit of MSD versus simulation time.

It is important to emphasize that when calculating the self-diffusion coefficient, the initial quadratic segment of the MSD curve is discarded. This is the case, given that the initial sharp rise in the MSD plot is a result of a non-steady molecule behaviour while evolving in the available free pore volume. This non-diffusive motion continues until collisions with the channel walls or other molecules take place. After the movement in this initial phase, the MSD starts reflecting the actual translational diffusion of the adsorbate molecules (Lins & Nascimento, 1997; Nicholas et al., 1993).

For the purpose of calculation stability, different simulation times (50, 100, 200, 300, and 400 ps) and 573 and 723 K were used. The results are discussed in the next section of this chapter.

All MD simulation runs were carried out, visualized, and analyzed carefully using the Forcite module of Accelrys Inc. Materials Studio 6.0 software installed on the CMLP-3331 computer station at the University of Western Ontario.

4.5 Results and Discussion

4.5.1 Self Diffusivity Calculations Stability

As already stated, in the present study, the stability of self diffusivity calculations for both n-dodecane and benzothiophene were investigated at 573 K and 723 K considering different simulation times (50, 100, 200, 300, and 400 ps).

Figures 4.2 and 4.3 report the self-diffusion coefficient for n-C12 and BZT, respectively, as a function of the simulation time and temperature. Results always show a higher self diffusivity at low simulation times (50 and 100 ps). Following this initial period, self diffusivity values obtained become both lower and stabilized at a simulation times of 300 and 400 ps. It should be mentioned that this generic behaviour was observed for both n-C12 and BZT cases.

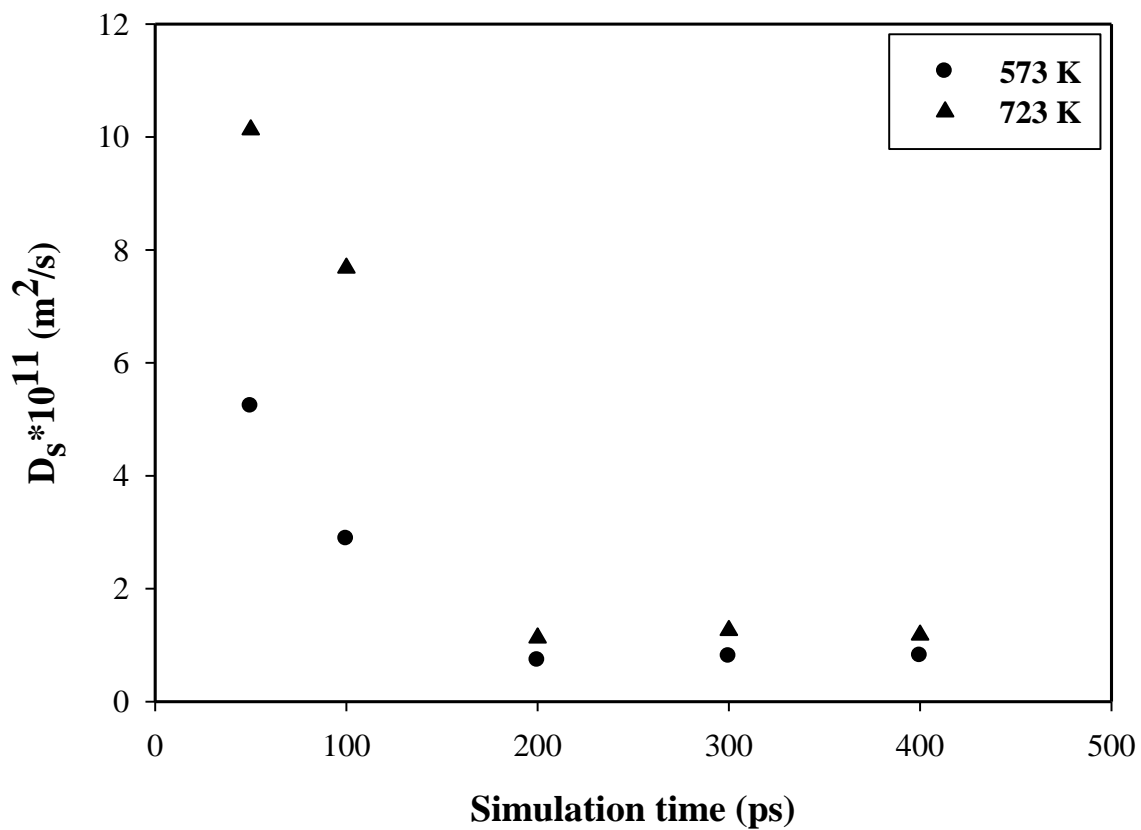


Figure 4.2. Self diffusivity of n-dodecane as a function of simulation time (molecule loading = 1/ u.c).

On the basis of the results reported in Figures 4.2 and 4.3, it is considered that 400 ps is an adequate total molecular dynamic simulation time to establish self diffusivity coefficients as attempted in the present study.

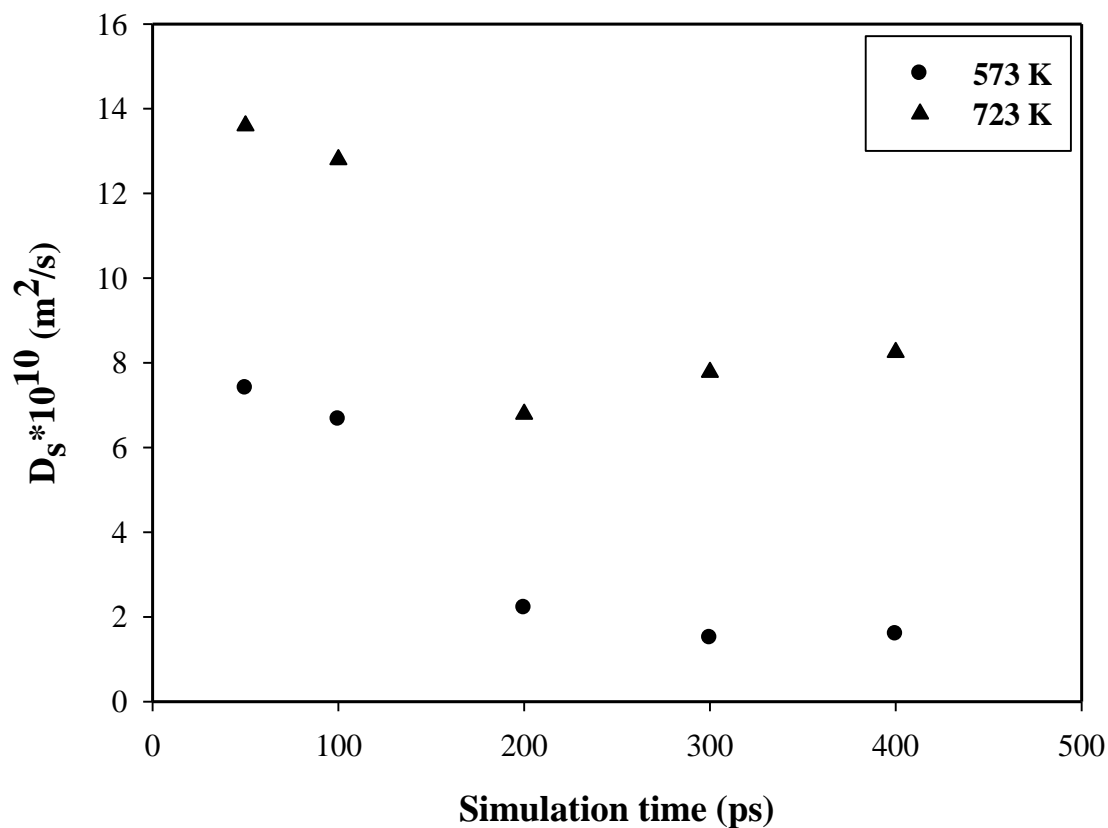


Figure 4.3. Self diffusivity of benzothiophene as a function of simulation time (molecule loading = 1 / u.c).

4.5.2 Self Diffusivity of n-Dodecane

n-Dodecane is a normal paraffin with 12 carbon atoms and a 4.9 Å molecular diameter (Tukur & Alkhattaf, 2005). Since the ZSM-5 zeolite exhibits dimensions of 5.2 × 5.8 Å and 5.1 × 5.2 Å for straight and zigzag channels respectively, n-dodecane is expected to have no diffusional constraints.

4.5.2.1 Temperature Effect on n-Dodecane Self Diffusivity

The self-diffusion coefficient of n-dodecane was found to increase noticeably with temperature. This result is shown in Figure 4.4, where the self diffusivity as a function of temperature is reported. For example, the self-diffusion coefficient of n-C12 at 723 K is about 1.5 times greater than that at 573 K.

The same effect of temperature on n-C12 self diffusivity was found by Runnebaum & Maginn (1997) in silicalite structures using MD simulations. In addition, using the experimental technique QENS, the same effect of temperature on the self diffusivity of n-dodecane was observed by Jovic (2000).

Chain molecules, such as n-C12, can be thought of as becoming “flexible” as temperature is increased. However, with its inherent increased flexibility, the “chain like” molecule can move rapidly between structure configurations. This process continues until n-C12 adopts the configuration with the lowest barrier to diffusion. Thus, the self diffusivity coefficient is as a result increased (Runnebaum & Maginn, 1997).

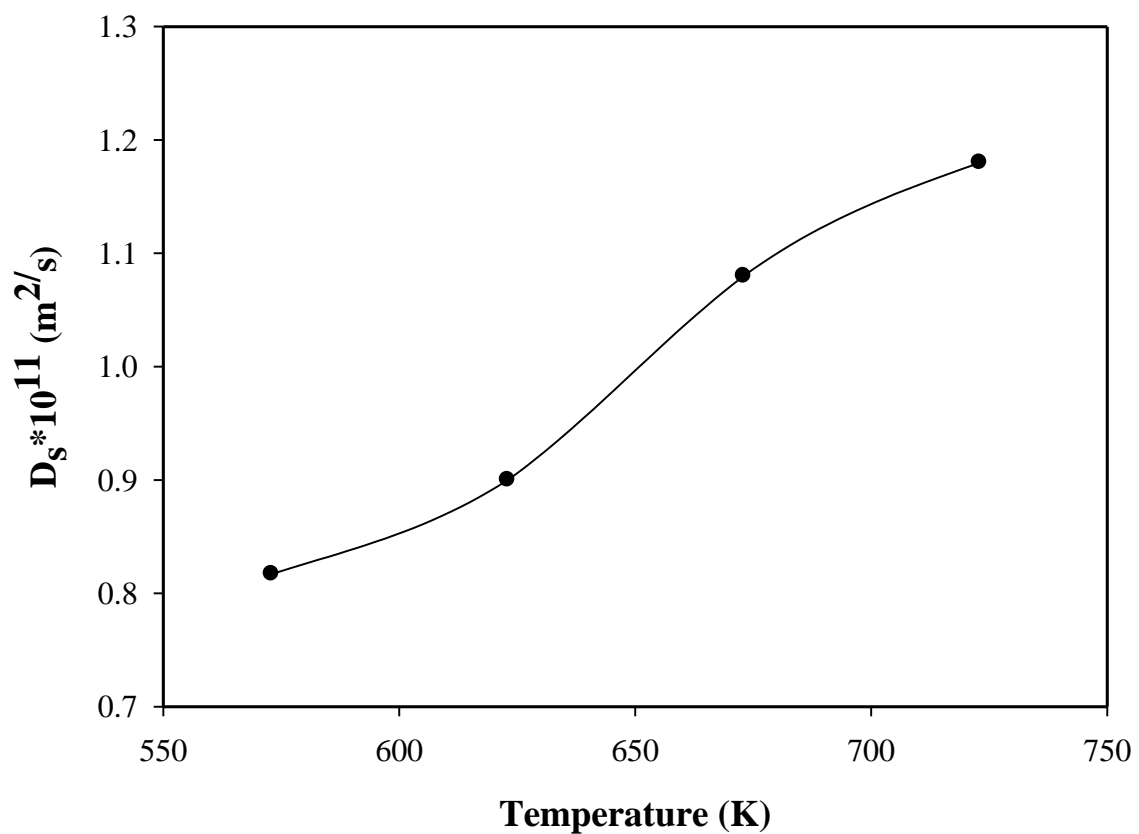


Figure 4.4. Self diffusivity of n-dodecane as a function of simulation temperature

(molecule loading = 1 / u.c, and simulation time is 400 ps).

4.5.2.2 Molecule Loading Effect on n-Dodecane Self Diffusivity

The effect of changing the molecule loading per unit cell (concentration) on the self diffusivity coefficient of n-dodecane was studied at a constant temperature (723 K). Results obtained showed a concentration dependence of the self diffusivity as reported in Figure 4.5.

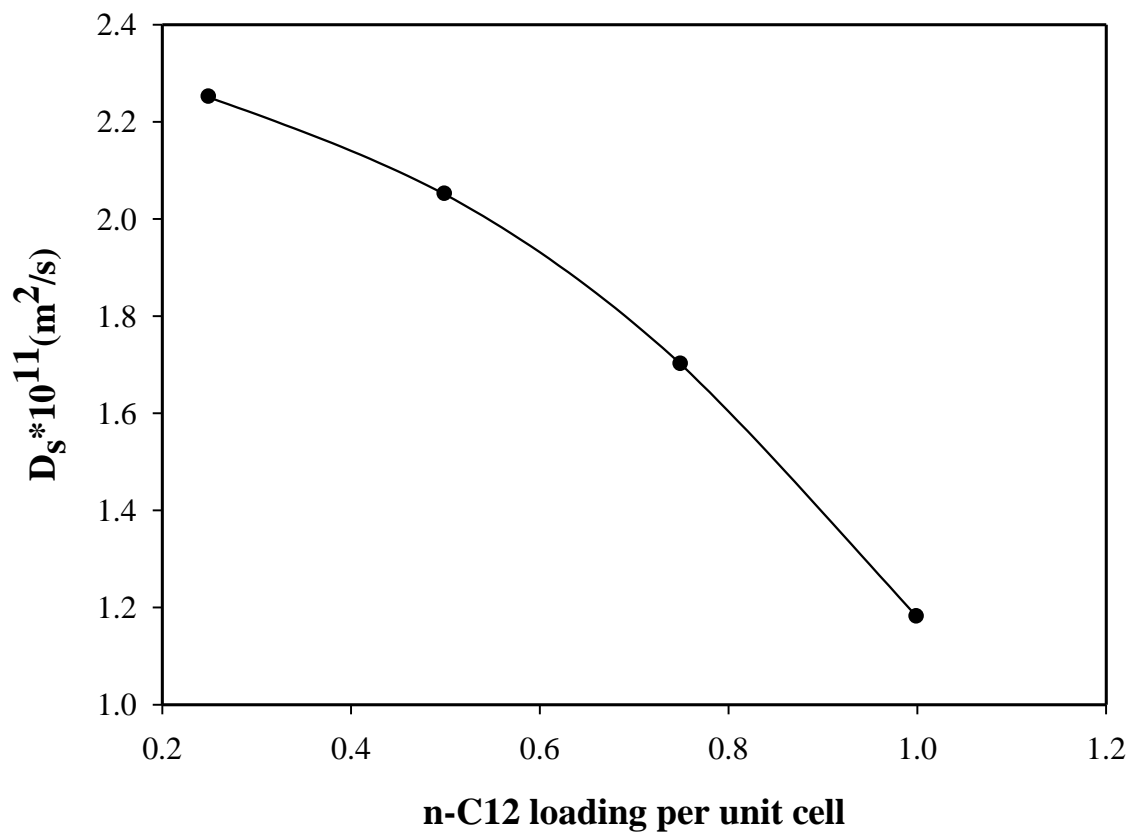


Figure 4.5. Self diffusivity of n-dodecane as a function of molecule loading per unit cell (Temperature is 723 K and simulation time is 400 ps).

Kärger & Pfeifer (1987) described five different types of concentration dependencies of the self diffusivity (obtained with PFG NMR measurements). In general, these concentration dependencies were ascribed to differences in the interaction between the framework atoms and diffusing molecules. For example, interactions with different cations in the zeolites or the presence of strong and weak adsorption sites can result in these dependencies (Schuring, 2002). On this basis, the observed behaviour of n-dodecane self-diffusion with the loading in this study belongs to Type I. This type of

dependency was found for molecules adsorbed on large pore zeolites and undergoing no specific interaction (Kärger & Pfeifer, 1987).

The same effect of molecule loading per unit cell on self diffusivity was found by Nicholas et al. (1993) and Hussain & Titiloye (2005) for short n-alkanes (methane, ethane, and propane) in silicalite at 300 K and 400 K.

4.5.3 Self Diffusivity of Benzothiophene

Benzothiophene is a sulfur containing compound with a kinetic molecular diameter of 6 Å (Contreras et al., 2008) compared to the 5.2×5.8 Å and 5.1×5.2 Å channels of the ZSM-5 zeolites. The upper critical molecular diameter required for chemical species to evolve in ZSM-5 zeolites is 6.6 Å (0.66 nm) or smaller which corresponds to durene (tetra-methyl-benzene). Durene is the molecule with the largest critical diameter able to diffuse out of the ZSM-5 zeolites during methanol conversion (Ravella et al., 1987). Based on this fact, benzothiophene can still diffuse inside the ZSM-5 pores.

4.5.3.1 Temperature Effect on Benzothiophene Self Diffusivity

Figure 4.6 reports the self-diffusion coefficient of BZT at different temperatures (fixed loading of 1 molecule per zeolite unit cell with a fixed simulation time of 400 ps). It can be observed that there is a BZT self diffusivity increase with temperature. The increase of BZT self diffusivity is very noticeable (about 5 times) as temperature changes from 573 K to 623 K, and becomes more modest after this temperature.

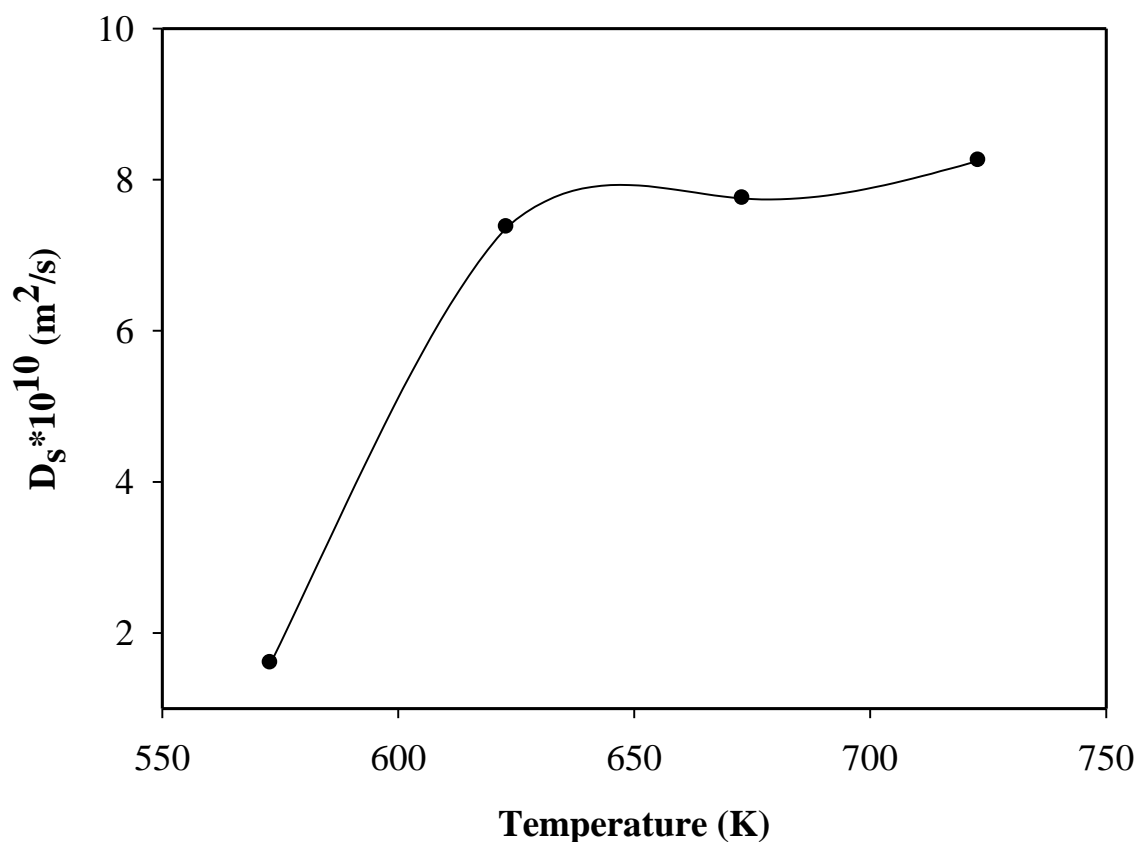


Figure 4.6. Self diffusivity of benzothiophene as a function of simulation temperature (molecule loading = 1 / u.c, and simulation time is 400 ps).

Regarding this result, it is very important to highlight that diffusion studies of benzothiophene in ZSM-5 zeolites are absent in the technical literature. It is believed however, that reported diffusion studies of aromatic hydrocarbons can be considered for the purpose of comparing the obtained results. Sastre et al. (1998) reported the self diffusivity obtained using MD simulations for o- and p-xylene in a flexible model of 10 and 12 member ring zeolites. Self diffusivity values found were in the same order of magnitude (10^{-10} m²/s) as the BZT self diffusivity calculated in the current research. In

addition, toluene self diffusivity in ZSM-5 produced a coefficient of the same order of magnitude as shown by Szczygieł & Szyja (2005) using MD simulations.

Concerning the benzothiophene self diffusivities calculated at various temperatures, they showed values of one order of magnitude higher than that for n-dodecane. This is in spite of the fact that benzothiophene has a kinetic molecular diameter of 6 Å while compared to 4.9 Å of n-dodecane. These results can be explained given the BZT molecule rigidity when compared to the long chain of n-dodecane molecule. The BZT molecule structure could be considered to move inside the ZSM-5 zeolite pores as a “free ball” while the n-dodecane molecule moves as a “spaghetti shaped” chain.

4.5.3.2 Molecule Loading Effect on Benzothiophene Self Diffusivity

The concentration dependence of BZT self diffusivity was studied at different molecule loadings and at 723 K. Results are reported in Figure 4.7. One can notice that BZT self diffusivity remains fairly constant and drops sharply at a loading of 1 molecule per unit cell. It is interesting to see that this behaviour resembles Type II of the five self diffusivity patterns reported by Kärger & Pfeifer (1987). The observed decrease in the self-diffusion coefficient at a sufficiently high concentration of BZT is an understandable consequence of mutual hindrance. This effect of mutual hindrance is found to be most significant for the large molecules (Kärger & Pfeifer, 1987).

Sastre et al. (1998) found that the self diffusivity of o-xylene, in a model structure of ZSM-5, is reduced with molecule loading increase. Another MD simulation study reported the same observation for benzene diffusion in the ZSM-5 zeolites

(Rungsirisakun et al., 2006). It is speculated that such a decrease in self diffusivity is a result of steric hindrance “friction” between diffusing molecules passing each other.

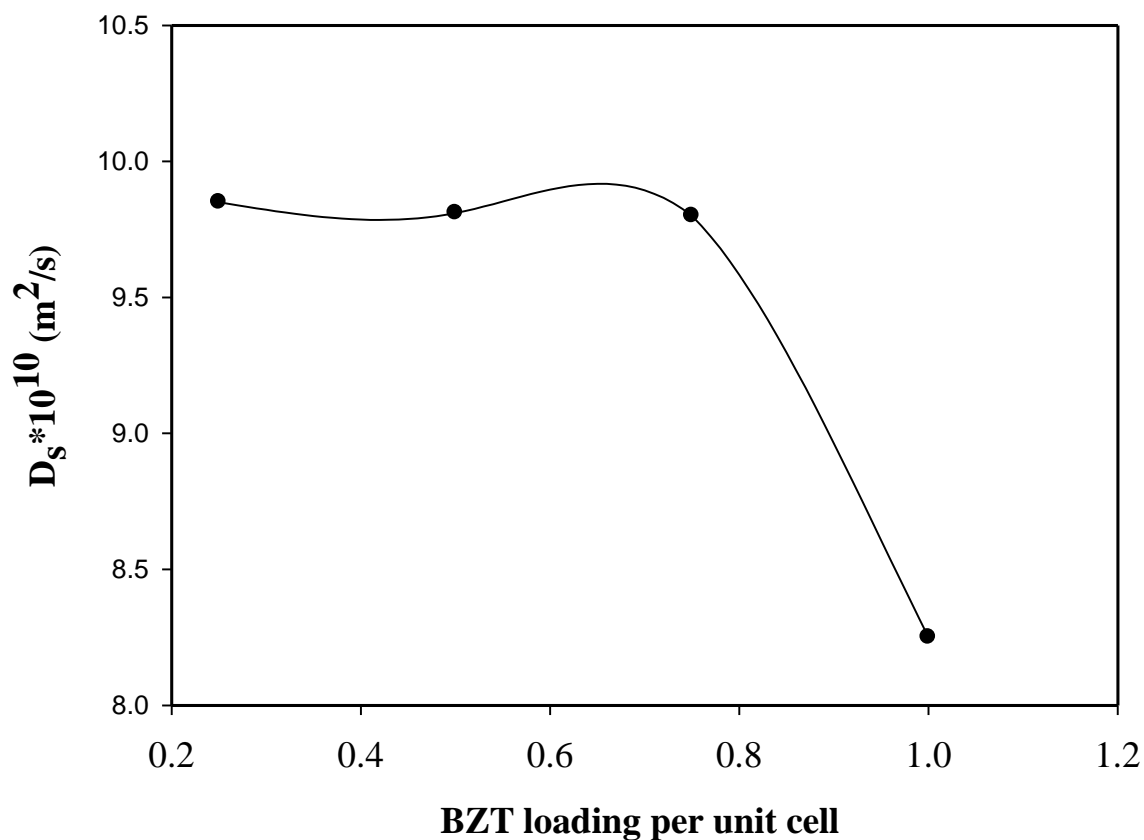


Figure 4.7. Self diffusivity of benzothiophene as a function of molecule loading per unit cell (Temperature is 723 K and simulation time is 400 ps).

In the current study, the significant decrease in benzothiophene self diffusivity at a molecule loading of 1 molecule/u.c can be attributed to the same issue. This friction between BZT molecules appears, however, not to be significant at low loadings (0.25, 0.5, and 0.75 molecules / u.c) as the self-diffusion coefficient remains fairly constant at these conditions.

4.6 Significance of the Results Obtained for the Catalytic Desulfurization of Light Diesel

Results reported in this chapter provide evidence that there are significant differences in the benzothiophene and n-C12 self-diffusivities in ZSM5 zeolites. Self-diffusivity differences promote benzothiophene selective adsorption in the early stages of the unsteady reaction in the CREC Riser Simulator, as can happen in a full industrial riser/downer circulating fluidized unit. In this manner, sulfur containing compounds have the increased opportunity of being removed leaving the main species contributing to light diesel quality essentially unchanged (e.g. n-C12). It is important to emphasize that the conditions selected for the MD simulations include the 350-450 °C range which is the temperature range used in the experimental part of this research as will be discussed in Chapters 5 and 6 of this thesis.

4.7 Conclusions

The following key points can be considered as conclusions for the current chapter:

- (a) Molecular Dynamics simulations allow calculating self-diffusion coefficients for BZT and n-dodecane.
- (b) Calculated self diffusivity coefficients show higher values for BZT than n-dodecane. This is true at all temperatures and in spite of BZT having a larger molecular diameter of 6 Å when compared to the 4.9 Å diameter of n-dodecane.
- (c) Results obtained are consistent with the BZT molecule rigid configuration, while compared to the “chain like” n-dodecane molecule. As a result, BZT molecules can move more freely than the n-dodecane molecules in ZSM-5 zeolites.

(d) Simulation results obtained are relevant for a desulfurization process to be implemented in a riser/downer fluidized unit where light diesel sulfur containing species can diffuse faster. As a consequence, they can be removed selectively using ZSM5 zeolites. This allows light diesel desulfurization with minimum paraffin cracking and hence, retaining the diesel quality.

CHAPTER 5

EXPERIMENTAL METHODS

5.1 Introduction

This chapter describes the experimental procedures and methods involved in the preparation, characterization and testing of the H-ZSM5 catalyst for the conversion of benzothiophene and diesel range model hydrocarbons (n-dodecane) used in the present study.

The first section of this chapter illustrates the procedure followed in the preparation of the H-ZSM5 pellets. The second section describes the different methods used to characterize the prepared catalysts samples. Theory and experimental procedures of various characterization techniques used in the present study are also briefly described. The third section provides a detailed description of the CREC Riser Simulator reaction system that is used for testing the activity of the prepared catalyst samples under fluidized bed reactor conditions. Moreover, as part of this section, operating conditions and materials used in thermal and catalytic runs are reported. In addition, a description of the analytical system used to quantify the reaction products is included. Finally, techniques used to characterize the spent catalyst samples are also reviewed in detail.

5.2 Catalyst Preparation and Materials

A ZSM-5 zeolite in ammonium form (CBV 3024E with $\text{SiO}_2/\text{Al}_2\text{O}_3 = 30$ and Na_2O content of 0.05 wt %) supplied by Zeolyst International, was calcined in a tube furnace at 550 °C under air flow for 5 hours using a ramping rate of 5 °C / min. This procedure is

well reported in the literature (Mitchell et al., 2011; Kim et al., 2003). Upon calcination, ammonia leaves the zeolite framework allowing obtaining the protonic form or H-ZSM5.

The catalyst pellet was then prepared using: (a) H-ZSM5 (active material), (b) fused alumina (Aluminum oxide, fused 99%) provided by Sigma Aldrich as a filler, and (c) colloidal silica (LUDOX AS-40 colloidal silica, 40 wt% suspension in water) from Aldrich as a binder.

The zeolites remain the principal source of catalytic activity. A binder is usually added as a glue to provide cohesion to the zeolite particles. On the other hand, a filler is added to make up the body of the catalyst. The function of the filler and binder is to provide physical integrity to the catalyst particles in terms of proper density, particle size and attrition resistance. The combination of binder and filler is designated in the present study as “catalyst matrix”. Most commercial FCC catalysts contain between 15 and 40 percent zeolite and between 15 and 30 percent binder with the balance being the filler (Fahim et al., 2010; Al-Khattaf, 2001).

In order to prepare 100 g of catalyst particles, 30 g of H-ZSM5 was mixed with 50 g fused alumina and 20 g silica sol. The resulting slurry was well mixed and enough water was added to form a homogeneous paste. Following this, the paste was pressed using a three-hole pellet presser. Finally, catalyst pellets were dried at 110 °C for one hour and then at 370 °C for three hours. The resulting zeolite pellets were then ground and sieved. This was done to recover the particles in the appropriate 53 to 100 µm size range. The pellets produced had a lower sphericity than the ones formed normally by spray drying.

However, these pellets were still adequate for fluidization under the conditions of the CREC Riser Simulator.

The model compound benzothiophene (C_8H_6S) (Thianaphthene, Aldrich 98% purity), was selected as the sulfur containing model compound in the diesel fraction. Diesel was simulated with n-dodecane (n-C12, Sigma Aldrich 99% purity).

5.3 Catalyst Characterization

Catalyst characterization is required to determine: (a) the physical properties of the prepared catalyst such as surface area and particle size, (b) the mechanical properties such as bulk density, (c) the chemical properties such as acidity and chemical composition, and (d) the structural properties such as crystallinity.

In most cases, three samples, namely: (i) the zeolite (H-ZSM5), (ii) the matrix (fused alumina and silica sol), and (iii) the prepared zeolite pellets, were characterized using the above mentioned techniques. This allowed, having a better understanding of the interaction and the contribution of both the zeolite and the matrix on the catalytic reaction.

5.3.1 Apparent Bulk Density and Particle Size Distribution

The apparent bulk density (ABD) of the catalyst pellet was assessed using a method established at the CREC laboratories. This method allows determining the average apparent bulk density of a catalyst by introducing a known weight of the catalyst in a known volume flask. Then, the flask was filled with isopropyl alcohol (2-propanol). After that, ABD was calculated by dividing the initial weight of catalyst by the difference

between the total flask volume and alcohol volume (mass of alcohol by its density) as in equation 5.1:

$$ABD = \frac{W_{cat}}{V_T - V_A} \quad (5.1)$$

where ABD is the apparent bulk density in g/cc, W_{cat} is the catalyst weight (0.6 g), V_T is the flask volume (5 cc), and V_A is the volume of isopropanol (9.62 cc) calculated as the ratio of isopropanol weight required to fill the flask (7.6 g) and the density of isopropanol (0.79 g/cc).

The particle size distribution (PSD) of the prepared H-ZSM5 pellets was determined using a Mastersizer 2000 from Malvern Instruments. The PSD analysis was performed at the Western Chemical and Biochemical Engineering Department common laboratory.

5.3.2 X-Ray Diffraction (XRD)

XRD is used for identification of crystal structures (qualitative analysis) such as those of zeolites materials. In addition, the compounds making up the catalyst sample can be clearly identified by the XRD pattern (quantitative analysis). A crystal is defined as a solid composed of atoms arranged in a periodic pattern in three dimensions. When a crystalline structure is bombarded with X-rays at different angles during a period of time, the X-rays are scattered by the electron clouds of different atoms making up that structure. At certain positions, the diffracted rays are formed and these can be sensed by a detector and recorded. For crystalline structures, the detected signal may be stronger at one or many positions of the samples. On the other hand, for non-crystalline structures (amorphous material), the XRD spectrum gives only a line showing noise from the

instrument. As all crystalline structures have unique X-ray diffraction patterns (like a fingerprint), a comparison of the diffractograms of unknown materials with different known structures leads to their positive identification (Hernandez Enriquez, 2003).

The X-ray diffractometer consists of an X-ray source, a detector and a sample holder. The X-ray source and the detector are at a fixed angle on the horizontal plane while the sample holder changes its angle (which is called scattering angle), at certain speeds during the analysis. X-rays are produced from the bombardment of a metal anode (the target) by high energy electrons from a heated filament in a Rontgen X-ray tube. Various materials are used to build the targets in the X-ray tubes. The most common ones are: Cu, Cr, Fe, Co, Mo, and Ag. The peak positions are recorded at 2θ degrees where θ is the diffraction angle which is radiation dependent. To transform the diffraction angles to lattice spacing or d-spacing, the Bragg equation is implemented as:

$$n\lambda = 2d\sin(\theta) \quad (5.2)$$

where n is an integer (usually equal to 1), λ is the wavelength of X-ray, d is the lattice spacing and θ is the angle of diffraction (Cullity, 1978).

An Ultima IV X-ray diffraction system from Rigaku Instruments was used to perform the X-ray analysis. This diffractometer consists of an X-ray generator (20-60 kV, 2-60 mA) with a Cu target, a scintillation counter detector and a sample holder. The system was operated in a step scanning mode, with a scanning speed (duration time) of 4 sec, and a scanning step of 0.03, increasing from 3 to 54.99 degrees in the 2θ diffractogram scale. The XRD analysis was performed at Western Chemical and Biochemical Engineering Department Common Laboratory.

5.3.3 SEM-EDX

Scanning Electron Microscopy coupled with Energy Dispersive X-ray (SEM-EDX) is a technique used for assessing the elemental composition of solids and to provide images of the particles. Using SEM-EDX, an electron beam is directed to the sample, located in a high vacuum chamber (10^{-5} to 10^{-6} torr) to avoid interferences from air and water molecules present in the atmosphere. The electrons interact with the surface atoms producing a signal that is collected through a series of detectors. The signal can be analyzed to obtain the elemental composition of the surface and its enhanced picture. SEM-EDX is an effective characterization tool for analysing zeolite samples as it allows determining silica to alumina ratio (Si/Al). In addition, the degree of ion exchange during zeolite synthesis can be determined through the sodium cation content quantification (Hernandez Enriquez, 2003; Gianetto, 1993).

A Hitachi S-4500 field emission SEM fully equipped with an EDAXTM EDX system was used in the present study (electron beam voltages: 5 kV, resolution: 2-60 μm). This system was employed for obtaining the elemental composition of the catalyst samples. The catalyst samples were coated with Au to reduce charge problems. The EDX system was also used to measure the elemental contents including Si, Al, O, and Na. SEM-EDX analyses were carried out in collaboration with Surface Science Western (SSW).

5.3.4 NH₃-TPD

The characterization of the acidity of zeolites is of great importance for the applications of these materials in chemical processes. Various methods have been successfully applied to study the active sites in zeolites. Most of these methods are based

on adsorption or desorption of gas phase probe molecules, which are selected on the basis of their reactivity and molecular size. Temperature programmed desorption using ammonia as a probe molecule (NH₃-TPD) has shown to be an essential tool to study the strength of acid sites available in zeolites. The principle of this method consists of causing desorption of chemisorbed NH₃ species and thereby determining the rate of desorption. The total acidity of the zeolite sample is related directly to the amount desorbed of NH₃ per unit weight of sample. Despite the simplicity of the TPD technique and the usefulness of the data obtained, the main limitations of this technique have to be pointed out. TPD gives an average value of acid strength rather than a distribution. In addition, during the desorption process, a re-adsorption may occur. In addition, desorption from weak sites is hindered by adsorbates on strong sites. Furthermore, the main limitation of the TPD method is being not capable of distinguishing between acid sites types such as Brønsted or Lewis sites (Chester & Derouane (Eds.), 2009).

NH₃-TPD experiments were performed in the present study using a Micromeritics AutoChem II analyzer equipped with a thermal conductivity detector (TCD). A catalyst sample (0.1 - 0.3 g) contained in a U-shape quartz cell was degassed for 2 hours at 500 °C. The sample was then brought to saturation for 1 h at 100 °C using a gas mixture of NH₃ and helium gas (5% NH₃ and 95% He). The sample was then purged, at the same temperature, with He for 1 hour at a rate of 50 ml/min in order to remove physically adsorbed ammonia. Following this, the temperature was increased linearly at 15 °C/min until 500 °C was reached, with flowing He. As the temperature was increased, the ammonia desorbed and the TCD signal was recorded. The generated report includes the TCD signal versus time and temperature.

Furthermore, with the help of a calibration curve, the amount of NH_3 desorbed per unit weight of catalyst can be calculated simply by integrating the resultant peaks. The total acidity per unit weight of catalyst is related to this amount and to the molar volume.

5.3.5 Pyridine FTIR

Fourier Transform Infrared Spectroscopy (FTIR) using pyridine as a probe molecule can overcome the main limitation of TPD. In other words, this characterization technique can assess the zeolite acidity based on Brønsted or Lewis sites concentrations. The lone-pair electrons of a pyridine nitrogen atom are involved in different types of interaction with the surface acid sites. Three modes of pyridine adsorption have been reported: (1) protons transfer at Brønsted acid sites to form pyridinium ion (PyH^+) which is thermally stable, (2) electron transfer at Lewis acid sites (molecularly coordinated pyridine), and (3) hydrogen bonding pyridine to the surface hydroxyl groups. All three modes of adsorption display IR spectra peaks at different wavelengths and can be identified by their IR absorption bands. Pyridine coordinated with the Lewis centers yields a peak at 1450 cm^{-1} , while protonated pyridine on the Brønsted centers yields a peak at 1540 cm^{-1} . Both complexes also yield a peak at 1490 cm^{-1} . The multi-bands in the spectral region of $1580\text{--}1660\text{ cm}^{-1}$ are generally assigned to hydrogen-bonded pyridine (Chester & Derouane (Eds.), 2009; Tonetto et al., 2004).

The zeolite samples were dried, in situ, being heated under N_2 flow at $550\text{ }^\circ\text{C}$ and cooled to $100\text{ }^\circ\text{C}$. The samples were kept at $100\text{ }^\circ\text{C}$ and saturated with pyridine using a N_2 stream containing pyridine. Adsorption of pyridine was allowed for 1 hr. Then, the samples were flushed with pure N_2 , at $100\text{ }^\circ\text{C}$ for 90 minutes, in order to remove weakly

adsorbed pyridine. Following this, samples were collected and ground into a fine powder with an agate mortar. Finally, diffuse reflectance infrared spectroscopy (DRIFTS) measurements were recorded using a Bruker IFS55 FTIR spectrometer operating at a 4 cm^{-1} resolution and 100 scans. All FTIR spectra were collected at room temperature. FTIR analyses were carried out in collaboration with Surface Science Western (SSW).

5.3.6 N₂ Adsorption

The principle of measuring the total surface area of a solid by physisorption of a gas consists of determining the number of gas molecules required to cover the surface of the solid with a monolayer of adsorbate. If the area occupied by one molecule is known, the surface area of the solid can be calculated from the number of adsorbed gas molecules measured volumetrically. The adsorption of a gas on a solid is usually characterized by an isotherm. The isotherm represents the amount of gas adsorbed on the solid surface at a given temperature and partial pressure at equilibrium.

The most common characterization technique for determining the specific surface area of porous materials is the so called BET (Brunauer, Emmet, and Teller). The BET method is based on the adsorption and condensation of N₂ at liquid N₂ temperature. The principle of BET measurement starts with determining the point at which a monolayer of gas molecules covers the surface of the catalyst. Each adsorbed molecule occupies an area of the surface comparable to its cross sectional area.

The BET equation describes the relationship between the volume of gas adsorbed at a given partial pressure and the volume adsorbed at monolayer coverage as:

$$\frac{P}{V_{\text{ads}}(P_0 - P)} = \frac{1}{V_m C} + \frac{(C-1)P}{V_m C P_0} \quad (5.3)$$

where V_{ads} represents the quantity of gas adsorbed at gas partial pressure P , P_0 represents the saturation pressure of the gas at the experimental temperature, V_m represents the volume of gas adsorbed at monolayer coverage, and C is a constant.

The specific surface area of the catalyst may then be calculated from V_m , if the average area occupied by an adsorbed molecule is known. Thus, the specific surface area is given by the following equation:

$$\text{SSA} = \frac{V_m A_P N}{V_0} \quad (5.4)$$

where SAA is the specific surface area, A_P is the area of surface occupied by a single gas molecule (0.162 nm^2 for N_2 molecule), N is Avogadro's number, and V_0 is the molar volume of gas at STP.

The BET equation provides a good representation of the relative pressures P/P_0 between 0.05 and 0.3. This relative partial pressure range is usually used for surface area measurements. The adsorption in micropores (pore diameters less than 2 nm), which is significant in zeolites, cannot be determined by the BET with P/P_0 values below 0.05. The amount of adsorbed gas is too small to be accurately measured (Satterfield, 1980). However, the BET method can still be valuable as a reference for comparing with other surface area measurement techniques.

DFT (density functional theory) provides a better alternative for BET measurements of microporous solids such as zeolites. DFT has received considerable attention in recent years. DFT is a powerful method giving surface area and pore size distribution from experimental adsorption isotherms (Chester & Derouane (Eds.), 2009; Tonetto et al., 2004). DFT describes the adsorption process at the gas/solid interface of pores with slit-like or cylindrical geometry.

The t-plot method (Lippens & Boer, 1965) allows assessment of external surface area and micropore volume by plotting the adsorbed volume against the statistical thickness t of the adsorbed nitrogen layer. This method accounts for adsorption in both micropores and external surface. It uses a thickness curve type Harkins and Jura with a relative pressure range between 0.05 and 0.7 as:

$$t - \text{plot} = [13.99 / (0.034 - \log(P/P_0))]^{0.5} \quad (5.5)$$

The specific surface area and pore volume of the catalyst samples used in the current research were determined by physisorption of nitrogen using a Micromeritics ASAP 2010 Automatic Adsorption Analyzer.

A catalyst sample, being typically 0.1 to 0.3 g, was placed in the quartz sample tube and weighed. Then, the sample was degassed for 3 hrs at 300 °C. After that, nitrogen adsorption was carried out at 77 K. The relative pressure (P/P_0) ranging from 10^{-6} to 1 of the adsorption isotherms was calculated using a reference saturation vapor pressure. The specific surface area was calculated according to BET, Langmuir, and DFT methods. Furthermore, the pore volume was determined with the t-plot method. Moreover, porosity

distribution by DFT analysis was obtained using nitrogen adsorption isotherm data and a cylindrical pore model.

5.4 Reaction System

5.4.1 The Riser Simulator

All of the experimental runs were carried out in the CREC Riser Simulator (de Lasa, 1992). The CREC Riser Simulator is a bench scale internal recycle batch reactor. This reactor is designed for catalyst testing and allows one to obtain reliable data for kinetic modeling of fluid catalytic cracking (FCC) reactions (Kraemer, 1991). The CREC Riser Simulator has been used extensively to study desulfurization reactions over H-ZSM5 zeolites catalysts using the ethyl mercaptan conversion (Hernandez Enriquez, 2003) and the thiophene conversion (Jaimes, 2009).

The CREC Riser Simulator reactor is a well-mixed reactor unit that works under fluidized conditions. It has a volume of about 50 cm³ and a 1 g catalyst capacity. It combines a batch of catalyst and a batch of reactant, operating isothermally at a constant volume of reaction mixture throughout a predetermined reaction time. It consists of two outer shells, a lower section and an upper section that permit easy loading and unloading of catalyst.

This reactor is designed in such a way that an annular space is created between the outer portion of the basket and the inner part of the reactor shell containing the basket. This annular space facilitates the recirculation of gaseous reactants and/or products by the rotation of an impeller positioned above the catalyst basket. A metallic gasket seals the two chambers. An impeller is located in the upper section of the reactor. A packing gland

assembly with a cooling jacket supports and seals the impeller shaft. Upon rotation of the shaft, gas is forced outward from the center of the impeller towards the walls. This creates a lower pressure in the central region of the impeller. It induces a flow of gas upward through the catalyst chamber from the bottom of the reactor annular region where the pressure is slightly higher. This upward flow, gives a fluidized bed of catalyst particles as well as intense gas mixing inside the reactor. A schematic diagram of the Riser Simulator is shown in Figure 5.1.

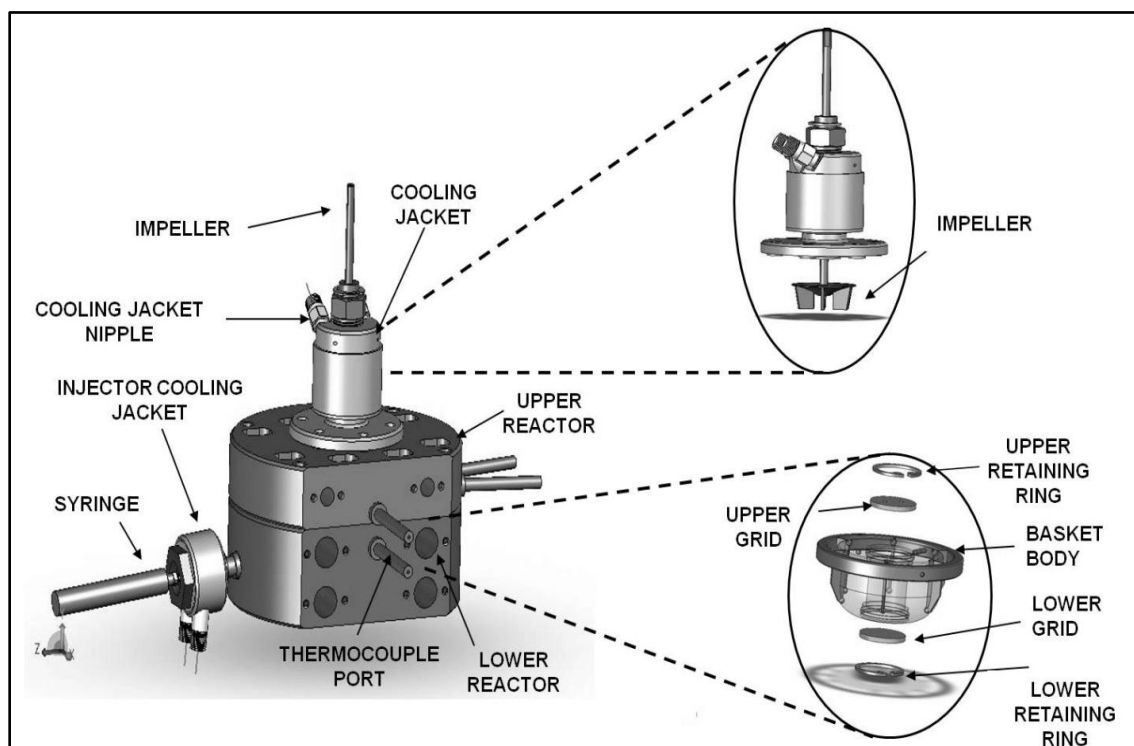


Figure 5.1. Schematic diagram of the CREC Riser Simulator with components at the time of assembly.

The CREC Riser Simulator operates in conjunction with some other accessory items, such as (a) a vacuum box (VB), (b) a gas chromatograph (GC), (c) a series of sampling

valves, (d) a timer, (e) two pressure transducers and, (f) two temperature controllers. The sampling system also allows sending the reaction products to the analytical system. A schematic diagram of the CREC Riser Simulator, along with the major accessories is illustrated in Figure 5.2.

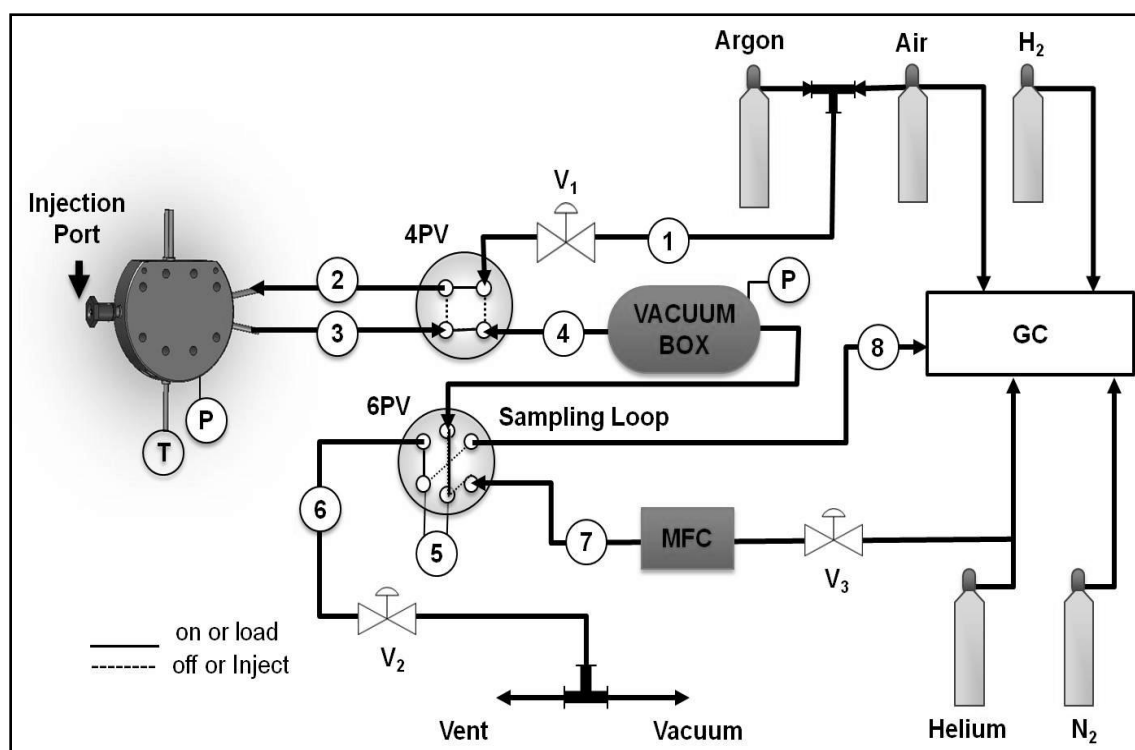


Figure 5.2. Schematic description of the CREC Riser Simulator, with associated valves, and accessories: (MFC: mass flow controller, 4PV: four port valve, 6PV: six port valve, V₁, V₂ and V₃: auxiliary on-off valves, P: pressure, T: temperature).

All the connections of the CREC Riser Simulator are manufactured using 1/8" stainless steel tubing, except the transfer line that carries the reaction products sample to the analytical system (line 8 in Figure 5.2). This line was replaced in the case of this study by SulfinertTM coated tubing, to avoid adsorption of sulfur compounds. Valve V₁ is

used to select the gas source (Air or Argon) to the reactor and vacuum system. Argon is used during the reaction periods as an inert gas while air is used during catalyst regeneration. Valve V_2 is used to vent the system or create a vacuum in the system. Valve V_3 is an isolation valve to control the product sampling. All valves are of the solenoid type and are controlled from the front control panel.

A 1/8" 4-port chromatographic valve (4PV) connects the reactor with the Air/Argon supply at one end, and with the vacuum system at the other end. In the open position, the gases pass through the 4PV, enter into the reactor through the inlet port, come out of the reactor through the outlet port, back into the 4PV, and finally to the vacuum box. While in the closed position, the reactor is completely isolated from the system; thus any gas flowing to the 4PV will by-pass the reactor and goes straight to the vacuum box.

The vacuum box, which is connected to the 4PV, is a stainless steel vessel. The vacuum box is internally coated with SilcoNertTM 2000. This is in order to avoid sulfur adsorption in the vacuum box which causes carry over between experimental runs. The vacuum box has a volume of about 1000 cm³. This large volume allows quick and easy evacuation of gas products as well as unreacted species from the smaller volume CREC Riser Simulator reactor. Additionally, a large pressure difference can be attained using a vacuum pump in order to remove the reactor content effectively. The sampling loop is of 2 cm³ in volume and is also internally coated with SilcoNertTM 2000.

Two pressure transducers (OMEGA PX303-050A5V) rated at 50 psia maximum pressure are installed in both the reactor and the vacuum box to allow the monitoring of the pressure during the experiment, as well as to make sure that complete and

instantaneous evacuation occurs in the reactor. Both of the transducers are connected to analog/digital cards, supplied by Cole Parmer (A/D, model L-08109-27). For data collection, the GWBASIC code is used.

Two temperature controllers (OMEGA CN9600A) are used to display and control the reactor temperature. Another OMEGA CN9000A unit is used to control and display the vacuum box temperature. Additional readings such as room, cooling jacket water, and transfer lines temperatures are displayed using a OMEGA DP462 unit. Temperature controllers are calibrated to work with K type OMEGA thermocouples.

The reaction time is set with a timer connected to the actuator of the 4PV. This timer is linked to a micro-switch located in the manual injector. It starts with the manual injection of the feed, and when the preset time expires, the reactor contents are evacuated to the vacuum box through the four-port valve. The evacuation process is almost instantaneous because of the significant pressure difference between the reactor and the vacuum box. Consequently, the reaction is terminated with the evacuation of the reactor.

A 1/8" 6-port chromatographic valve (6PV) is installed following the vacuum box. The 6PV has two permitted positions: "load" or "inject", with two independent paths for the gases to move through. The "load" position is used to fill up the sample loop with this path leading from the vacuum box to the vent/vacuum pump. The "inject" position connects the sample loop with the helium carrier gas supply, and allows the sending of the sample to the GC/MS analytical system.

The 4PV, 6PV, and the vacuum box are located inside a heated box. A thermocouple placed inside the heated box is used to measure and control the temperature of the

vacuum system. The vacuum box temperature was always set above 280 °C to avoid any condensation of products. The temperature of the transfer line connecting the 6PV and the GC was also kept above 280 °C, using a heating tape.

Prior to experiments, the reactor and vacuum box volumes were assessed according to the procedure described in Appendix B. The reactor volume was found to be 56.55 cm³. This volume includes the reactor, the connecting lines within the reactor, and the 4-port valve (4PV). The vacuum box volume was found to be 1150.14 cm³. This volume includes the vacuum box, the connecting lines, the 6PV, and the sample loop.

5.4.2 Experimental Procedure

Thermal and catalytic runs were performed using the previously described CREC Riser Simulator. About 0.8 g of catalyst was loaded in the reactor basket and the reaction system was sealed, and leak tested. Then, the catalyst was further calcined at 550 °C under air flow for 25 min. After that, the reactor temperature was set to the desired reaction temperature and argon gas was circulated to flush the system. Using a calibrated gas tight Hamilton syringe, 0.16 g of reactant mixture was weighed and injected into the reactor. Once the reaction time was reached, the reaction products were evacuated from the reactor and sent to the analytical system through the heated transfer line. All experimental runs were repeated three times to secure reproducibility of results.

Mixtures of benzothiophene and n-dodecane were reacted at: (a) around atmospheric pressure, (b) mild temperatures (350, 375, 400, 425, and 450 °C), (c) short contact times (3, 5, and 7 seconds), and (d) 6 wt % benzothiophene concentration. The maximum temperature of 450 °C was chosen to diminish the thermal cracking of both

benzothiophene and hydrocarbons. The catalyst to oil ratio (cat/oil) was set at 5 and the impeller velocity at 5700 rpm to get a well fluidized bed.

A typical experimental run in the CREC Riser Simulator consists of a number of procedural steps. These various steps are followed with the change in pressure recorded by the pressure transducer. A typical pressure profile in the Riser Simulator is shown in Figure 5.3. This Figure shows that prior to the injection of the reactant into the reactor, the pressure of the reactor was about 15 psia, whereas the vacuum box is kept at low pressure of 3.7 psia. To maintain this difference in pressure, the reactor and VB are isolated by closing the 4PV. At the time of the reactant injection into the CREC Riser Simulator, the reactant rapidly vaporizes, causing an abrupt increase in reactor pressure (A-B). Another stage follows the reactant vaporization, whereby reaction takes place and gaseous products are formed, causing an expansion in the system (B-C). Once the preset reaction time is completed, the 4PV is automatically switched to connect the reactor and the vacuum box. The initial large difference in pressure between these two chambers causes the evacuation of reaction products from the reactor into the VB. This evacuation, which occurs instantaneously due to the significant differences in pressure and volume of the reactor and VB, leads to a sudden drop in the reactor pressure and consequent rapid pressure stabilization in both chambers pressures (C-D). The reported condition in Figure 5.3, display total pressure changes from A to C and corresponds to a three seconds reaction time run of benzothiophene/n-dodecane mixture.

A regeneration cycle was required after each catalytic run to burn any amount of coke formed. The reactor temperature was set at 550 °C during the catalyst regeneration process for 25 minutes under air flow.

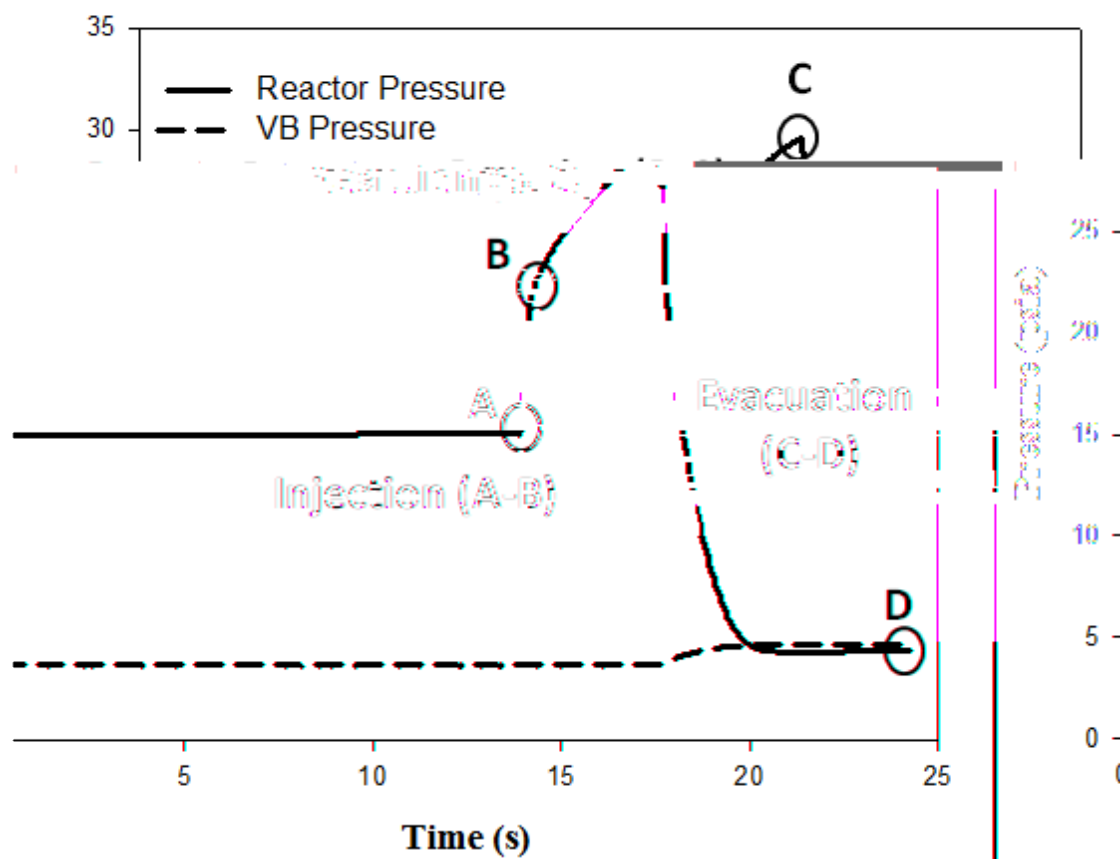


Figure 5.3. Typical pressure profile in the CREC Riser Simulator.

5.4.3 Analytical System

An Agilent 5973N Mass Selective Detector (MSD) was used to identify the reaction products. An Agilent 6890N Gas Chromatograph (GC) equipped with a Flame Photometric Detector (FPD) and a Flame Ionization Detector (FID) allowed the products quantification.

The MSD was operated in the scan mode using the parameters listed in Table 5.1. The reaction products were identified comparing the peaks found with the MSD Ion Detector to the the data in the available library from G1701DA MSD ChemStation software. The

product peaks from the MSD were then assigned to the peaks which appeared in the FID/FPD chromatograms at the same retention times.

Table 5.1. Mass Selective Detector parameters and settings.

Parameter/Setting	Value
Transfer Temperature	280 °C
Tune file	ATUNE.U
EM Voltage	0
Solvent delay	0 min
Acquisition mode	SCAN
Threshold	150 counts
Sampling rate 2 ⁿ	2
Mass range	5 - 500
Scan/sec	2.97

The FPD was utilized for the selective detection of benzothiophene in hydrocarbons mixtures. A calibration curve correlating peak areas and amounts of benzothiophene was established prior to the experimental runs. In addition, the FID was employed to quantify the hydrocarbon species and low concentration sulfur species produced from the reaction using a response factor (RSF). All GC/FPD/FID calibration data including the BZT calibration curve, and the FID response factor (RSF) for sulfur species are shown in detailed in Appendix C of this dissertation.

Two 5%-phenyl-methylpolysiloxane capillary columns, HP-5MS and HP-5, with a length of 30 m, a nominal diameter of 0.25 mm, and a nominal film thickness of 0.32 μm permitted the separation of the compounds present in the samples. Both columns were

connected to the back inlet of the GC. The first column end was linked to the MSD, while the second column end was split between two capillary columns: one reaching an FID and the other an FPD. In this way, each single injection produced three signals, one per detector. This configuration allowed the identification and the quantification of various hydrocarbon products as well as sulfur species in hydrocarbons mixture with low sulfur content. The detailed method used for each detector is shown in detail in Table 5.2.

The GC oven temperature program used in the current research includes: (a) initially holding the oven at 35 °C for 10 min, (b) increasing the oven temperature to 70 °C with a ramping rate of 8 °C/min, (c) holding the oven temperature at 70 °C for 8 min, (d) increasing the oven temperature to 250 °C with a ramping rate of 15 °C/min, and finally (f) holding the oven temperature at 250 °C for 5 min. This temperature program was found the best to give peaks separation and integrity.

The GC/MSD analytical system was operated using the MSD Productivity ChemStation, which is an integrated GC/MS software application covering various post run calculations including data acquisition, processing, and reporting.

Table 5.2. GC method and parameters.

Parameter/Setting	Value	
Inlet		
Mode	Split	
Gas	He	
Temperature	270 °C	
Pressure	31.1 psia	
Split Ratio	30	
Column 1	Agilent 19091S-433 350 °C Max	
Detector	MSD	
Outlet	Vacuum	
Mode	Constant flow	
Flow	1.1 ml/min	
Column 2	Agilent 19091J-413 350 °C Max	
Detector	FID/FPD	
Outlet	Ambient	
Mode	Constant flow	
Flow	1.0 ml/min	
Detectors	FID	FPD
Temperature	250 °C	250 °C
H ₂ Flow	40 ml/min	50 ml/min
Air Flow	450 ml/min	60 ml/min
Makeup gas type	N ₂	N ₂
Makeup Flow	45 ml/min	60 ml/min
Lit offset	2.0	2.0
Position	Front Detector	Back Detector

5.4.4 Quantification of Carbonaceous Material in Spent Catalyst Samples

The coke deposited on the catalyst surface after experiments was measured in wt % using a Total Organic Carbon Analyzer (TOC-V) from Mandel with a Solid Sample Module (SSM-5000).

A sample of about 40 mg was weighed and loaded in the sample “boat” of the TOC instrument. Following this, the sample was burned at 900 °C to produce CO₂ gas, which was then absorbed using a soda lime granular CO₂ absorber. With the aid of computer software (TOC-Control V) from SHIMADZU, the amount of coke burned was quantified in mg by converting the resultant peak area to the weight of coke through a calibration curve developed prior to the experiments. The catalyst sample remains were then discarded.

In addition, the sulfur amount in the coke was determined using Inductively Coupled Plasma (ICP) mass spectrometry and following a method developed by Khan et al. (2012). About 100 mg of spent catalyst sample were placed in a digestion tube containing 1 ml HNO₃ and 1 ml HCL. The tube was then sealed with a screw cap and placed into the ultrasonic bath (VWR Scientific Products, USA, Model 75HT; 117V, 205 W, with an analogue timer 0 to 35 minute, and heater 0 to 85 °C) for sonication. The digestion process was performed at 80 °C for 2 hours. Following this, the sample solution was decanted and diluted in a 50 ml volumetric flask using de-ionized water. The diluted solution was then filtered to an ICP tube using a disposable syringe (10 ml NORM-JECT, Latex free) through a syringe filter (0.2 µm Supor membrane from Pall Corporation, U.S.A.). Finally, the total sulfur was measured by using an ICP-OES (Varian Vista Pro;

CCD Simultaneous, Australia) Auto Sampler. ICP analysis was conducted in collaboration with the Civil and Environmental Engineering Department of Western University.

CHAPTER 6

RESULTS AND DISCUSSION

6.1 Introduction

This chapter reports and discusses the experimental results and findings for the current research on the catalytic conversion of BZT over a H-ZSM5 zeolite catalyst.

The first section of this chapter describes and reviews the main characterization results for the prepared H-ZSM5 zeolite pellets. On the other hand, the second section of the current chapter shows the detailed results obtained from the thermal and catalytic runs of pure n-C12 and BZT/n-C12 mixture samples including conversion, selectivity, and products distribution. Moreover, this chapter also includes a detailed discussion of these experimental results in order to establish a reaction rate model and provide insights on the reaction mechanism for BZT conversion over H-ZSM5 zeolites.

6.2 Catalyst Characterization

6.2.1 ABD and PSD

Fluidization in moving bed reactors is dependent on catalyst density. The Average Particle Size (APS) and the Particle Size Distribution (PSD) can significantly affect fluidization characteristics (Satterfield, 1980). The Apparent Bulk Density (ABD) of the prepared zeolite pellets was found to be 1580 kg/m³ and the average particle size was assessed at 50.46 μm . According to Geldart's powder classification groups (Geldart, 1973), such particles with an Average Particle Size of 50.46 μm and Apparent Density of

1580 kg/m³ belongs to group B. Group B particles display good fluidization at or only slightly above Minimum Fluidization Velocity. It is important to mention that the H-ZSM5 before pelletization displays a low ABD (650 Kg/m³) and a small particle size (about 1 micron). Hence, it is impractical to fluidize such a highly cohesive powder in the CREC Riser Simulator or any equivalent fluidized bed unit.

However, after pelletization, pellet crushing and particle sieving in the 53-100 micron range, the resulting particles fluidize very well, providing a suitable material for the extension of the results of this study to a large scale process. This significant finding was the result of being able to control both the density and the changes in the size of the particles using an inert matrix with about one micron of H-ZSM5 dispersed crystallites.

6.2.2 XRD

XRD analysis was carried out to assess the crystallinity of the H-ZSM-5 zeolites used in this research. The H-ZSM-5 before calcinations as received from the manufacturer, and H-ZSM5 after calcination at 550 °C for 5 hrs under air flow, showed typical XRD patterns as reported in Figure 6.1. This result shows that zeolite crystallinity was not affected by the calcination process.

Both sample structures showed a crystalline phase only with no amorphous phase identified. This is in agreement with the fact that zeolites are highly crystalline materials. In addition, these XRD patterns are very similar to the ones reported in the literature (de Lasa et al., 2006; Treacy & Higgins, 2001). ZSM-5 or calcined ZSM-5 (H-ZSM5) characteristic peaks in the XRD patterns are usually at 2 θ diffraction angles of 7.94, 7.95, 8.01, 8.84, 8.88, and 8.90 degrees (Treacy & Higgins, 2001). These XRD peaks were

indeed found for the zeolite samples used sometimes with little shifts in the peak positions due to the variations between different X-ray sources. There were also other XRD peaks at 25.5, 35, 37.7, 43.3, and 52.5 (Figure 6.1) which were assigned to the filler (fused alumina) of the silica alumina matrix.

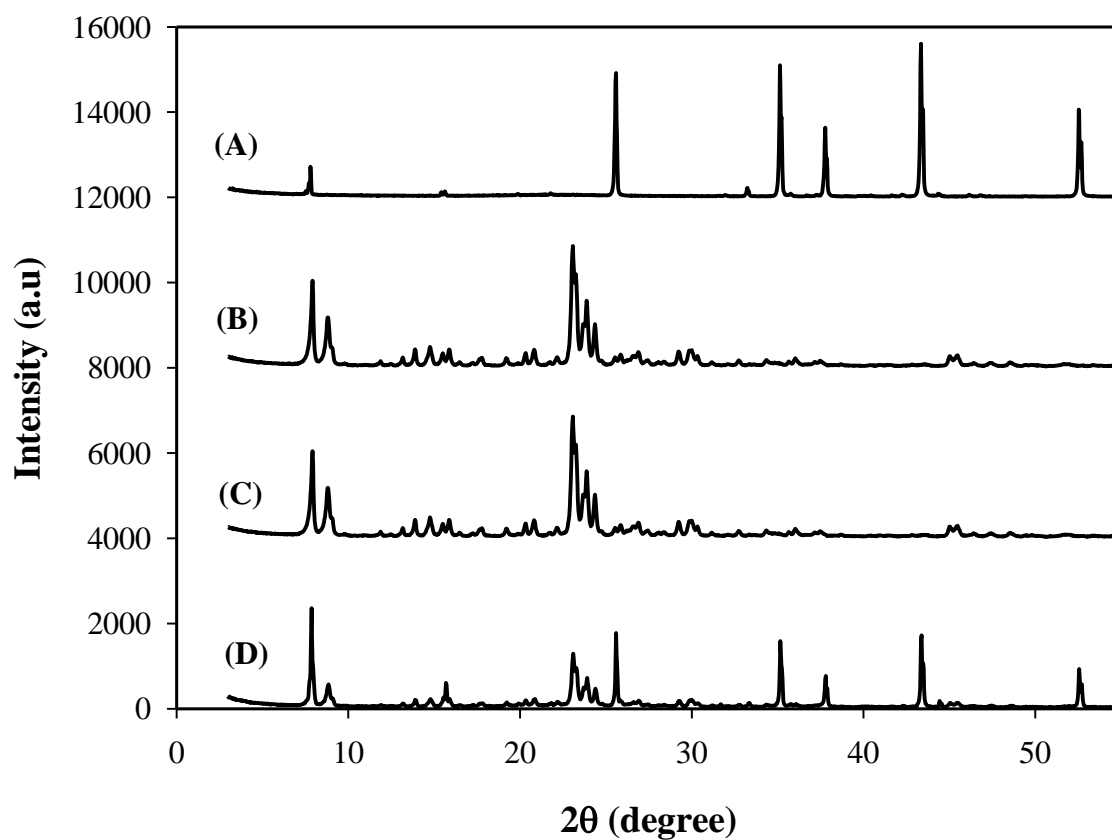


Figure 6.1. XRD patterns for the catalyst samples: (A) matrix alone with incorporated fused alumina filler, (B) fresh H-ZSM5 (before calcinations), (C) H-ZSM5 after calcinations, and (D) catalyst pellets containing 30 wt % of H-ZSM5 and 50 wt % fused alumina filler.

6.2.3 SEM-EDX

Table 6.1 reports the results of SEM-EDX analysis for the catalyst samples namely: (a) the parent H-ZSM5 zeolite, (b) the matrix, and (c) the catalyst pellet (with 30 wt % of H-ZSM5).

Table 6.1. SEM-EDX analysis results in wt %. Reported values are averages of three runs with standard deviation of ± 2 .

Element	H-ZSM5	Matrix	Pellet
Si	54.14	24.09	48.13
Al	3.07	34.76	10.23
O	42.78	41.14	41.62
Na	< 0.05*	n/a	< 0.05*
Si/Al	17.65	0.69	5.05

*The lowest level detected by the instrument is 0.05%

SEM-EDX results for the parent zeolite (H-ZSM5) were in agreement with the supplier data. As received zeolite was reported to have a silica to alumina ratio of 30 atomic ratio ($\text{SiO}_2/\text{Al}_2\text{O}_3 = 30$). This is equivalent to an elemental ratio (Si/Al) of 15. In this respect, SEM-EDX analysis shows a Si/Al of 17 which is in agreement with the expected value of 15, with the difference being within experimental error. On the other hand, the matrix elemental analysis shows a high Al and a smaller Si content. This anticipated result is due to the 75% fused alumina component of the matrix.

The pelletized zeolites exhibited a lower Si/Al ratio than the parent zeolite prior to pelletization. This result is consistent with the high Al contribution of the matrix which

was 50 wt % of the entire pellet. In other words, the matrix diluted the original zeolite sample yielding a bulk Si/Al ratio of 5.

It can also be observed in Table 6.1 that the sodium content of the H-ZSM5 zeolite and the pellet samples were below the detectable limit of 0.05wt%. This result shows the successful ion exchange process for the H-ZSM5. Furthermore, it confirms that no ion exchange is required after zeolite pelletization.

6.2.4 NH₃-TPD

Acidity of zeolite samples was characterized by Temperature Programmed Desorption (TPD) using NH₃ as a probe molecule. Utilizing this method, the total acidity and acid strength distribution can be obtained from the total peak area and relative area of TPD peaks at lower and higher temperatures. NH₃-TPD can differentiate sites by sorption strength only and cannot distinguish between Brønsted or Lewis acid sites (Tonetto et al., 2004).

At first, it was found in a separate experiment developed with catalyst pellets made from fused alumina and silica sol (matrix) only, that NH₃ adsorption was not significant. This is due to the fact that no peaks were detected from NH₃ desorption. In other words, the matrix displayed the desirable effect of not contributing to the total acidity of the zeolite pellets.

A typical TPD profile from an acid type zeolite displays two desorption peaks, termed LTP and HTP (low temperature peak and high temperature peak, respectively). The H-ZSM5 zeolite typically exhibits two distinctive peaks: the low temperature peak at 210 - 255 °C and the high temperature peak at 420 - 465 °C. Generally, the LTP and the HTP

correspond to weak and strong acid sites, respectively (Chester & Derouane (Eds.), 2009; Shirazi et al., 2008).

Figure 6.2 shows both the NH_3 -TPD results for the H-ZSM5 zeolite and for the zeolite once pelletized. Both samples produced two characteristic peaks: the LTP and the HTP. Furthermore, as expected, both the LTP and the HTP intensities were lower for the pellet given that it contained a diluted H-ZSM5 fraction with 30 wt % H-ZSM5.

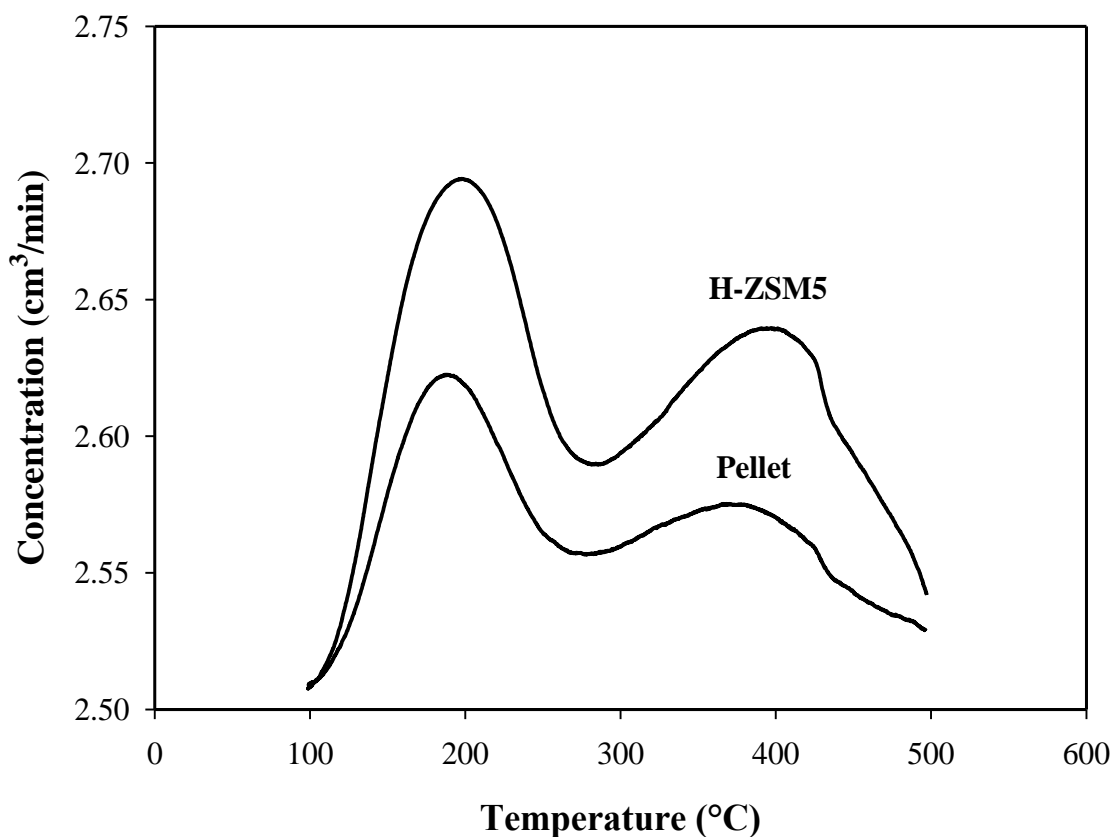


Figure 6.2. NH_3 -TPD spectra for: (a) the H-ZSM5 zeolite and (b) the catalyst pellets containing 30 wt % zeolite.

The total acidity of the H-ZSM5 zeolite and the zeolite pellet are reported in Table 6.2. This provides additional confirmation that the silica-alumina matrix was not

contributing to the total acidity of the catalyst pellet. In summary, the acidity of the 30 wt % H-ZSM5 was the main factor in determining the catalyst pellet acidity.

Table 6.2. Acid properties of zeolite samples.

	H-ZSM5	Pellet
Total Acidity (mmolNH ₃ / g)	0.788	0.211
Brønsted/Lewis sites ratio	1.9	1.2

6.2.5 Pyridine FTIR

As stated in Chapter 5, Fourier Transform Infrared Spectroscopy (FTIR) using pyridine as a probe molecule can be used to provide additional acidity information with respect to the TPD data. In other words, this characterization technique can be employed to assess zeolite acidity based on Brønsted or Lewis sites concentrations. The lone-pair electrons of a pyridine nitrogen atom are involved in different types of interactions with the surface acid sites.

Figure 6.3 shows the FTIR spectra for all catalyst samples used in the current research. It can be noted that no pyridine adsorption was observed on the matrix. This result is in agreement with previous results from TPD. In addition, a standard run was conducted using a H-ZSM5 zeolite sample before pyridine saturation which shows the basis of this analysis. Pyridine saturated samples of H-ZSM5 and zeolite pellets showed all FTIR characteristic peaks of pyridine. The Brønsted acid sites peak at 1540 cm⁻¹ and Lewis acid sites peak at 1450 cm⁻¹ were detected in both samples. In addition, other peaks at 1490 cm⁻¹ and in the region of 1580-1660 cm⁻¹ can be observed. This represents

the resulting complex from Brønsted and Lewis acid sites, and hydrogen-bonded pyridine, respectively.

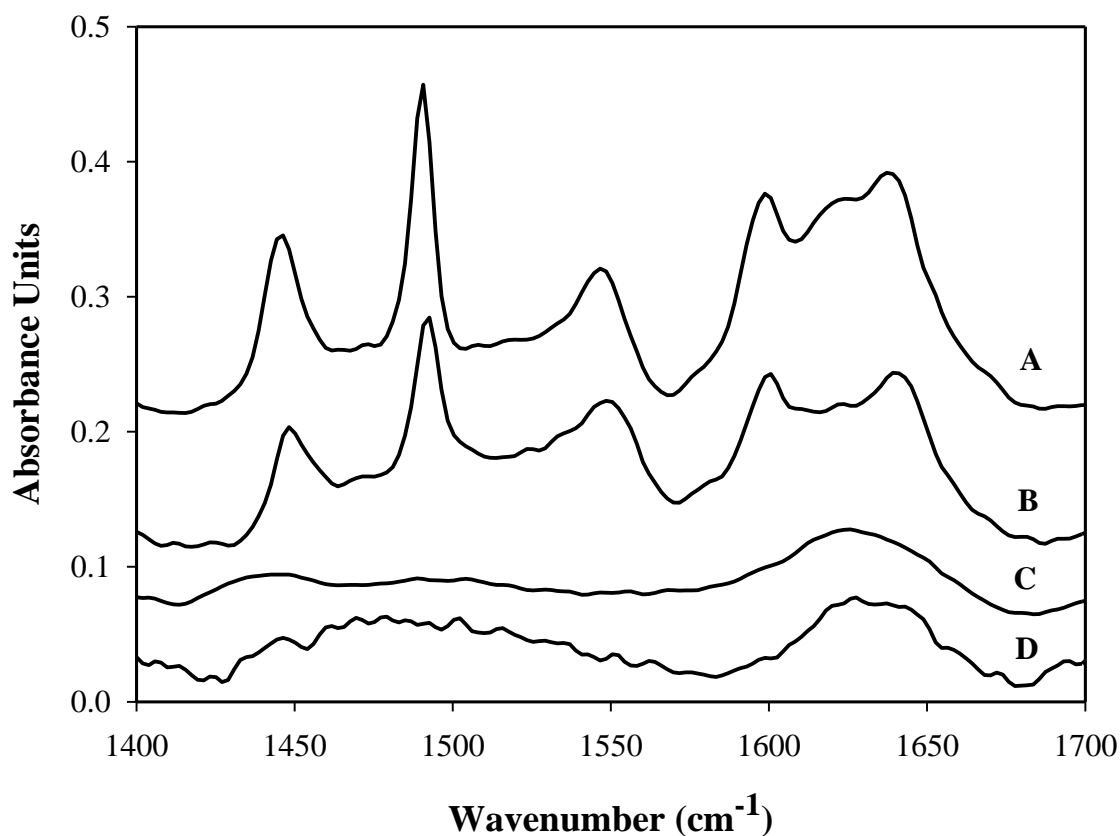


Figure 6.3. FTIR spectra of pyridine for: (A) catalyst pellets with 30 wt % H-ZSM5, (B) H-ZSM5 zeolites, (C) matrix, and (D) H-ZSM5 before pyridine adsorption.

The peaks at 1540 cm^{-1} and 1450 cm^{-1} were used to quantify the Brønsted and Lewis acid sites concentrations, respectively. Table 2 reports the Brønsted/Lewis acid sites ratios for both the H-ZSM5 zeolites, and the catalyst pellets with 30 wt % H-ZSM5.

It can be noted that Brønsted acid sites are the dominant sites over Lewis acid sites. It can also be observed that the Brønsted/Lewis ratio decreased after pelletization from

almost two to 1.2. In this respect, an approximate 50% reduction in Brønsted/Lewis ratio was found by Tonetto et al. (2004), using HY zeolite pellets. This observation was attributed to the zeolite dehydroxylation during the calcination step of the pelletization process.

6.2.6 N₂ Adsorption

Figure 6.4 reports the nitrogen adsorption-desorption isotherms of: (a) the H-ZSM5 zeolites, (b) the silica alumina matrix and, (c) the catalyst pellets with 30 wt % H-ZSM5.

The shape of the adsorption isotherms of both the H-ZSM5 zeolites and the zeolite pellets is of Type I in the BET classification. This is typical for microporous solids (Brunauer et al., 1940). The volume adsorbed at a very low relative pressure (P/P_0) is significant for H-ZSM5, being reduced substantially for the catalyst pellets with 30 wt % H-ZSM5.

For the matrix, the volume adsorbed at very low pressure is very small with the matrix displaying a type III adsorption isotherm. This can be explained given the mesoporous structure of the matrix. Thus, the total volume adsorbed by the matrix gives a corresponding very low surface area. This is mainly due to the low surface area of fused alumina which makes 75% of the matrix.

In summary, in the pellet structure, the micropores are essentially given by the H-ZSM5 with most of mesopores being supplied by the pellet matrix.

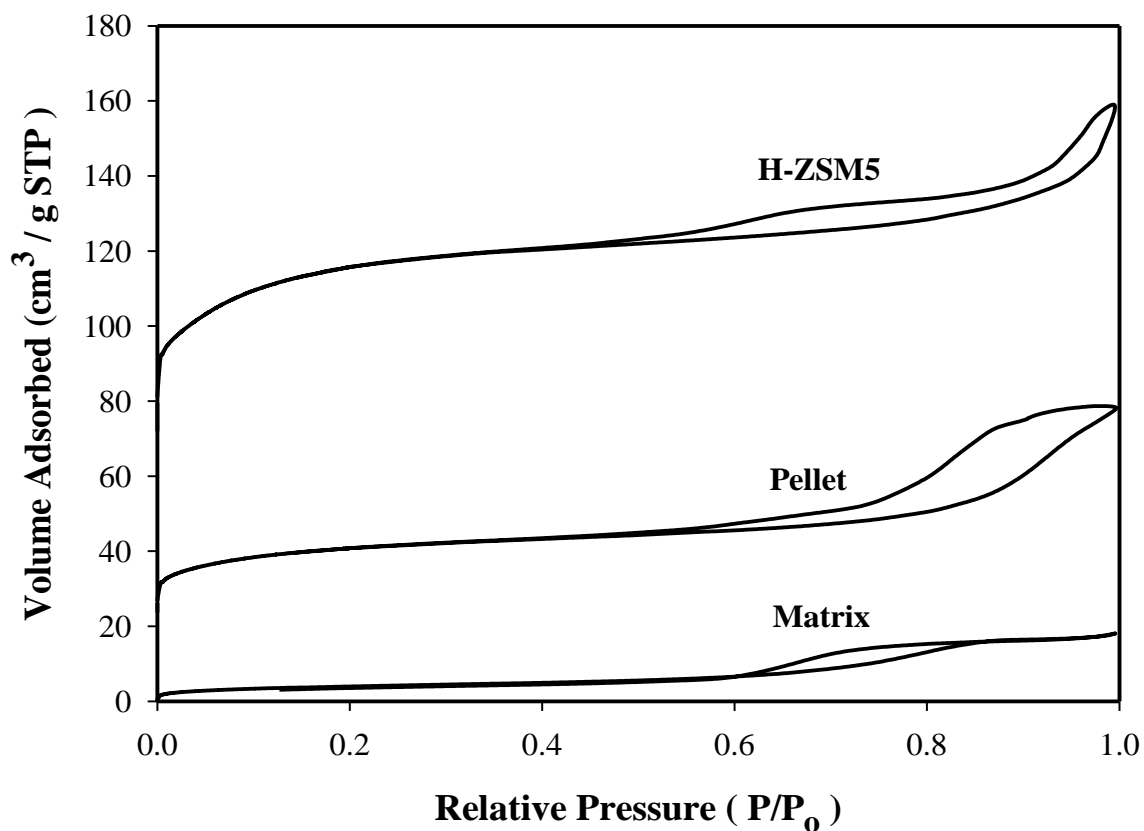


Figure 6.4. Adsorption-desorption isotherms of nitrogen on: (a) H-ZSM5 zeolites, (b) matrix and (c) zeolite pellets.

As stated before in the experimental part of this thesis, the adsorption in micropores (pore diameters less than 2 nm), which is significant in zeolites, cannot be determined by the BET with P/P_0 values below 0.05. On the other hand, DFT provides a better alternative for the quantification of surface area and pore size distribution in microporous solids such as zeolites.

Table 6.3 reports the specific surface area (SSA), pore volume (PV), and median pore diameter computed from the nitrogen adsorption on: (a) H-ZSM5, (b) the matrix, and (c) the catalyst pellets. It can be observed that the BET and the Langmuir methods greatly

underestimate the value of SSA for the H-ZSM5 zeolites and the pellets, with SSA decreasing in the following order: $SSA_{\text{BET}} < SSA_{\text{Langmuir}} < SSA_{\text{DFT}}$.

Table 6.3. Specific surface area SSA (m^2/g), pore volume PV (cm^3/g), and Median Pore Diameter (\AA).

	Sample		
	H-ZSM5	Matrix	Pellet
SSA (BET) ^A	411	14	141
SSA (Langmuir)	509	17	175
SSA (DFT) ^B	596	8	197
Micropores SSA (t-plot) ^C	266	0.16	81
External SA (t-plot)	144	14	59
Micro PV (t-plot)	0.116	≈ 0	0.036
Micro PV (DFT)	0.117	0	0.036
Total PV (DFT)	0.219	0.026	0.114
Total PV ^D	0.227	0.026	0.108
Median Pore Diameter (H-K) ^E	6.1	18	6.8

A. Calculated using the BET equation in the range of $0.05 < P/P_o < 0.33$

B. Obtained using Density Functional Theory: pores are assumed to be of cylindrical geometry on an oxide surface. The numerical method considers non-negative regularization, and no smoothing.

C. Calculated using the t-plot method: thickness curve type Harkins and Jura:

$$t - \text{plot} = [13.99 / (0.034 - \log(P/P_o))]^{0.5}$$

D. Measured at $P/P_o \sim 0.98$

E. Calculated using Horvath-Kawazoe: Cylindrical Pore Geometry (Saito and Foley) and Cheng and Yang correction.

As one can notice, adsorption in micropores is not properly described by the BET equation. BET is based on a multilayer adsorption which is not possible occur in these small pores. Furthermore, the Langmuir isotherm model assumes a monolayer adsorption on a homogeneous surface. Thus, neither BET nor Langmuir Model allow for the filling of micropores as hypothesized and as a result, SSA calculated using DFT provides a better alternative (Tonetto et al., 2004).

Regarding the SSAs for the matrix, they were almost the same using BET and Langmuir methods. However, SSA was much lower when using DFT. These results can be explained given the mesoporous structure of the matrix. In other words, the matrix structure contains mesopores only and DFT is unable to account for them yielding a small SSA. As a result, and for the matrix, the BET and Langmuir results should be considered as more reliable than DFT.

The micropore specific surface area and external surface area obtained using the t-plot method, are reported in Table 6.3. In both cases, the parent H-ZSM5 zeolite showed higher values than the catalyst pellet. The matrix produced much lower values. As mentioned before, this method is based upon the fact that both micropores and external surface area contribute to the adsorption process.

In addition, the data in Table 6.3 reports that the micropore volume obtained from the t-plot method is in agreement with that from the DFT calculations. Before pelletization, the H-ZSM5 zeolite has three times more micropore volume than the catalyst pellet while the matrix displays a negligible micropore volume. The same agreement can be observed between the Total Pore Volume resulting from the DFT and the volume adsorbed close to

saturation ($P/P_o \sim 0.98$). The latter is calculated using the volume of liquid (Gursvitch's rule) in Table 6.3. Thus, one should note that the pelletization process decreases the total pore volume of the H-ZSM5 to about the half of its initial value.

On the other hand, the Median Pore Diameter was obtained using the Horvath-Kawazoe approach (Horvath & Kawazoe, 1983). This approach initially assumes that the adsorption isotherm follows Henry's law. However, the correction proposed by Cheng and Yang (Cheng & Yang, 1994) for the deviation of isotherm data from Henry's law must be used at higher pressures. In addition, the cylindrical pore geometry proposed by Saito and Foley (Saito & Foley, 1991) for zeolites and FCC catalysts was employed. Table 6.3 reports a pore diameter of 6.1 Å for the H-ZSM5 catalyst which in agreement with the well known ZSM-5 pore diameters (5-6 Å). The same results can be observed for the zeolite pellets confirming that the pelletization process had no impact on pore geometry. However, the matrix showed a much higher Median Pore Diameter compared to zeolite samples due to its mesoporous structure.

6.3 Catalyst Stability

The total catalyst lifetime is of crucial importance for the economics of a chemical process. The lifetime of a catalyst is determined by its chemical, thermal, and mechanical stability. Catalyst stability is influenced by a number of factors including: (a) coking, (b) decomposition, and (c) poisoning. Catalyst deactivation can be followed by measuring activity or selectivity as a function of time. Catalyst activity can be restored by regeneration before ultimately replacing the catalyst (Hagen, 2006).

The stability of the prepared H-ZSM5 pellet was investigated in continuous (without regeneration) and cyclic (with regeneration) modes using pure n-dodecane samples. These runs were performed in the CREC Riser Simulator at 450 °C, with a catalyst to oil ratio of 5, and a reaction time of 7 seconds. These conditions were selected to emulate the extreme reaction conditions that will be used later in the catalytic runs of the present study.

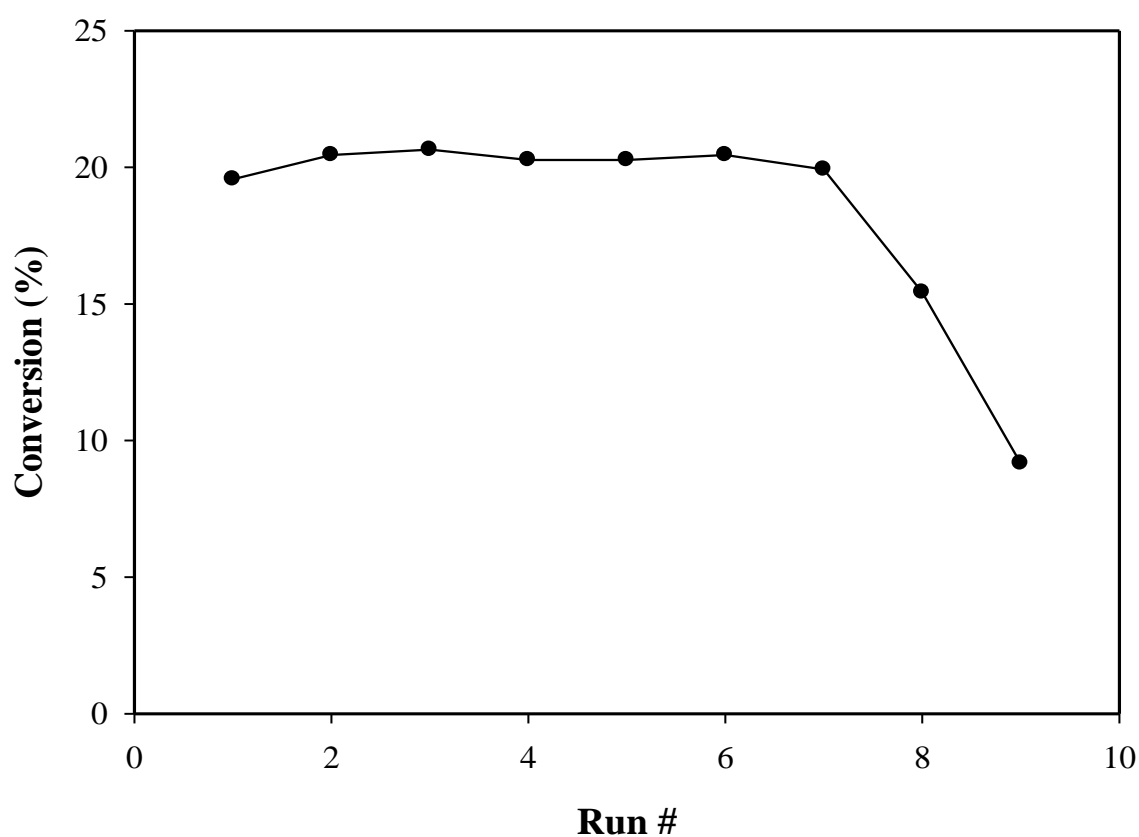


Figure 6.5. Conversion of n-dodecane versus run number. Reaction conditions: 450 °C, cat/oil = 5, 7 seconds reaction time, and without catalyst regeneration in between runs.

Figure 6.5 reports the conversion of n-dodecane with the number of consecutive runs without catalyst regeneration. It can be concluded that the catalyst pellet can maintain its

activity for seven continuous runs before being deactivated. Catalyst deactivation can explain the quick decrease in n-dodecane conversion in the last two runs. The loss of activity in this case can be assigned to coke formation which causes active sites losses and zeolite pores blockage.

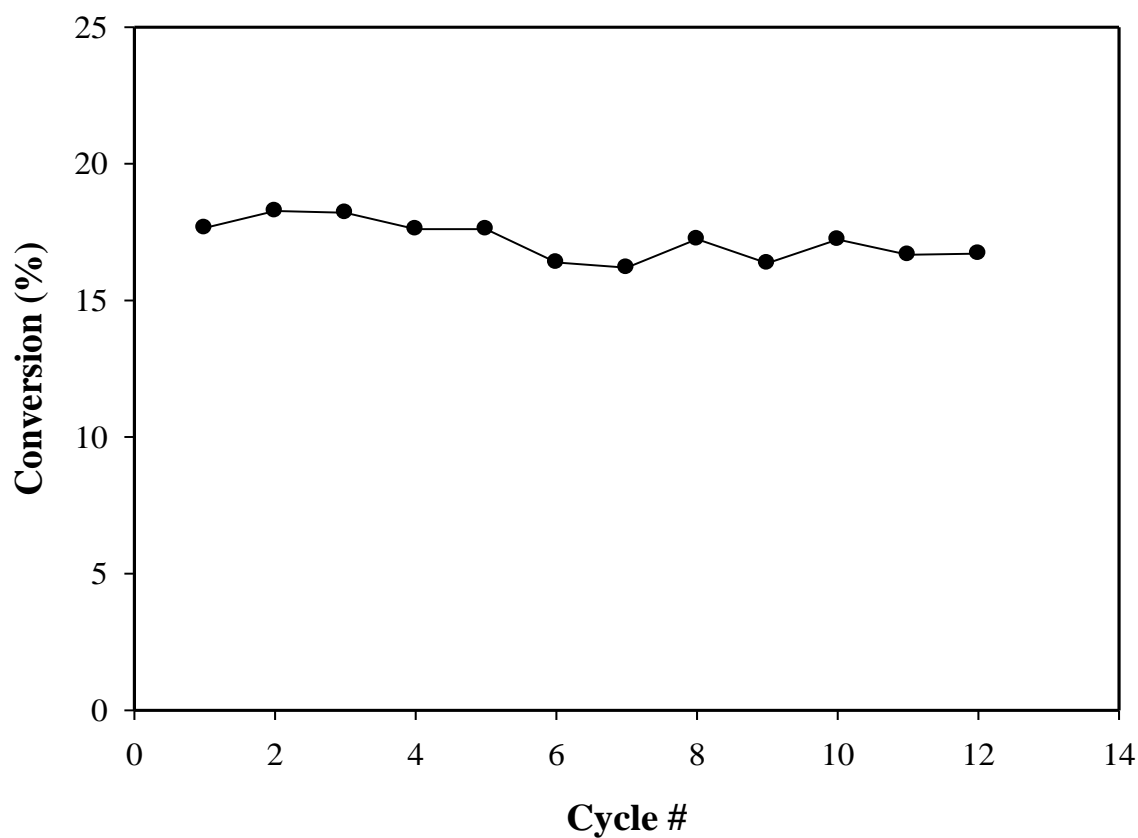


Figure 6.6. Conversion of n-dodecane versus cycle number. Reaction conditions: 450 °C, cat/oil = 5, 7 seconds reaction time, and with catalyst regeneration in between runs.

On the other hand, runs developed in the cyclic mode, where a catalytic cracking run is followed by a catalyst regeneration run, showed stable catalyst activity. Figure 6.6 reports n-dodecane conversion as a function of number of cycles. One can see that n-dodecane

conversion remains fairly constant throughout several reaction-regeneration cycles. In fact, there was no catalyst deactivation after 12 consecutive cycles. This result confirms that the prepared H-ZSM5 pellet can maintain its activity for a long time-on-stream if run in the cyclic reaction-regeneration mode. Moreover, it also indicates that the regeneration procedure used (550 °C under air flow for 25 minutes) is suitable to burn all coke formed and fully restore the catalyst activity after each run.

6.4 Thermal and Catalytic Runs

Thermal and catalytic runs with the prepared H-ZSM5 based catalyst were performed in the CREC Riser Simulator. A mixture of 6 wt % benzothiophene (BZT) dissolved in n-dodecane (n-C12) was reacted in an Argon environment at around atmospheric pressure, mild temperatures (350 °C - 450 °C), contact times of 3, 5, and 7 seconds, catalyst to oil ratio of 5, and 5700 rpm impeller velocity. In addition, catalytic cracking of n-dodecane was investigated with 100% pure n-C12 samples at the same above mentioned conditions. All runs were repeated three times to ensure reproducibility of experimental results. Mass balance closures, which include all chemical species fed and removed from the reactor, were in the range of $\pm 6\%$. Selected mass balances are shown in Appendix D.

The gas phase products from the reaction were analyzed in an Agilent GC-MS system described in Chapter 5 of this dissertation. The coked catalyst samples were analyzed for Total organic carbon using TOC Analyzer while the amount of sulfur in coke was determined by ICP analysis following the procedure described in Chapter 5.

6.4.1 Thermal Cracking

Thermal cracking runs or blank runs were performed with an empty reactor or no catalyst loaded in the CREC Riser Simulator unit. These runs were developed to determine possible conversion of benzothiophene and n-dodecane via thermal cracking. Thermal cracking runs were performed at 450 °C and 7 seconds contact times which were considered the most severe conditions for the experiment.

n-Dodecane conversion displayed very small values of 0.35 % and 0.56 % in pure n-C12 and in a 6 % benzothiophene mixture, respectively. On the other hand, no conversion was observed for benzothiophene due to thermal cracking. Based on these results, thermal cracking was neglected under the conditions studied. It was concluded that the conversion observed during the catalytic runs truly represents the H-ZSM5 catalytic activity.

6.4.2 Catalytic Runs

The prepared zeolite catalyst was tested for the catalytic conversion of benzothiophene. The reactant mixture contained 6 wt % benzothiophene diluted in n-C12. In addition, catalytic cracking of n-dodecane was investigated with 100 % pure n-C12 samples.

6.4.2.1 Benzothiophene Conversion

Figure 6.7 reports the benzothiophene conversion using a mixture of 6 wt % BZT dissolved in n-dodecane. Benzothiophene conversion increases progressively with

reaction time in the 3 - 7 seconds range, reaching a maximum value of about 47 %, at the highest temperature and reaction time (450 °C and 7 seconds).

It is important to highlight these conversion values reported in Figure 6.7 include both the converted fraction in the gas phase and the converted benzothiophene as coke on catalyst. The conversion calculations are detailed in Appendix E.

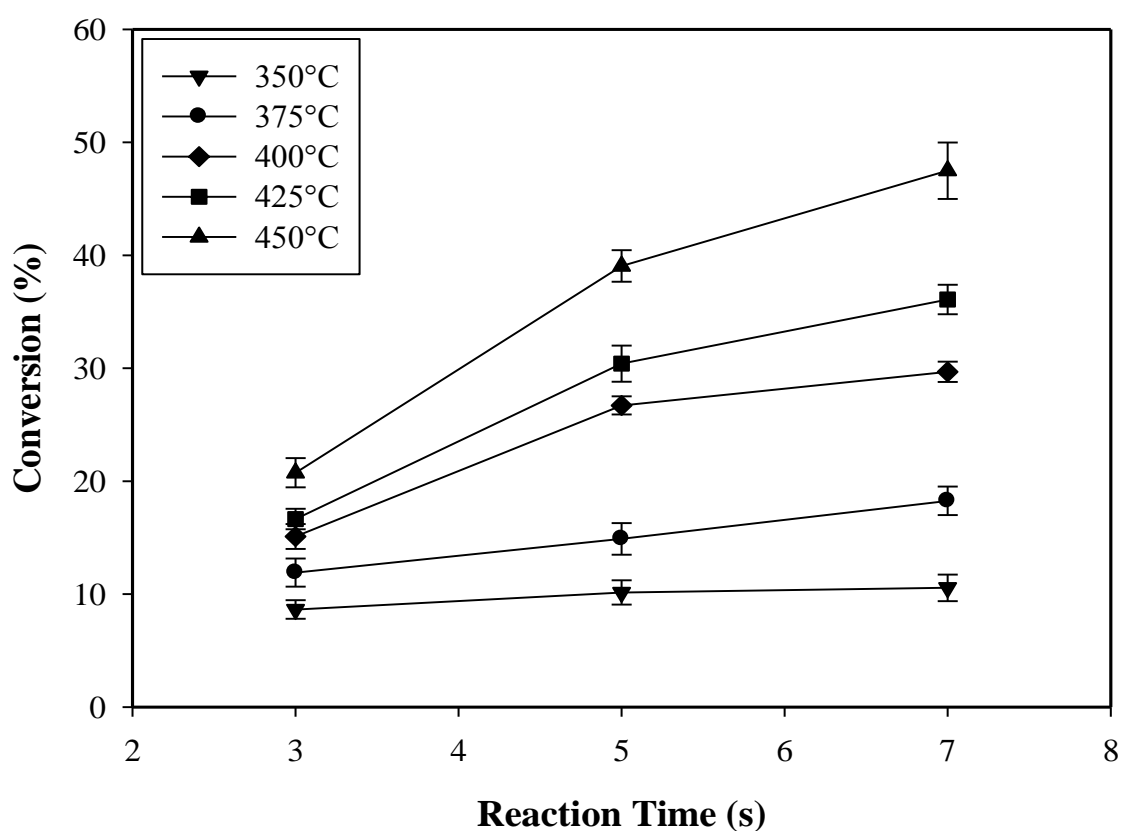


Figure 6.7. Total conversion of benzothiophene as a function of reaction time. Reaction conditions: $T = 350, 375, 400, 425, \text{ and } 450 \text{ }^{\circ}\text{C}$, $\text{cat/oil} = 5$. Feed composition is 6 wt % benzothiophene / 94 wt % n-dodecane. Error bars correspond to standard deviation of three repeats.

In more detailed, Figures 6.8 and 6.9 report benzothiophene conversion into gas phase products and as coke, respectively. It can be thus proven that the H-ZSM5 catalyst is able to selectively remove the sulfur containing compound (BZT) as coke with a very little fraction converted in the gas phase to alkyl-BZT.

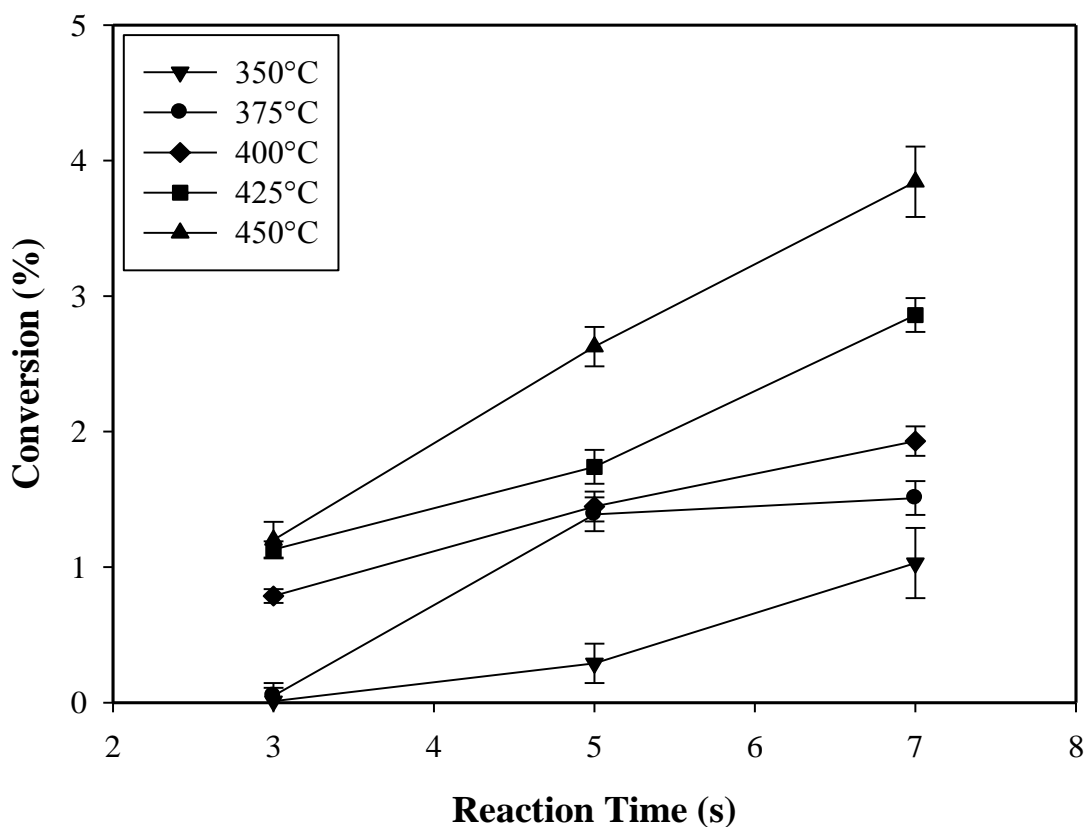


Figure 6.8. Conversion of benzothiophene in gas phase products as a function of reaction time. Reaction conditions: $T = 350, 375, 400, 425, \text{ and } 450 \text{ } ^\circ\text{C}$, $\text{cat/oil} = 5$. Feed composition is 6 wt % benzothiophene / 94 wt % n-dodecane. Error bars correspond to standard deviation of three repeats.

Furthermore, referring to the same Figures (6.8 and 6.9), it can be concluded that lower temperatures (350 °C and 375 °C) favor benzothiophene removal as coke with a

small fraction converted in the gas phase (less than 1.5 %). In addition, gas phase products from benzothiophene conversion at these lower temperatures and at a lower contact time (3 seconds) were found to be negligible (less than 0.05 % conversion).

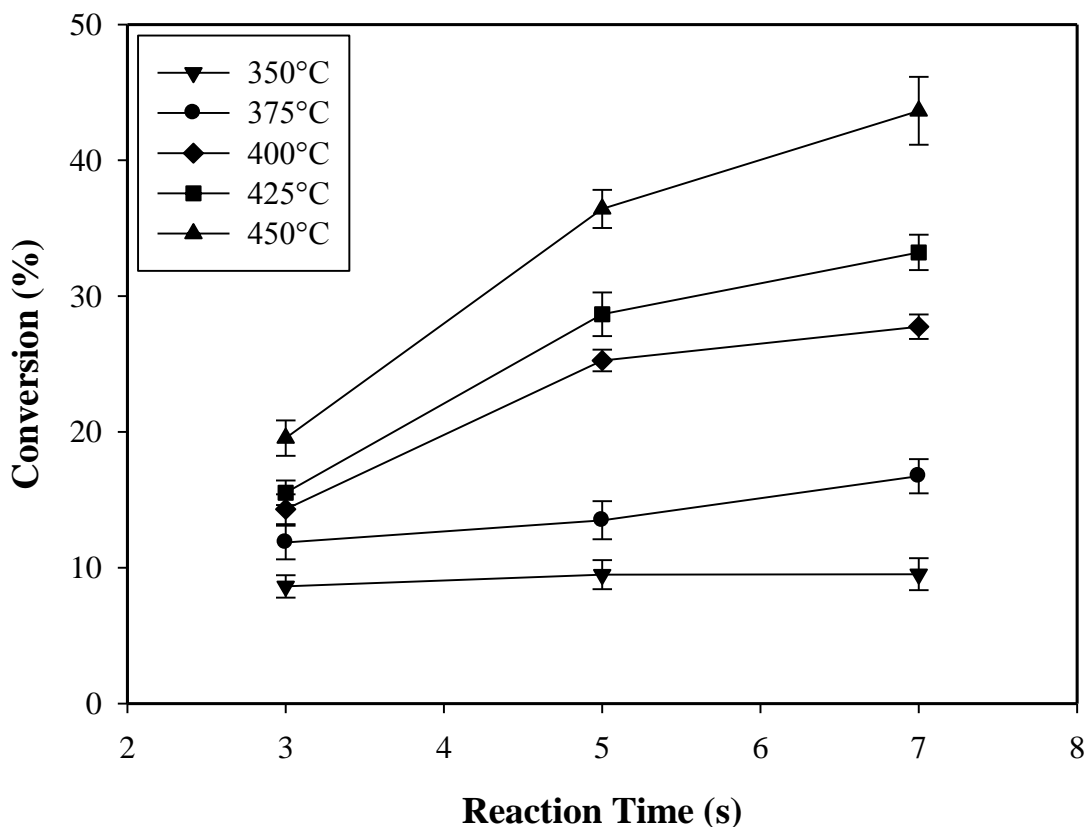


Figure 6.9. Conversion of benzothiophene as coke-on-catalyst as a function of reaction time. Reaction conditions: $T = 350, 375, 400, 425, \text{ and } 450 \text{ }^{\circ}\text{C}$, $\text{cat/oil} = 5$. Feed composition is 6 wt % benzothiophene/94 wt % n-dodecane. Error bars correspond to standard deviation of three repeats.

At higher temperatures (400 $^{\circ}\text{C}$ - 450 $^{\circ}\text{C}$) however, gas phase products from benzothiophene are increased. These gas phase products are mainly alkylated benzothiophenes ($\text{C}_1\text{-C}_3$ benzothiophenes). In all cases however, no H_2S gas was

detected. This result suggests that benzothiophene cracking is not visible under the studied reaction conditions.

Benzothiophene has a critical molecular diameter of 6 Å (Contreras et al., 2008) while compared to the 5-6 Å size of H-ZSM5 pores. In spite of this, benzothiophene can diffuse towards the H-ZSM5 active sites with some hindrance. Furthermore, at higher temperatures, zeolite pores can expand, facilitating the benzothiophene diffusional process. It is reported that the effective ZSM-5 catalytic pore size lies between 6.62 Å and 7.27 Å at 300 °C and can increase to 7.64 Å at 370 °C (Borm et al., 2010). This fact can explain the higher benzothiophene conversion at higher temperatures even if lower adsorptions are expected.

On the other hand, alkylated benzothiophenes exhibit larger molecular diameters than benzothiophene and therefore these species can experience increased diffusional constraints into the 5-6 Å H-ZSM5 pores. However, as discussed above, at higher temperatures, zeolite pores may expand allowing alkylated benzothiophene species to leave the zeolite framework. This can also explain the higher benzothiophene conversion into gas phase products observed at 400 °C - 450 °C when compared to 350 °C - 375 °C.

Finally, as will be reviewed in the upcoming sections, benzothiophene shows a higher selective conversion over n-dodecane than with this being true for all the cases considered in this research work.

6.4.2.2 Conversion of n-Dodecane

Figures 6.10 and 6.11, report the conversion of n-dodecane using a pure feed (100 wt % of C12) and a mixture (94 wt % of C12 with the balance being BZT), respectively. It can be noted that n-dodecane conversion increases progressively with temperature and reaction time in the 3 - 7 seconds range.

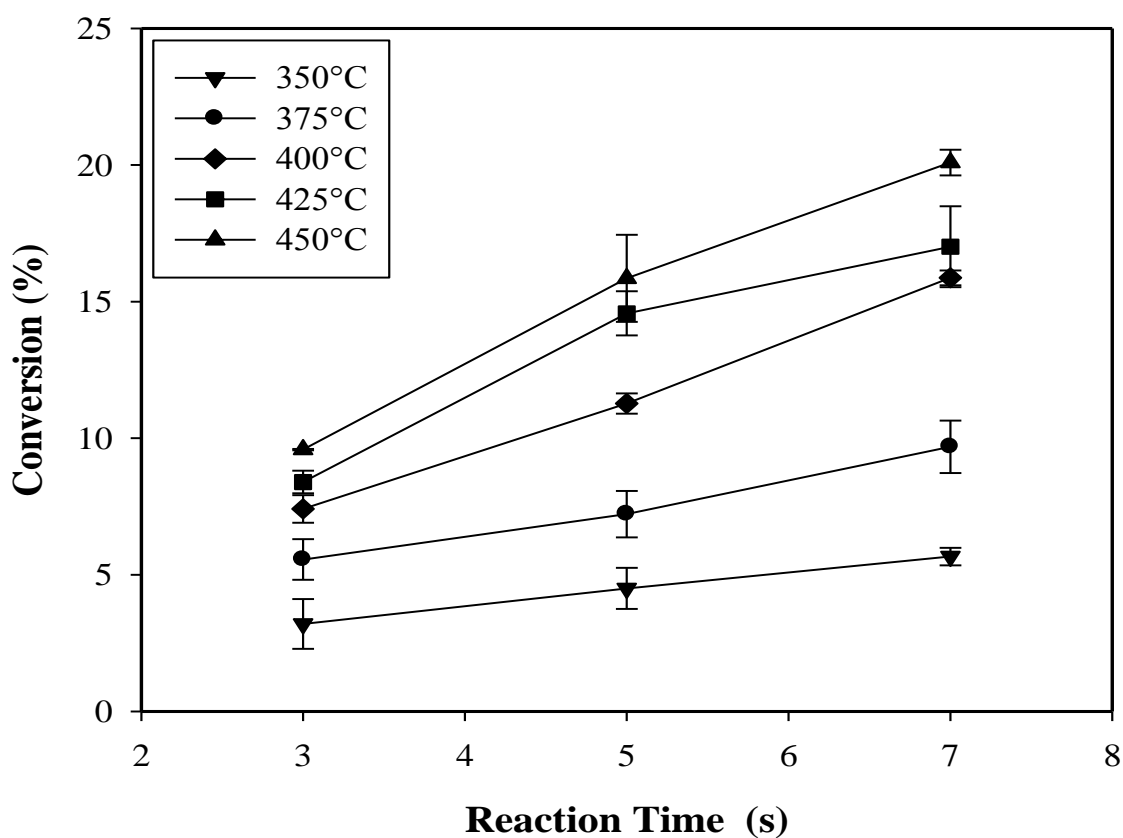


Figure 6.10. Conversion of n-dodecane as a function of reaction time. Reaction conditions: $T = 350, 375, 400, 425, \text{ and } 450 \text{ }^\circ\text{C}$, $\text{cat/oil} = 5$. Feed composition is 100 wt % n-dodecane. Error bars correspond to standard deviation for three repeats.

At the highest temperature and reaction time (450 °C and 7 seconds), n-dodecane conversion was about 20 % and 18 % in pure and mixture samples, respectively. In all cases, the pure samples displayed higher conversion of n-dodecane than the mixture samples.

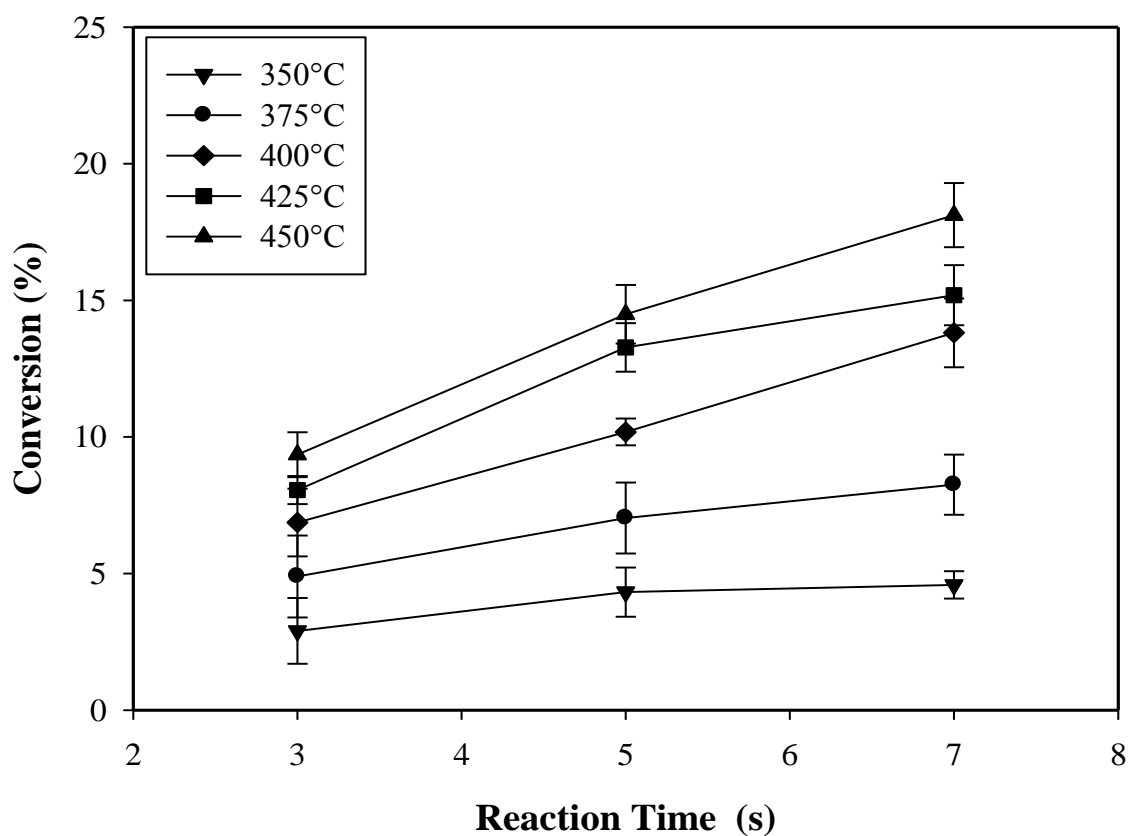


Figure 6.11. Conversion of n-dodecane as a function of reaction time. Reaction conditions: $T = 350, 375, 400, 425, \text{ and } 450$ °C, cat/oil = 5. Feed composition is 6 wt % benzothiophene / 94 wt % n-dodecane. Error bars correspond to standard deviation for three repeats.

The difference in n-dodecane conversion in the pure and mixture samples was more than 2 % at 400 - 450 °C and 7 seconds reaction time. However, at 350 - 375 °C and same reaction time the difference was only about 1 % or less. Moreover, lower reaction times (3 and 5 seconds) showed much less difference in n-dodecane conversion than 7 seconds at all temperature investigated.

Figure 6.11 shows that the presence of benzothiophene in the reactant feed has a detrimental effect on the conversion of n-dodecane. In other words, when present in the feed mixture, benzothiophene reduces n-dodecane cracking, competing effectively for the same acid sites with this being true, in spite of its larger molecular diameter. Benzothiophene has a 6 Å molecular diameter compared to 4.9 Å of n-dodecane. Thus, while in principle, n-dodecane is expected to diffuse faster than benzothiophene in the 5-6 Å H-ZSM5 zeolite pores, there are other factors that affect configurational diffusivity in H-ZSM 5 as considered in Chapter 4. This leads to benzothiophene with strong adsorption affinity to the H-ZSM5, occupying first adsorption sites under the unsteady state operation of the CREC Riser Simulator equivalent to a batch well mixed unit.

Furthermore, one can also notice that at higher temperatures and high contact times, there are even higher conversion differences between benzothiophene and n-dodecane (47 % versus 20 %). This can be justified given that at higher thermal levels, benzothiophene experiences less diffusional constraints as a consequence of the expected pores expansion of H-ZSM5 zeolite framework.

6.4.3 Products Distributions

The product distribution in the gas-phase was determined with the combined GC-MS system as described in Chapter 5. Selected chromatograms from catalytic runs of benzothiophene / n-dodecane mixtures are shown in Figures 6.12, 6.13, and 6.14.

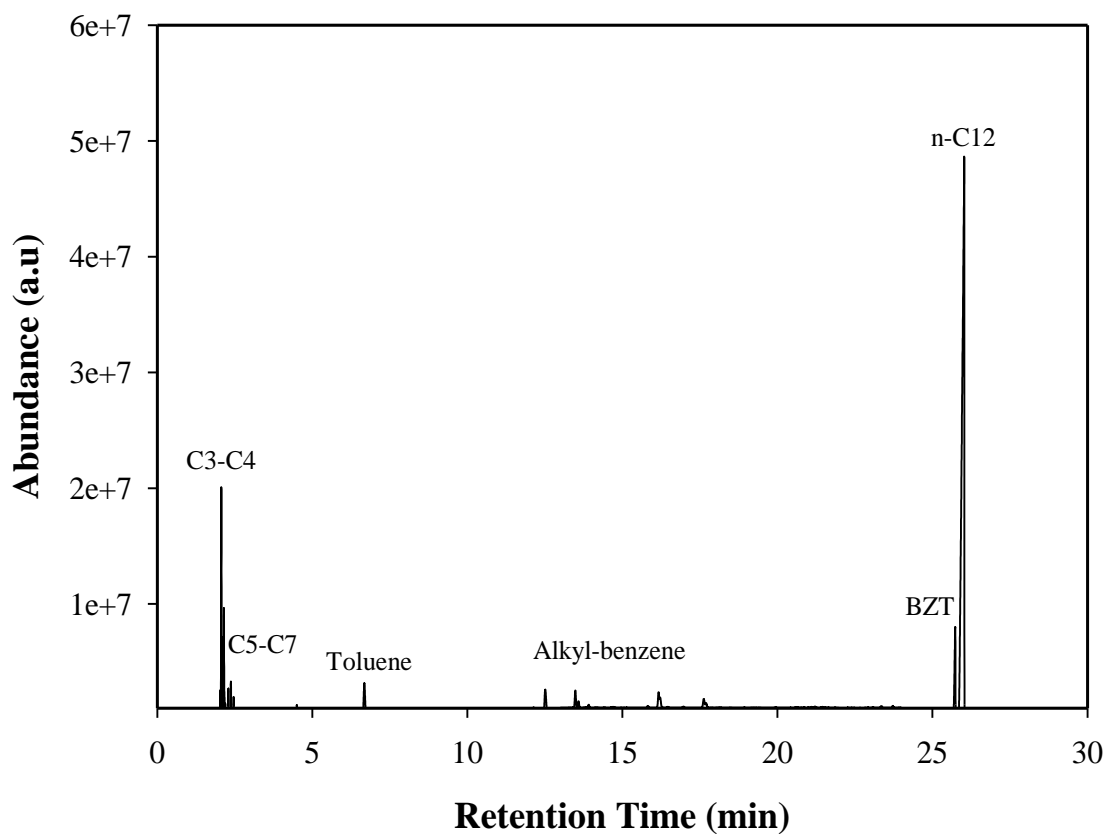


Figure 6.12. FID signal of hydrocarbon gas-phase products from 6 wt % benzothiophene / 94 wt % n-dodecane conversion and unconverted reactants at 450 °C, cat/oil = 5, and 7 seconds reaction time.

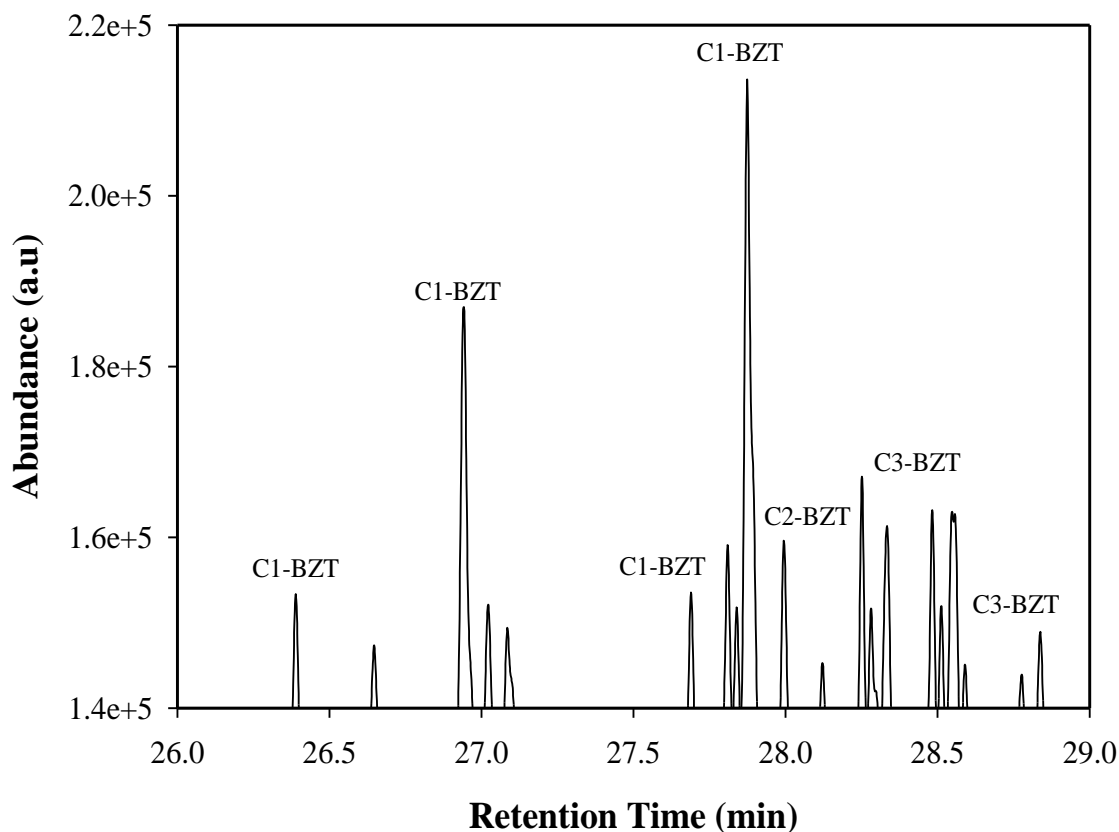


Figure 6.13. FID signal of sulfur gas phase products from 6 wt % benzothiophene / 94 wt % n-dodecane conversion at 450 °C, cat/oil = 5, and 7 seconds reaction time.

As stated before in Chapter 5 of this thesis, the FID has a response factor (RSF) of 1 for hydrocarbons species only. So, FID chromatogram peaks areas such these reported in Figure 6.12 are directly used to obtain weight fractions of hydrocarbons products. However, FID can only be used to quantify sulfur containing compounds if its RSF is known. Subsequently, one can relate the FID chromatogram peaks areas such these reported in Figure 6.13 to their weight fractions. The procedure used for this purpose is detailed in Appendix C.

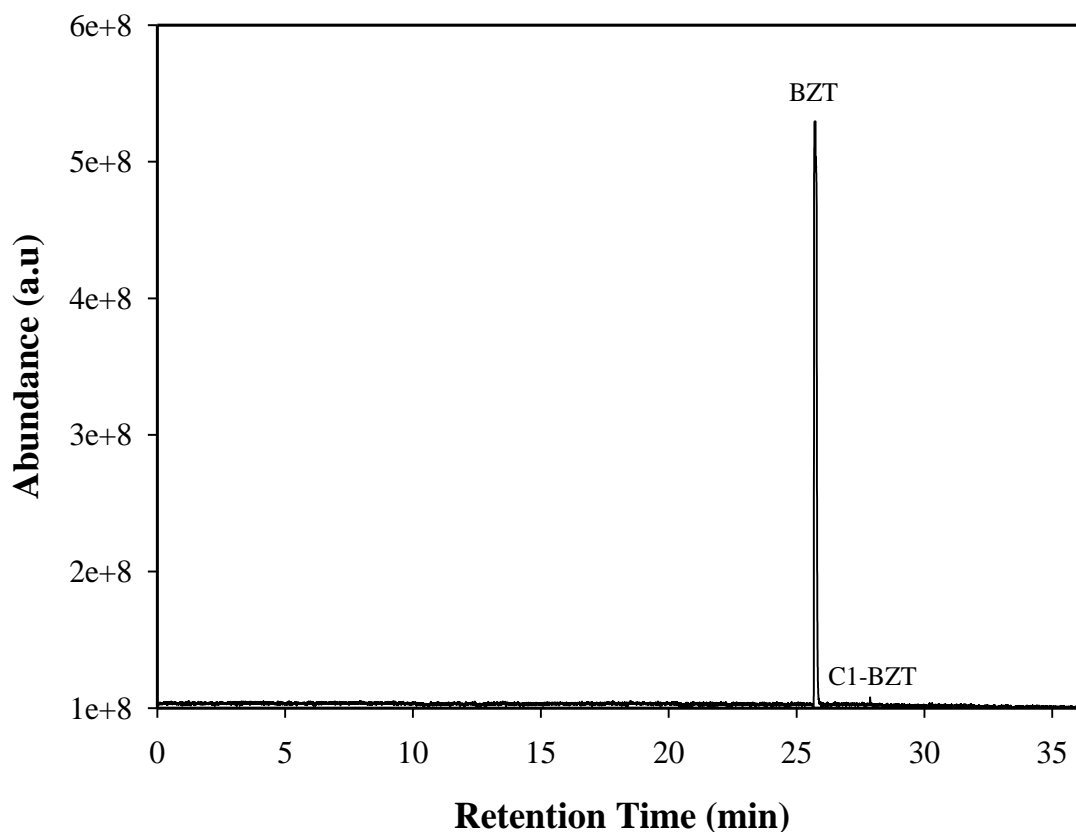


Figure 6.14. FPD signal showing unconverted benzothiophene and traces sulfur species from 6 wt % benzothiophene / 94 wt % n-dodecane conversion at 450 °C, cat/oil = 5, and 7 seconds reaction time.

In addition, the coke deposited on the catalyst was measured using the total organic carbon (TOC-V) analyzer while sulfur in coke was analyzed by ICP after acid digestion as explained in the experimental part of this dissertation. Table 6.4 reports a summary for products analysis from catalytic conversion of pure n-dodecane and a 6 wt% benzothiophene / n-dodecane mixture sample. It includes product distributions, coke on catalyst, sulfur in coke, and the total conversion.

Table 6.4. Hydrocarbon and sulfur products distribution from catalytic conversion of pure n-dodecane and benzothiophene / n-dodecane mixture at 450 °C, cat/oil = 5, and 7 seconds reaction time.

	Reactant mixture	
	100 wt % n-C12	n-C12 / 6 wt % BZT
Hydrocarbon Products (wt %)		
C ₃ - C ₄	14.21	13.33
C ₅ -C ₁₀ ^a	1.99	1.91
C ₅ -C ₇ ⁼	1.55	1.38
Aromatics ^b	2.35	1.86
unconverted n-C ₁₂	79.90	77.88
Sulfur Species (ppm)		
C1-benzothiophene		396
C2-benzothiophene		51
C3-benzothiophene		109
unconverted benzothiophene (wt %)		3.58
Coke (wt %) ^c	0.40	0.93
Sulfur (wt %) ^d		0.24
n-C12 conversion (%)	20.49	18.52
Benzothiophene conversion (%)		47.48

^a include paraffins and cycloparaffins

^b include benzene, toluene, and alkyl-benzenes

^c weight coke / weight catalyst

^d weight sulfur / weight catalyst

It can be observed in Table 6.4 that the converted n-dodecane produced mainly light hydrocarbons (C3 and C4). In addition, there is an appreciable amount of C5-C10 paraffins and cycloparaffins in the cracking products. Furthermore, the small fraction of olefins in the products can be attributed to the cracking mechanism over zeolites. It is well known that n-alkane cracking proceeds via a monomolecular or a bimolecular reaction pathway in which alkenes are formed as intermediates (Lugstein et al., 1997; Ono & Kanae, 1991; Guisnet & Magnoux, 1989). The low yield of aromatic hydrocarbons especially in the products of the mixture samples catalytic reaction is of significant importance. High production of aromatics is not in the advantage of the diesel fuel combustion quality. In other words, the cetane number of diesel fuel decreases as its aromatics content increases (Cooper & Donnis, 1996).

Concerning the catalytic conversion of benzothiophene, the sulfur products are mainly C1-C3 alkyl-benzothiophenes, and sulfur in coke. There was no H₂S found in the gas phase products. This result in turn points towards the difficulty of benzothiophene cracking under the studied conditions.

It is important to point out that the same product distribution patterns were observed under all reaction conditions studied (temperatures of 350 °C to 450 °C, and reaction times 3, 5, and 7s). However, at lower temperatures (350 °C - 375 °C) and low reaction time (3s), the quantification of sulfur products in gas phase alkyl-benzothiophenes was not easy due to their low concentrations.

More detailed product distributions from thermal and catalytic runs are reported in Appendix E (Tables E.1-E.7) of this dissertation.

6.5 Benzothiophene Adsorption Selectivity

In order to investigate the competitive conversion of benzothiophene and n-dodecane, a selectivity parameter according to (Jaimes & de Lasa, 2009) can be defined as follows:

$$S_{\text{BZT}} = \frac{X_{\text{BZT}}/W_{\text{BZT}}}{X_{\text{C12}}/W_{\text{C12}}} \quad (6.1)$$

where X_{BZT} and X_{C12} are the benzothiophene and n-dodecane conversions respectively based on W_{BZT} and W_{C12} , the corresponding weight fractions of benzothiophene and n-dodecane in the reactant mixtures.

At close initial reactant concentrations, a selectivity parameter of more than 1 indicates that benzothiophene conversion is higher than n-dodecane conversion. On the other hand, at relatively close conversions of both species, variations in the selectivity parameter are related to their initial concentrations (Jaimes & de Lasa, 2009).

The selectivity parameter lumps the combined effects of adsorption and reaction surpassing the value of 30 in all cases studied as in Figure 6.15. Given the significant differences in gas-phase concentrations between n-dodecane and benzothiophene, these results confirm that there is either a higher adsorption affinity of benzothiophene versus n-dodecane or alternatively a much higher intrinsic rate of benzothiophene desulfurization compared to n-dodecane cracking rate.

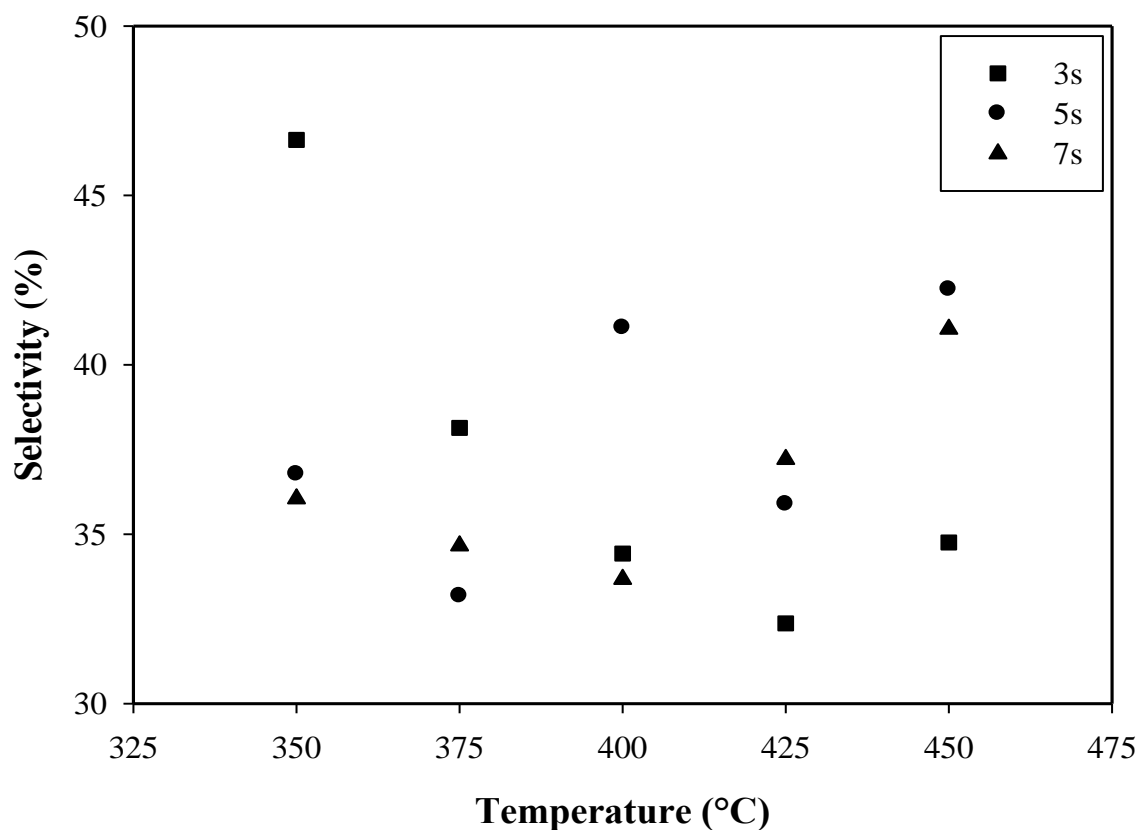


Figure 6.15. Selectivity of benzothiophene as a function of reaction time. Reaction conditions: $T = 350, 375, 400, 425,$ and 450 °C, $\text{cat/oil} = 5$. Feed composition is 6 wt % benzothiophene / 94 wt % n-dodecane.

6.6 Effect of Reactants Initial Concentrations on Catalytic Conversion

In order to explore the reaction order of the benzothiophene reaction, experiments with different initial benzothiophene concentrations (0.5, 2, 4, 6, 8 wt %) in n-dodecane were developed at 450 °C, $\text{cat/oil} = 5$, and 7 seconds reaction time. The results are shown in Figure 6.16.

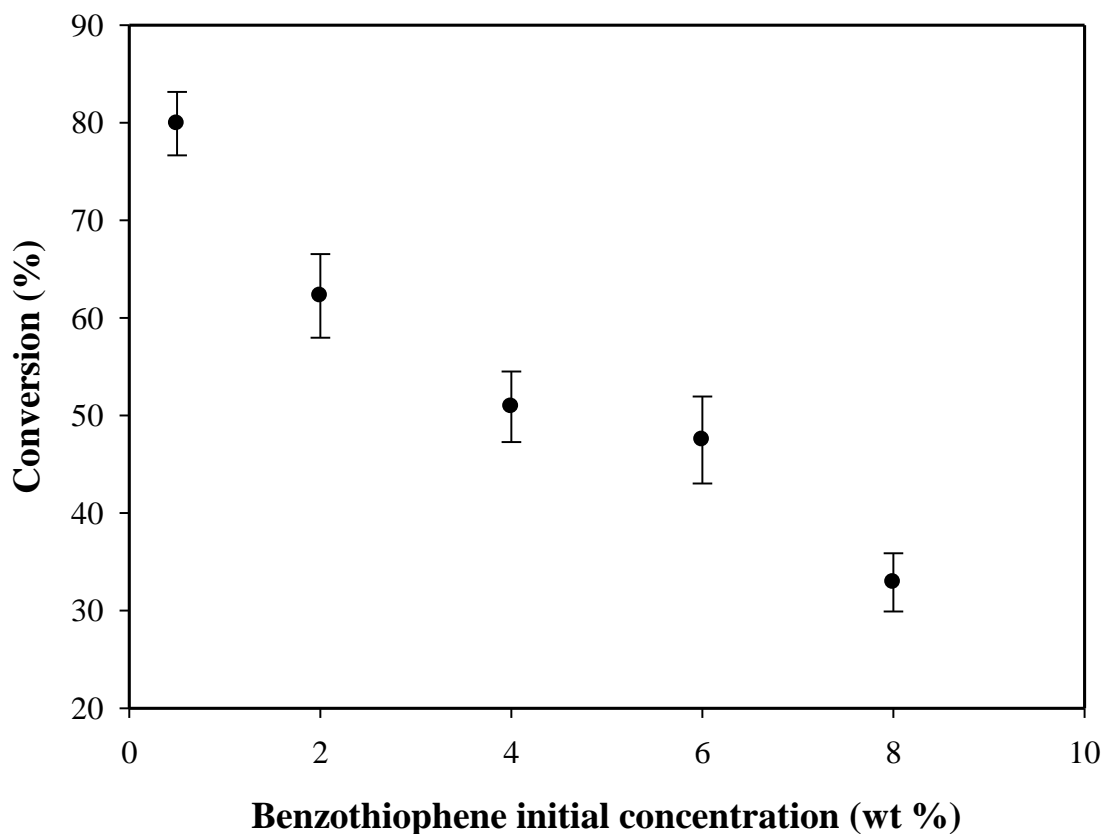


Figure 6.16. Benzothiophene total conversion versus benzothiophene initial concentration. Reaction conditions: $T = 450\text{ }^{\circ}\text{C}$, cat/oil = 5, and 7 seconds reaction time. Error bars correspond to standard deviation of three repeats.

It can be observed from Figure 6.16 that benzothiophene conversion decreases when increasing its initial concentration in the reactant mixture. In other word, there is a negative impact on the benzothiophene conversion when its initial concentration in the feed increases. This is a direct indication of a negative reaction order for benzothiophene conversion. This important experimental observation will be discussed in more detailed in the next Chapter of this dissertation (Chapter 7), when deriving the reaction rate expression for benzothiophene.

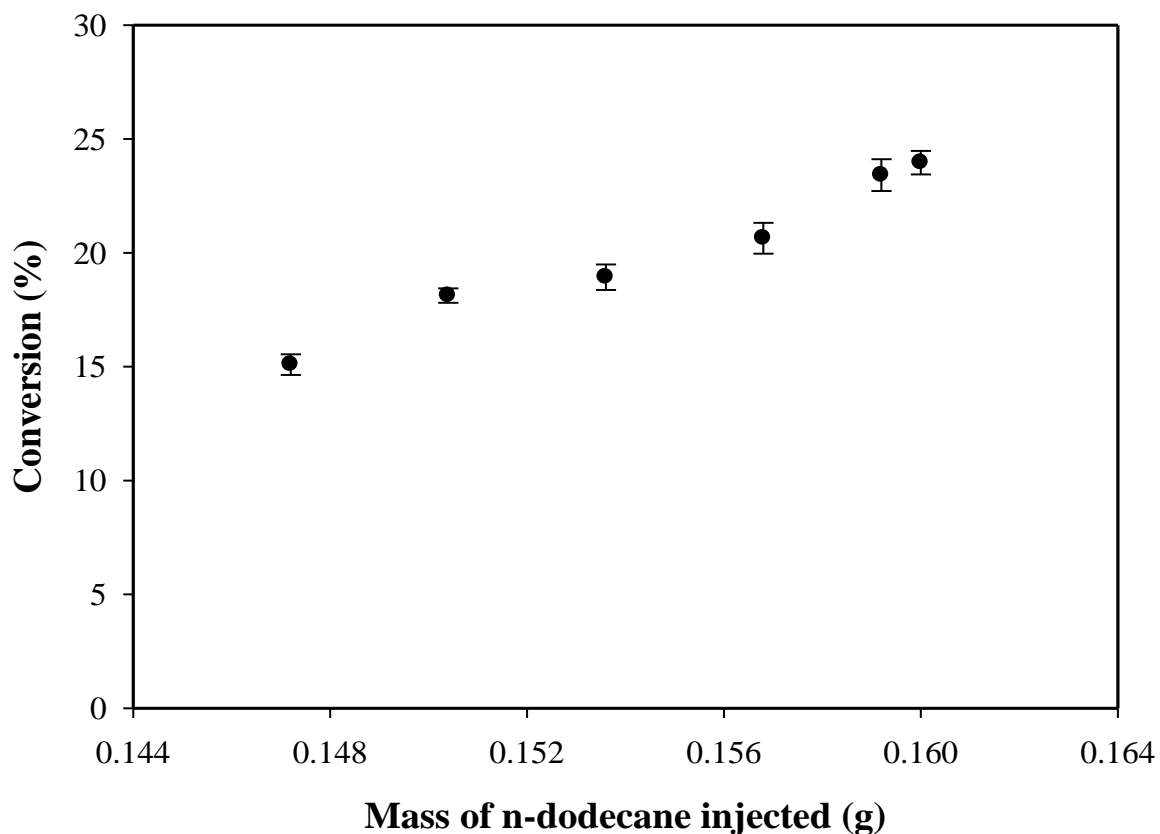


Figure 6.17. n-Dodecane conversion versus its mass injected in the Riser Simulator. Reaction conditions: $T = 450\text{ }^{\circ}\text{C}$, $\text{cat/oil} = 5$, and 7 seconds reaction time. Error bars correspond to standard deviation of three repeats.

In addition, Figure 6.17 reports the conversion of n-dodecane versus its weight injected in the Riser Simulator. Moreover, it can be considered that Figure 6.17 represents the conversion of n-dodecane in mixture samples with different initial benzothiophene concentrations. It is observed that n-dodecane conversion is slightly dependent on its initial concentration. The n-dodecane conversion deviates from the well known first order behavior of n-alkane cracking where the conversion is independent of initial concentration. This important result suggests that as benzothiophene increases in

the feed mixture, the n-dodecane cracking is suppressed. This can be thought of as benzothiophene occupying more active catalytic sites. In turn, this observation indicates the necessity of incorporating the benzothiophene initial concentration in the rate expression of n-dodecane as will be discussed in Chapter 7 of this thesis.

6.7 Conclusions

The following key points can be considered as the main conclusions from the current chapter:

- (a) The H-ZSM5 zeolite dispersed in the silica-alumina matrix of the present study is a suitable catalyst for the removal of sulfur containing species from light diesel.
- (b) The H-ZSM5 catalyst displays favorable structural, physical, chemical, and mechanical properties as shown using standard techniques for catalyst characterization namely: NH₃-TPD, pyridine FTIR, N₂-adsorption, XRD, PSD, and ABD.
- (c) The H-ZSM5 catalyst successfully removes sulfur containing species as demonstrated in the CREC Riser Simulator using benzothiophene and n-dodecane blends. It is also proven that both benzothiophene and n-dodecane conversions increase with reaction time and temperature.
- (d) The H-ZSM5 catalyst displays higher conversions using pure n-C12 than with mixtures comprised of 94 wt % n-C12 and 6 wt % BZT. These trends are especially important at higher temperatures.
- (e) The H-ZSM5 catalyst shows higher benzothiophene conversion than n-dodecane. These findings happen in spite of benzothiophene having a 6 Å critical molecular

diameter when compared to 4.9 Å diameter of n-dodecane. These results are attributed to both zeolite pores expansion and H-ZSM5 high sulfur containing species adsorption affinity. Benzothiophene is removed mainly as coke on catalyst with a small fraction being converted into alkyl-benzothiophene species (C1-C3 benzothiophene).

- (f) Benzothiophene displays high adsorption affinity as assessed by adsorption selectivity calculations.
- (g) The increase of benzothiophene initial concentration leads to a decrease in benzothiophene total conversion suggesting a negative reaction order. In addition, it shifts the known first order behaviour of n-alkanes cracking (in this case n-dodecane).

CHAPTER 7

KINETIC MODELING

7.1 Introduction

The present chapter reports the kinetic modeling of the catalytic conversion of benzothiophene conversion on the H-ZSM5 zeolite catalyst. The first section addresses the reaction mechanism of benzothiophene desulfurization using H-ZSM5 zeolite. Following this, the main assumptions of the proposed heterogeneous kinetic model are stated. After that, the system of partial differential equations that are used in the kinetic model are established. Finally, the results of the kinetic modeling including various kinetic constants, adsorption constants, and activation energies are reported and analyzed.

7.2 Benzothiophene Reaction Mechanism

Regarding benzothiophene reaction mechanism and based on the product distribution results as reported in Chapter 6 of this thesis, it can be stated that benzothiophene mainly undergoes alkylation reactions. In fact, alkyl-benzothiophene species present in the gas-phase products have a molecular diameter such that these species can diffuse out of the zeolite pores. However, alkyl-benzothiophene species with a larger alkyl groups are formed and trapped in the zeolite pore network due to their larger kinetic diameter (product shape selectivity). In addition, the benzothiophene reaction over H-ZSM5 zeolite may produce bulkier sulfur molecules species, trapped in zeolite cages and likely end up as coke on catalyst, via transalkylation reactions.

Gutiérrez-Alejandre et al. (2006) using FTIR showed that benzothiophene interacts with the hydroxyl group of acid zeolites namely, H-ZSM5 and H-MOR. Similar findings are reported by Jaimes & de Lasa (2009) converting thiophene on a H-ZSM5 zeolite based catalyst.

Hence, it is postulated that benzothiophene alkylation reaction over H-ZSM5 zeolite proceeds via benzothiophene protonation on a Brønsted acid site. Following this initial step, the resulting carbenium ion reacts with an olefin produced by the cracking of the co-reactant n-alkane (n-dodecane in this case). This reaction mechanism is shown in Figure 7.1.

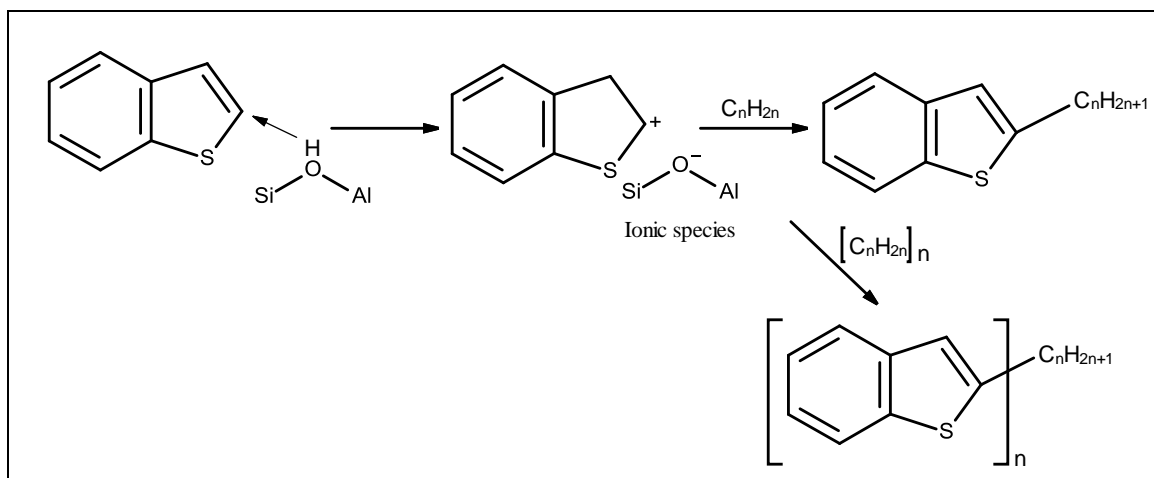


Figure 7.1. Benzothiophene alkylation mechanism over H-ZSM5 zeolite catalyst.

It is important to mention that the produced alkyl-benzothiophene isomerizes through an alkyl shift mechanism resulting in alkyl-benzothiophenes with alkyl groups placed in different positions in the benzothiophene structure (Richard et al., 2007; Valla et al., 2007). For instance, alkyl shift involving product species as shown in Figure 7.1 (2-alkylbenzothiophene) leads to 3, 5, and 7-alkylbenzothiophene.

7.3 Kinetic Model Development

An essential step in benzothiophene kinetic modeling is to identify the main product species. In addition, due to a large number of compounds involved, it is necessary to lump the compounds into groups according to their molecular characteristics and boiling point range. One should note that the more lumps a model includes, the more model parameters are involved and as a consequence more experimental data is needed. Generally, it is accepted that kinetic models with four or five lumps produce a satisfactory predictions (Valla et al., 2006).

Hence and for the purpose of the current research, the reaction system is simplified by lumping the product species into groups. Two lumps are defined for benzothiophene conversion: (a) SD (alkyl-benzothiophene in the light diesel boiling point range), (b) SC (sulfur which remains as coke on catalyst). The proposed network for benzothiophene conversion in the current study is shown in Figure 7.2.

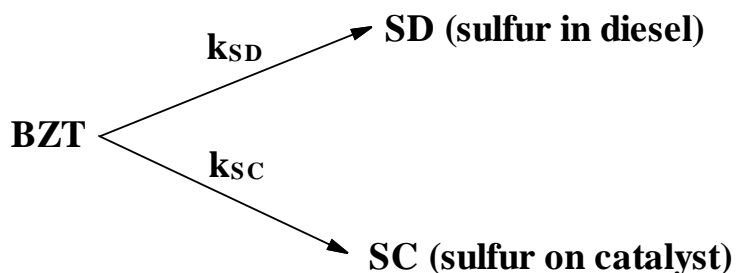


Figure 7.2. Proposed reaction network for benzothiophene conversion.

In addition, the proposed kinetic model involves n-dodecane conversion, the model compound used to represent the light diesel fraction. In the same way, the products observed for n-dodecane cracking are grouped as follows: (a) non-aromatic hydrocarbons

or HC which include paraffins, olefins, and cyclo-paraffins, (b) aromatic hydrocarbons or Ar which include benzene, toluene, and alkyl-benzenes.

The proposed network for n-dodecane conversion in the current study is shown in Figure 7.3. It is important to highlight that the coke formation on catalyst contributed by n-dodecane cracking is not considered in the proposed kinetic model. This is based on the experimental observation that n-dodecane conversion remains fairly constant for continuous seven runs without catalyst regeneration. These runs were performed at the most severe reaction conditions considered in the current research (450 °C reaction temperature and 7 seconds contact time).

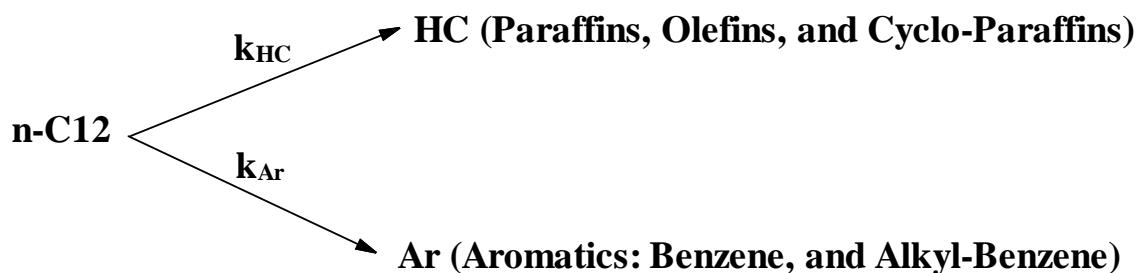


Figure 7.3. Proposed reaction network for n-dodecane cracking.

The selected reaction networks for benzothiophene and n-dodecane, along with the experimental data reported in Chapter 6, allows proposing a “parallel” heterogeneous kinetic model including all observable reactant and product species. Moreover, given the significant importance of selective sulfur species adsorption as discussed in Chapter 2 of this thesis (section 2.6), a Langmuir-Hinshelwood mechanism is considered for the kinetic model development. It is important to emphasize that this type of mechanism is found best to model the competitive adsorption of reactants and products. The main assumptions for the kinetic model are as follows:

1. The adsorption of benzothiophene is stronger than that of n-dodecane. This is based on the experimental observations as reported in Chapter 6 (Figure 6.15).
2. The surface chemical reaction is the rate limiting step and it is considered not to be affected by the reverse reaction step.
3. The formation of alkylated benzothiophene species in the diesel range (SD) is a result of the reaction of adsorbed benzothiophene with a short olefin produced by adsorbed n-dodecane cracking. Thus, the rate equation for the formation of SD can be written as:

$$r_{SD} = \frac{k_{SD} K_{BZT} C_{BZT} K_{C12} C_{C12}}{(1 + K_{BZT} C_{BZT} + K_{C12} C_{C12})^2} \quad (7.1)$$

where, r_{SD} is the reaction rate for sulfur species in diesel range with its rate constants k_{SD} , K_{BZT} is the adsorption constant of benzothiophene, K_{C12} is the adsorption constant of n-dodecane, and C_{BZT} is the concentration of benzothiophene while C_{C12} is the concentration of n-dodecane.

4. The formation of alkylated benzothiophene species as coke on catalyst (SC) is a result of the reaction of adsorbed benzothiophene with a larger olefin produced by adsorbed n-dodecane cracking. Therefore, the rate equation for the formation of SC can be written as:

$$r_{SC} = \frac{k_{SC} K_{BZT} C_{BZT} K_{C12} C_{C12}}{(1 + K_{BZT} C_{BZT} + K_{C12} C_{C12})^2} \quad (7.2)$$

where, r_{SC} is the reaction rate for sulfur species ending as coke on catalyst with its rate constants k_{SC} , K_{BZT} is the adsorption constant of benzothiophene, K_{C12} is the

adsorption constant of n-dodecane, and C_{BZT} is the concentration of benzothiophene while C_{C12} is the concentration of n-dodecane.

5. The non-aromatic hydrocarbons (HC), and the aromatic hydrocarbons (Ar) are produced by the cracking of adsorbed n-dodecane. As a result, the rate equations for HC and Ar can be written as:

$$r_{HC} = \frac{k_{HC}K_{C12}C_{C12}}{(1 + K_{BZT}C_{BZT} + K_{C12}C_{C12})} \quad (7.3)$$

$$r_{Ar} = \frac{k_{Ar}K_{C12}C_{C12}}{(1 + K_{BZT}C_{BZT} + K_{C12}C_{C12})} \quad (7.4)$$

where, r_{HC} is the reaction rate for non-aromatics hydrocarbon formation, r_{Ar} is the reaction rate for aromatics hydrocarbon formation, k_{HC} and k_{Ar} are the corresponding rates constants, K_{C12} is the adsorption constant of n-dodecane, K_{BZT} is the adsorption constant of benzothiophene, and C_{C12} is the concentration of n-dodecane while C_{BZT} is the concentration of benzothiophene. It is important to incorporate benzothiophene adsorption in the above two equations. This is in order to account for the observed effect of benzothiophene initial concentration on n-dodecane conversion experimentally (Chapter 6).

Based on all of the above mentioned steps and assumptions, the rate of consumption of benzothiophene can be summarized as in equation 7.5. The detailed derivation is shown in Appendix F of this thesis.

$$-r_{BZT} = \frac{(k_{SD} + k_{SC})K_{BZT}C_{BZT}K_{C12}C_{C12}}{(1 + K_{BZT}C_{BZT} + K_{C12}C_{C12})^2} \quad (7.5)$$

where, r_{BZT} is the reaction rate for benzothiophene reaction with its rate constants k_{SD} , k_{SC} , K_{BZT} is the adsorption constant of benzothiophene, K_{C12} is the adsorption constant of n-dodecane, and C_{BZT} is the concentration of benzothiophene while C_{C12} is the concentration of n-dodecane.

Assuming that n-dodecane has a low adsorption constant, at high concentration of benzothiophene $K_{BZT}C_{BZT} \gg 1 + K_{C12}C_{C12}$. Therefore, the reaction order becomes negative with respect to benzothiophene. This behaviour is shown experimentally in Chapter 6 (Figure 6.16) where benzothiophene conversion decreases as its initial concentration increases. In other words, the higher the concentration of benzothiophene the slower the reaction takes place. In this respect, it can be stated that benzothiophene inhibits the reaction.

Similarly, the rate equation for the cracking of n-dodecane can be written with a first order kinetics in the numerator as:

$$-r_{C12} = \frac{(k_{HC} + k_{Ar})K_{C12}C_{C12}}{(1 + K_{BZT}C_{BZT} + K_{C12}C_{C12})} \quad (7.6)$$

where, r_{C12} is reaction rate for n-dodecane cracking with its rate constants k_{HC} , k_{Ar} , K_{C12} is the adsorption constant of n-dodecane, K_{BZT} is the adsorption constant of benzothiophene, and C_{C12} is the concentration of n-dodecane while C_{BZT} is the concentration of benzothiophene.

It can be observed that when $K_{BZT}C_{BZT} \gg 1 + K_{C12}C_{C12}$ the reaction rate displays a negative order with respect to benzothiophene. This in turn can explain the experimental observation reported in Chapter 6 (Figure 6.17), where n-dodecane

conversion decreases slightly as the benzothiophene initial concentration increases. This fact can justify the benzothiophene adsorption influence on the cracking reaction rate equation.

7.4 System of Ordinary Differential Equations

In general, any kinetic model is comprised of several ordinary differential equations which are obtained by substituting the rate equation of each reactant and product into the reactor design equation. For the current research, the CREC Riser Simulator design equation is considered. This equation assumes a bench-scale isothermal well mixed batch reactor unit. The CREC Riser Simulator design equation can be written as:

$$r_i = \frac{V_R}{W_c} \frac{dC_i}{dt} \quad (7.7)$$

where r_i is the reaction rate of i , V_R is the Riser Simulator volume (cm^3), W_c is the weight of the catalyst loaded (0.8 gcat), C_i is the concentration of i (mol/cm^3), and t is time (s).

The concentration of any species (C_i) is related to its weight fraction (y_i) as:

$$C_i = \frac{y_i W_{hc}}{MW_i V_R} \quad (7.8)$$

where W_{hc} is the total mass of hydrocarbons injected in the Riser Simulator (g), MW_i is the molecular weight of i (g/mole), and V_R is the Riser Simulator volume (cm^3).

After substituting equation 7.8 into equation 7.7 and after the required algebraic steps, the CREC Riser Simulator design equation is obtained in terms of species weight fractions as:

$$\frac{dy_i}{dt} = \frac{W_c}{V_R} \left(\frac{MW_i V_R}{W_{hc}} \right) r_i \quad (7.9)$$

The next step is the substitution of all rate equations (7.1, 7.2, 7.3, 7.4, 7.5, and 7.6) into the Riser Simulator design equation 7.7 (in terms of concentration) and 7.9 (in terms of weight fraction), equivalent to a well mixed batch reactor where the catalyst is fluidized. As a result, one can obtain:

For Benzothiophene:

$$\frac{dC_{BZT}}{dt} = \frac{-W_c}{V_R} \frac{(k_{SD} + k_{SC})K_{BZT} C_{BZT} K_{C12} C_{C12}}{(1 + K_{BZT} C_{BZT} + K_{C12} C_{C12})^2} \quad (7.10)$$

Further considering,

$$C_{BZT} = \frac{y_{BZT} W_{hc}}{MW_{BZT} V_R} \quad (7.11)$$

and,

$$C_{C12} = \frac{y_{C12} W_{hc}}{MW_{C12} V_R} \quad (7.12)$$

One can establish the benzothiophene consumption rate equation in the CREC Riser Simulator in terms of species mass fractions as:

$$\frac{dy_{BZT}}{dt} = \frac{-W_C}{V_R} \frac{\beta K_{BZT} K_{C12}}{(1 + \alpha K_{BZT} y_{BZT} + \beta K_{C12} y_{C12})^2} (k_{SD} + k_{SC}) y_{BZT} y_{C12} \quad (7.13)$$

$$\text{where } \alpha = \frac{W_{hc}}{MW_{BZT} V_R} \quad \text{and} \quad \beta = \frac{W_{hc}}{MW_{C12} V_R}$$

For n-dodecane:

$$\frac{dC_{C12}}{dt} = \frac{-W_C}{V_R} \frac{(k_{HC} + k_{Ar}) K_{C12} C_{C12}}{(1 + K_{BZT} C_{BZT} + K_{C12} C_{C12})} \quad (7.14)$$

Similarly, the consumption of n-dodecane in the CREC Riser Simulator can be evaluated in terms of mass fractions using the following equation:

$$\frac{dy_{C12}}{dt} = \frac{-W_C}{V_R} \frac{K_{C12}}{(1 + \alpha K_{BZT} y_{BZT} + \beta K_{C12} y_{C12})} (k_{HC} + k_{Ar}) y_{C12} \quad (7.15)$$

For sulfur in diesel (SD):

$$\frac{dC_{SD}}{dt} = \frac{W_C}{V_R} \frac{k_{SD} K_{BZT} C_{BZT} K_{C12} C_{C12}}{(1 + K_{BZT} C_{BZT} + K_{C12} C_{C12})^2} \quad (7.16)$$

and

$$\frac{dy_{SD}}{dt} = \frac{W_C}{V_R} \frac{v_{SD} \beta K_{BZT} K_{C12}}{(1 + \alpha K_{BZT} y_{BZT} + \beta K_{C12} y_{C12})^2} k_{SD} y_{BZT} y_{C12} \quad (7.17)$$

$$\text{where } v_{SD} = \frac{MW_{SD}}{MW_{BZT}}$$

For sulfur in coke (SC):

$$\frac{dC_{SC}}{dt} = \frac{W_C}{V_R} \frac{k_{SC} K_{BZT} C_{BZT} K_{C12} C_{C12}}{(1 + K_{BZT} C_{BZT} + K_{C12} C_{C12})^2} \quad (7.18)$$

and

$$\frac{dy_{SC}}{dt} = \frac{W_C}{V_R} \frac{v_{SC} \beta K_{BZT} K_{C12}}{(1 + \alpha K_{BZT} y_{BZT} + \beta K_{C12} y_{C12})^2} k_{SC} y_{BZT} y_{C12} \quad (7.19)$$

$$\text{where } v_{SC} = \frac{MW_{SC}}{MW_{BZT}}$$

For non-aromatic hydrocarbons (HC):

$$\frac{dC_{HC}}{dt} = \frac{W_C}{V_R} \frac{k_{HC} K_{C12} C_{C12}}{(1 + K_{BZT} C_{BZT} + K_{C12} C_{C12})} \quad (7.20)$$

and

$$\frac{dy_{HC}}{dt} = \frac{W_C}{V_R} \frac{v_{HC} K_{C12}}{(1 + \alpha K_{BZT} y_{BZT} + \beta K_{C12} y_{C12})} k_{HC} y_{C12} \quad (7.21)$$

$$\text{where } v_{HC} = \frac{MW_{HC}}{MW_{C12}}$$

For aromatic hydrocarbons (Ar):

$$\frac{dC_{Ar}}{dt} = \frac{W_C}{V_R} \frac{k_{Ar} K_{C12} C_{C12}}{(1 + K_{BZT} C_{BZT} + K_{C12} C_{C12})} \quad (7.22)$$

and

$$\frac{dy_{Ar}}{dt} = \frac{W_C}{V_R} \frac{v_{Ar} K_{C12}}{(1 + \alpha K_{BZT} y_{BZT} + \beta K_{C12} y_{C12})} k_{Ar} y_{C12} \quad (7.23)$$

$$\text{where } v_{Ar} = \frac{MW_{Ar}}{MW_{C12}}$$

where MW_{SD} , MW_{SC} , MW_{HC} , and MW_{Ar} are the average molecular weights for sulfur in diesel species, sulfur in coke, non-aromatic hydrocarbons, and aromatic hydrocarbons respectively. These molecular weights were determined based on the yield and molecular weight of individual components formed within each class.

Furthermore, each kinetic constant k_i , can be postulated to change with reactor temperature T , following the Arrhenius type equation:

$$k_i = k_{i0} \exp\left(\frac{-E_i}{RT}\right) \quad (7.24)$$

where E_i represents the energy of activation, R is the universal gas constant, and k_{i0} is the pre-exponential factor.

In the same way and on the basis of adsorption thermodynamics, one can relate the adsorption constant K_i with the reaction temperature T , as:

$$K_i = K_{i0} \exp\left(\frac{-\Delta H_i}{RT}\right) \quad (7.25)$$

where ΔH_i is the heat of adsorption, and K_{i0} is the pre-exponential factor.

7.5 Kinetic Parameters Estimation

The derived rate equations, as can be noted from the previous section are highly non-linear with respect to their parameters. In particular, adsorption constants for benzothiophene and n-dodecane (K_{BZT} and K_{C12}) appear both in the numerator and the denominator of each equation.

Therefore, the estimation of kinetic parameters was developed applying non-linear least-squares fitting using MATLAB software. Two built-in available subroutines were used: LSQCURVEFIT for the minimization of the objective function and ODE113 for the numerical integration of differential equations.

The evaluation of model parameters was conducted using experimental data at different temperatures. The reaction rate constants were expressed using an Arrhenius type of temperature dependence as in equation 7.24 in order to take into account the temperature dependence of the experimental data. Based on these considerations, each rate constant (k_i) yields two parameters (k_{i0} and E_i).

The same principle is true for adsorption constants of both benzothiophene and n-dodecane using equation 7.25. Therefore, each adsorption constant (K_{BZT} or K_{C12}) will generate two parameters (K_{i0} and ΔH_i). These parameters k_{i0} , E_i , K_{i0} and ΔH_i are called intrinsic kinetic parameters.

The optimization criteria are that all rate and adsorption constants are positive, the activation energy for the reaction is positive, and the heat of adsorption (ΔH) is negative. This is to be consistent with physical principles (Kilanowski & Gates, 1980; Rahman et

al., 2010). The optimization criteria used was based on a minimum sum of squares (SSQ) defined as:

$$SSQ = \sqrt{\sum_{i=1}^N (x_{i, \text{exp}} - x_{i, \text{pred}})^2} \quad (7.26)$$

where $x_{i, \text{exp}}$ and $x_{i, \text{pred}}$ are the mass fraction percentages of component i obtained experimentally and predicted by the kinetic model, respectively.

Table 7.1. Intrinsic kinetics parameters of the proposed kinetic model along with their 95% confidence intervals and standard deviations.

Parameter	Value	95% CI	STD
k_{SDo}^a	2.52×10^2	51.231	27.78
E_{SD}^b	46.02	8.568	4.65
k_{SCo}^a	2.10×10^3	41.439	224.74
E_{SC}^b	39.81	10.719	5.81
k_{HCo}^a	1.65×10^2	32.343	17.54
E_{HC}^b	25.28	4.901	2.66
k_{Aro}^a	45.6	2.812×10^2	152.87
E_{Ar}^b	199.01	1.928×10^3	830.91
K_{BZTo}^c	2.63	3.21E-01	0.17
ΔH_{BZT}^b	-35.29	11.352	6.19
K_{Cl2o}^c	3.38×10^{-2}	8.6×10^{-2}	0.01
ΔH_{Cl2}^b	-20.13	26.060	0.11
DOF	258		

^a[cm³ gcat⁻¹ s⁻¹], ^b[KJ/mol], ^c[cm³ mol⁻¹], DOF = $m - p$, where m is the number of experimental data points, and p is the number of model parameters.

The values of the estimated 12 kinetic parameters along with their 95% confidence intervals (CI) are reported in Table 7.1. It can be noted that all estimated parameters display acceptable 95% CI. However, the estimation of kinetic parameters for the aromatics lump (k_{ArO} and E_{Ar}) involves high confidence intervals. This may be attributed to the error in the analysis of small quantities of aromatics in the product stream. This result is consistent with observations of others (Rahman et al., 2010). Moreover, the ability of establishing the 12 model parameters is consistent with the DOF (degree of freedom) in this analysis with 270 experimental data points considering three repeats for each run. As reported in Table 7.1, $DOF = 258$.

Furthermore, the obtained kinetic parameters are in a good agreement with the experimental observations of products distribution. For example, the energy of activation for sulfur in diesel range species (E_{SD}) is higher than that of sulfur on catalyst products (E_{SC}). This result indicates the favourable path for benzothiophene conversion of forming coke on catalyst which was previously indicated by higher conversion values in Chapter 6. However, the difference of only 7 KJ/mol may indicate that this path is significantly influenced by product shape selectivity. The same interpretation can be stated for a higher intrinsic kinetic constant for SC over SD.

In the same way, the activation energy of aromatics formation out of n-dodecane cracking (E_{Ar}) is much higher than that of non-aromatics hydrocarbons (Paraffins, olefins, and cyclo-paraffins). The opposite is true for the intrinsic kinetic constant where k_{HC} is much greater than k_{Ar} . These results in turn indicate that n-dodecane cracking reaction is unlikely produce aromatic species.

Moreover, the strong adsorption of benzothiophene over n-dodecane is quite apparent. This is true considering both the intrinsic adsorption constants and the energies of adsorption. In other words, the intrinsic adsorption constant for n-dodecane is very low when compared to the benzothiophene intrinsic adsorption constant. On the other hand, the intrinsic energy of adsorption ($-\Delta H$) for benzothiophene displays a lower value of -35 KJ/mol compared to -20 KJ/mol for n-dodecane.

The dependence of kinetic parameters on each other is examined through the cross-correlation coefficients matrix reported in Table 7.2. It can be noted that most of the cross-correlation coefficients are below 0.9 with only three of them exceeding this value. Hence, it can be concluded that the kinetic model as proposed is not over-parameterized.

Table 7.2. Cross-correlation coefficients for the kinetic model optimized parameters

	k_{SDo}	k_{SCo}	k_{HCo}	k_{Aro}	K_{BZTo}	K_{C12o}	E_{SD}	E_{SC}	E_{HC}	E_{Ar}	ΔH_{BZT}	ΔH_{C12}
k_{SDo}	1.000											
k_{SCo}	-0.638	1.000										
k_{HCo}	0.007	-0.006	1.000									
k_{Aro}	-0.045	-0.045	-0.045	1.000								
K_{BZTo}	0.283	0.283	0.290	-0.047	1.000							
K_{C12o}	-0.007	0.006	-0.914	0.045	-0.290	1.000						
E_{SD}	0.948	-0.641	-0.006	-0.036	-0.142	0.006	1.000					
E_{SC}	-0.027	0.645	-0.013	-0.036	-0.142	0.013	-0.713	1.000				
E_{HC}	0.037	-0.002	0.233	-0.036	-0.136	-0.236	0.010	0.070	1.000			
E_{Ar}	-0.290	-0.290	-0.292	0.158	-0.302	0.292	-0.231	-0.231	-0.233	1.000		
ΔH_{BZT}	0.292	0.292	0.298	-0.052	0.816	-0.298	-0.115	-0.115	-0.110	-0.329	1.000	
ΔH_{C12}	-0.037	0.002	-0.233	0.036	0.136	0.236	-0.010	-0.070	-0.954	0.233	0.110	1.000

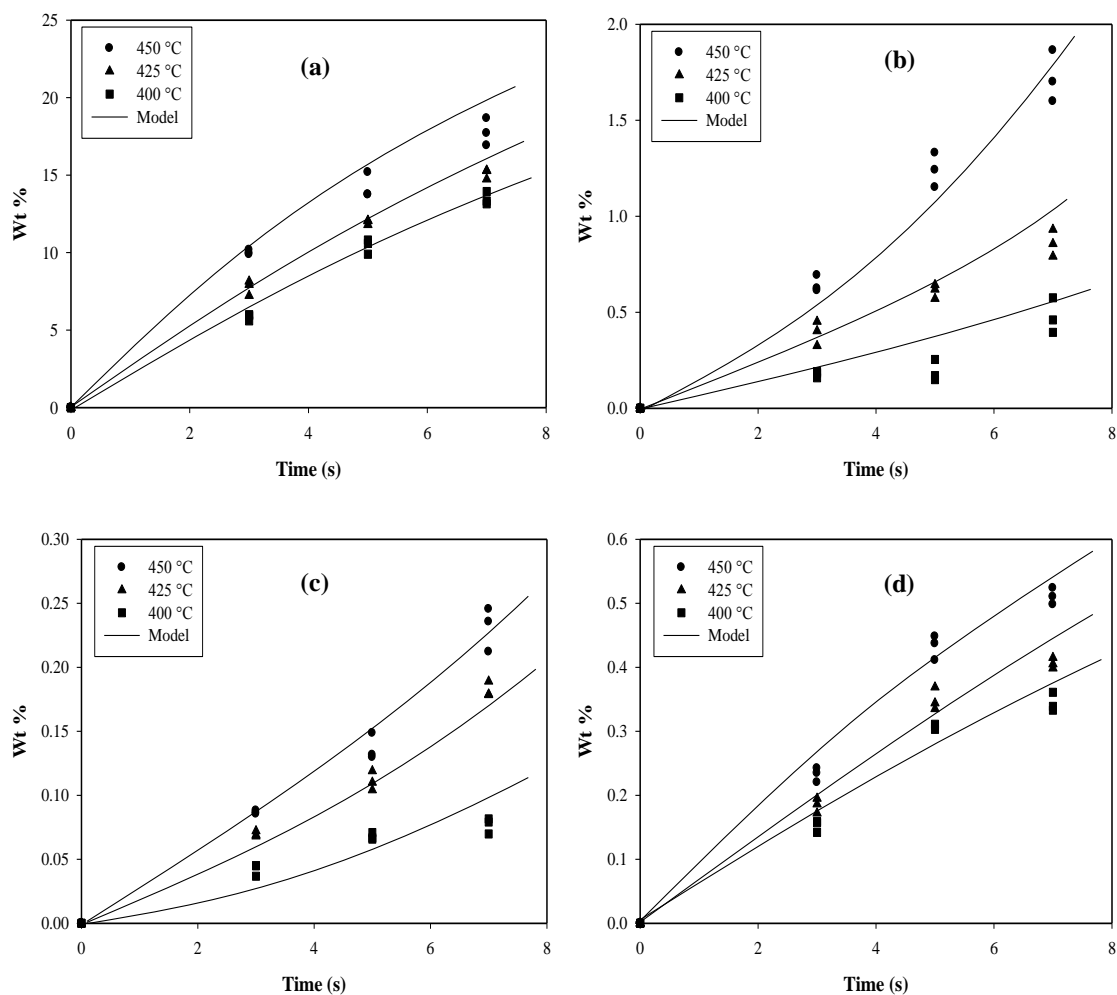


Figure 7.4. Comparison between experimental and predicted reaction products yields as a function of reaction time at different reaction temperatures with: (a) Hydrocarbons, (b) Aromatics, (c) Sulfur species in diesel range, and (d) Sulfur in coke.

In order to validate the obtained kinetic model, one has to establish a comparison between the experimental data and the results predicted by the model. With this aim, reaction products yields obtained experimentally are compared with the predicted yields by the model in the 400-450 °C range.

More specifically, Figure 7.4 reports a comparison of the mass fraction percentages obtained experimentally and those predicted by the model as a function of reaction time for the reaction products, HC, Ar, SD, and SC, respectively. As shown in this Figure, it can be concluded that the proposed kinetic model adequately fits the experimental data within the limits of the experimental errors.

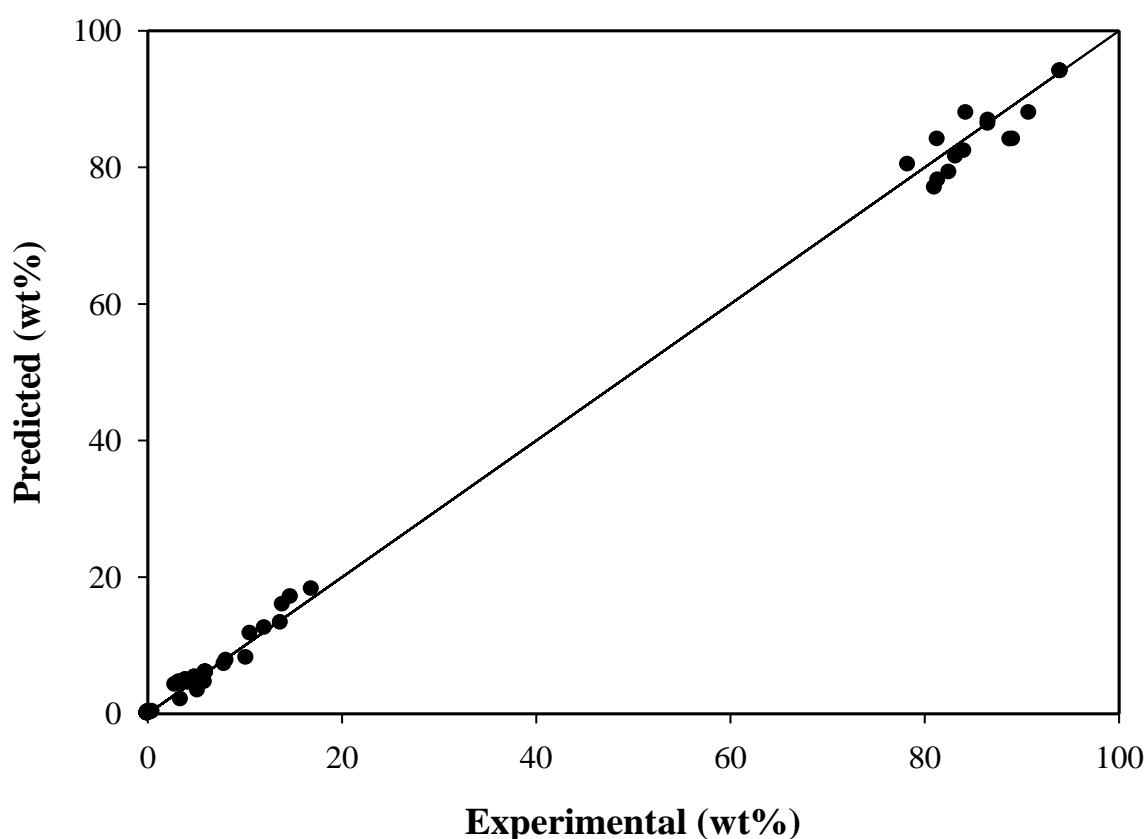


Figure 7.5. Parity plot showing the model prediction as opposed to the experimental data

Moreover, the parity plot of model predictions as compared to the experimental data is illustrated in Figure 7.5. It can also be inferred that the data is not clustered in horizontal or vertical lines. Horizontal bands may be the result of changes in the observed conversion caused by an independent variable which is not included in the kinetic model.

On the other hand, vertical lines are an indication of the kinetic model over-parameterization (El Solh et al., 2003; Moreira et al., 2012). The correlation coefficient R^2 was found to be 0.993. On this basis, it is concluded that the model predicts the experimental data appropriately.

7.6 Conclusions

The following conclusions can be drawn from this chapter of the current PhD dissertation:

1. Benzothiophene mainly undergoes alkylation reaction utilizing olefins available from the n-dodecane cracking.
2. Two separate species lumps networks are used for both benzothiophene and n-dodecane reactions. Sulfur species in the diesel range (SD) and sulfur in coke (SC) are involved in the benzothiophene conversion, while non-aromatic hydrocarbons (HC) and aromatic hydrocarbons (Ar) are involved in n-dodecane cracking.
3. A “parallel” heterogeneous kinetic model, based on Langmuir-Hinshelwood mechanism, for benzothiophene conversion over the H-ZSM5 catalyst is proposed. The model accounts for all reactants (benzothiophene and n-dodecane) and products (HC, Ar, SD, and SC).
4. The intrinsic kinetic parameters are estimated using non-linear least square fit of MATLAB and the experimental data at different reaction temperatures.
5. The estimated parameters justify well the observed product distribution, where benzothiophene is selectively removed as coke while n-dodecane cracking likely produces non-aromatic hydrocarbons.

6. The proposed kinetic model with a degree of freedom (DOF) of 258 is found adequately to describe the experimental data with a correlation coefficient R^2 of 0.993.

CHAPTER 8

CONCLUSIONS AND RECOMMENDATIONS

8.1 Conclusions

This dissertation provides a theoretical and experimental approach for the desulfurization of light diesel fraction hydrocarbons. It describes the catalyst preparation of H-ZSM5 zeolite pellets employing an inert silica-alumina matrix. In addition, standard characterization techniques are used to study physicochemical, mechanical, and structural properties of the prepared catalyst. The reactivity of the zeolite catalyst is established in the CREC Riser Simulator operating at mild temperatures (350-450°C) and pressure. n-Dodecane and Benzothiophene are selected to represent the light diesel hydrocarbons and its sulfur containing compounds, respectively. The experimental findings are reviewed using a basis of molecular dynamics (MD) calculations of self diffusivity of these species in ZSM-5 zeolites. Moreover, a heterogeneous kinetic model is developed using the experimental results and its kinetic parameters are estimated using non-linear regression analysis.

The main contributions and findings of the present research are as follows:

1. Fluidizable H-ZSM5 zeolite catalyst with an adequate APS and ABD is prepared using a matrix containing fused alumina as a filler, and silica sol as a binder. It is confirmed using SEM-EDX analysis that ion exchange is not necessary for final catalyst pellet.

2. TPD and FTIR analysis confirms the inert nature of the matrix used, with no observable acid sites. On the other hand, H-ZSM5 is the main source for catalyst acidity with presence of both types of acid sites Brønsted and Lewis. XRD results confirmed the high crystallinity of the ZSM-5 catalyst with no detectable amorphous phase. N₂ adsorption showed the low surface area property of the matrix with no micropores, and the high surface area of the H-ZSM5 zeolite.
3. The catalytic runs in the CREC Riser Simulator were valuable to demonstrate the high and selective conversion of benzothiophene compared to n-dodecane. In fact, benzothiophene is removed consistently in all runs as coke on catalyst with a negligible fraction being converted to alkyl-benzothiophene in gas phase products. On the other hand, there was a very modest cracking of n-dodecane yielding mainly lighter paraffins hydrocarbons and a small amount of aromatics. These findings point towards the product shape selective removal of benzothiophene in H-ZSM5 zeolite, with a final hydrocarbon product having an enhanced cetane number.
4. MD simulations showed higher self diffusion coefficients for benzothiophene over n-dodecane, with this being observed at all temperatures investigated. It is thus expected that in the case of benzothiophene/n-dodecane mixtures, benzothiophene will diffuse faster towards the zeolite active sites. This in turn minimizes the overall cracking of n-dodecane.
5. Experimental runs allowed postulating a “parallel” heterogeneous kinetic model involving lumped hydrocarbon species. This model also includes a Langmuir-Hinshelwood adsorption-reaction mechanism. It was found that the “parallel”

kinetic model adequately describes the CREC Riser Simulator experimental data for benzothiophene conversion over the H-ZSM5 catalyst. The estimated parameters for the kinetic model are found to be consistent with the experimental observations of products distribution. Furthermore, the determined kinetic parameters displayed low spans for the 95% confidence interval and low cross correlation coefficients.

8.2 Recommendations

The various findings of the present research point towards the viability of a downer/riser bed desulfurization process for light diesel fraction using a fluidizable H-ZSM5 zeolite catalyst. It is considered, however, that the following issues should be addressed:

Molecular Dynamics (MD) simulations:

1. The use of MD simulations was revealed to be an excellent tool for studying the diffusion of reactants in zeolite catalysts. However, it is recommended for future studies that species transport be coupled with adsorption phenomena in the MD simulations. This will allow for a better understanding of the various interactive effects between molecule transport and adsorption, as applicable to the desulfurization reaction using a HZSM-5 based catalyst.

Catalyst preparation and characterization:

1. The catalyst preparation method described in Chapter 5 was found to produce particles with adequate average particle size and density for fluidization in the

CREC Riser Simulator. However, it is recommended, for future research, to consider using a spray dryer for catalyst pelletization. This technique will allow obtaining particles with higher sphericity and very low attrition.

2. The acidity of H-ZSM5 is found to be the source of catalytic activity. As shown using FTIR analysis (Chapter 6), the zeolite catalyst samples used had both types of acid sites, namely Brønsted and Lewis acid sites. However, it was not a simple task to establish which chemical reaction was promoted or enhanced using a specific acid site type. As a result, it is recommended to use a customized H-ZSM5 zeolite with a single type of acid site (e.g. Brønsted acid sites) (Zheng, 2002). This will allow demonstrating the beneficial effect of Brønsted acid sites on the selective conversion of benzothiophene while reducing, at the same time, the influence of the non-selective Lewis acid sites.

Analytical system:

1. The analytical system for identifying and quantifying reaction products employed a Flame Photometric Detector (FPD) for benzothiophene and a Flame Ionization Detector (FID) for all the other sulfur containing species. This method may have some unavoidable inaccuracies, particularly when dealing with the low concentration of the gas phase sulfur containing species products. It is thus, suggested to consider the use of a Chemiluminescence detector (SCD) and/or a Pulsed Flame Photometric detector (PFPD), for future work, as recommended by others (Chambers & Duffy, 2003; Choudhary, 2007; Ma et al., 2005a; 2005b; Schulz et al., 1999).

Catalytic Runs:

1. Diesel fuel cuts used in oil refineries mainly contain paraffin compounds (more than 75%). Thus, there is a small fraction of aromatic compounds which has to be accounted for in light diesel desulfurization studies. Therefore, it is recommended that future reactivity runs be developed with a model of light diesel including a paraffin, an aromatic (e.g. naphthalene) and benzothiophene. This will allow investigating both the benzothiophene conversion and the interactive effects of aromatics and paraffins when being co-fed to the CREC Riser Simulator.
2. The desulfurization of diesel fuel cuts used in refineries is the final viability test of the proposed desulfurization technology. It is thus, recommended to extend the current research using refinery light diesel feeds doped with various amounts of benzothiophene levels.

REFERENCES

- Adapa, S., (2008), Removal of model sulphur compounds from hydrocarbon fractions by selective adsorption, PhD thesis, University of Kaiserslautern, Germany.
- Ahmed, K. W., (2011), Hydrodesulfurization of benzothiophene and dibenzothiophene over phosphorus modified CoMo/Al₂O₃, MSc. thesis, King Fahd University of Petroleum and Minerals, Dhahran, Saudi Arabia.
- Ainscough, A., Dollimore, D., (1987), Adsorption capacity of molecular sieve type carbons, *Langmuir*, 3, 708–713.
- Al-Baghli, N., Al-Khattaf, S., (2005), Catalytic cracking of a mixture of dodecane and 1,3,5 tri-isopropyl-benzene over USY and ZSM-5 zeolites based catalysts, *Studies in Surface Science and Catalysis*, 158, 1661–1668.
- Al-Khattaf, S., (2001), Diffusion and reaction of hydrocarbons in FCC catalysts, PhD thesis, University of Western Ontario, London, Canada.
- Al-malki, A., (2004), Desulfurization of gasoline and diesel fuels using non-hydrogen consuming techniques, MSc. thesis, King Fahd University of Petroleum and Minerals, Dhahran, Saudi Arabia.
- Ali, M., Almalki, A., Elali, B., Martinie, G., Siddiqui, M., (2006), Deep desulfurization of gasoline and diesel fuels using non-hydrogen consuming techniques, *Fuel*, 85, 1354–1363.
- Auerbach, S. M., Carrado, K. A., Dutta, P. K., (2003), *Handbook of zeolite science and technology*, Marcel Dekker Inc., New York.
- Babich, I. V, Moulijn, J. A., (2003), Science and technology of novel processes for deep desulfurization of oil refinery streams: a review, *Fuel*, 82, 607–631.
- Bhandari, V., Hyunko, C., Geunpark, J., Han, S., Cho, S., Kim, J., (2006), Desulfurization of diesel using ion-exchanged zeolites, *Chemical Engineering Science*, 61, 2599–2608.
- Bhide, S. Y., Yashonath, S., (1999), Dependence of the self-diffusion coefficient on the sorbate concentration: A two-dimensional lattice gas model with and without confinement, *The Journal of Chemical Physics*, 111, 1658-1668.
- Bogdanov, B., Georgiev, D., Angelova, K., Hristov, Y., (2009), Synthetic zeolites and their industrial and environmental applications, *International Science Conference*, Bulgaria.

Boita, T., Moreau, M., Richard, F., Pérot, G., (2006), Transformation of thiophenic compounds over acidic zeolites, *Applied Catalysis A: General*, 305, 90–101.

Borm, R. Van, Aerts, A., Reyniers, M.-F., Martens, J. A., Marin, G. B., (2010), Catalytic cracking of 2, 2, 4-trimethylpentane on FAU, MFI, and bimodal porous materials: influence of acid properties and pore topology, *Industrial & Engineering Chemistry Research*, 49, 6815–6823.

Brunauer, S., Deming, L. S., Deming, W. S., Teller, E., (1940), On a theory of the van der waals adsorption of gases, *Journal of American Chemical Society*, 62, 1723–1732.

Brunet, S., Mey, D., Perot, G., Bouchy, C., Diehl, F., (2005), On the hydrodesulfurization of FCC gasoline: a review, *Applied Catalysis A: General*, 278, 143–172.

Bunte, S. W., Sun, H., (2000), Molecular modeling of energetic materials: The parameterization and validation of nitrate esters in the COMPASS Force Field, *The Journal of Physical Chemistry B*, 104, 2477–2489.

Campos-Martin, J. M., Capel-Sanchez, M. C., Fierro, J. L. G., (2004), Highly efficient deep desulfurization of fuels by chemical oxidation, *Green Chemistry*, 6, 557–562.

Catlow, C., Freeman, C. M., Vessal, B., Leslie, M., (1991), Molecular dynamics studies of hydrocarbon diffusion in zeolites, *Journal of Chemical Society Faraday Transactions*, 87, 1947–1950.

Chambers, L., Duffy, M. L., (2003), Determination of total and speciated sulfur content in petrochemical samples using a pulsed flame photometric detector, *Journal of Chromatographic Science*, 41, 528–534.

Cheng, L., Yang, R., (1994), Improved Horvath-Kawazoe equations including spherical pore models for calculating micropore size distribution, *Chemical Engineering Science*, 49, 2599–2609.

Chester, A. W., Derouane (Eds.), E. G., (2009), *Zeolite characterization and catalysis: A tutorial*, fifth ed., Springer, New York.

Choudhary, T. V., (2007), Structure–Reactivity–Mechanistic considerations in heavy oil desulfurization, *Industrial & Engineering Chemistry Research*, 46, 8363–8370.

Contreras, R., Cuevasgarcia, R., Ramirez, J., Ruizazuara, L., Gutierrezalejandro, a, Puentelee, I., Castillovillalon, P., (2008), Transformation of thiophene, benzothiophene and dibenzothiophene over Pt/HMFI, Pt/HMOR and Pt/HFAU: Effect of reactant molecular dimensions and zeolite pore diameter over catalyst activity, *Catalysis Today*, 130, 320–326.

Cooper, B. H., Donnis, B. B. L., (1996), Aromatic saturation of distillates : an overview, *Applied Catalysis A: General*, 137, 203–223.

Cullity, B. D., (1978), *Elements of X-ray diffraction*, second ed., Addison-Wesley Publishing Company Inc., USA.

Daly, F. P., (1978), Hydrodesulfurization of benzothiophene over Co-Mo/Al₂O₃ catalyst, *Journal of Catalysis*, 51, 221–228.

de Lasa, H. I., Hernandez Enriquez, R., Tonetto, G., (2006), Catalytic desulfurization of gasoline via dehydrosulfidation, *Industrial & Engineering Chemistry Research*, 45, 1291–1299.

de Lasa, H. I., (1992), Riser simulator, U.S. Patent # 5 102 628.

Demontis, P., Suffritti, G. B., (2009), A comment on the flexibility of framework in molecular dynamics simulations of zeolites, *Microporous and Mesoporous Materials*, 125, 160–168.

Dietz, W. A., (1967), Response factors for gas chromatographic analyses, *Journal of Chromatographic Science*, 5, 68–71.

Dumont, D., Bougeard, D., (1995), A molecular dynamics study of hydrocarbons adsorbed in silicalite, *Zeolites*, 15, 650–655.

Dupuy, B., Laforge, S., Bachmann, C., Magnoux, P., Richard, F., (2012), Desulfurization of model FCC feedstocks by alkylation: Transformation of thiophenic compounds in presence of 2-methyl-1-pentene over acidic zeolites, *Journal of Molecular Catalysis A: Chemical*, 363-364, 273–282.

El Solh, T., Jarosch, K., de Lasa, H., (2003), Catalytic dry reforming of methane in a CREC Riser Simulator kinetic modeling and model discrimination, *Industrial & Engineering Chemistry Research*, 42, 2507–2515.

Fahim, M., Al-sahhaf, T., Elkilani, A., (2010), *Fundamentals of petroleum refining*, first ed., Elsevier B.V., Oxford.

Flanigen, E. M., Bennett, J. M., Grose, R. W., Cohen, J. P., Paton, R. L., Kirchner, R. M., Smith, J. V., (1978), Silicalite, a new hydrophobic crystalline silica molecular sieve, *Nature*, 271, 512–516.

Gary, J. H., Handwerk, G. E., (2001), *Petroleum refining technology and economics*, fourth ed., Marcel Dekker, Inc., New York.

Gauw, F. J. M., (2002), *Kinetic studies on alkane hydroisomerization over solid acid catalysts*, Technische Universiteit, Eindhoven, Netherlands.

- Geldart, D., (1973), Types of gas fluidization, *Powder Technology*, 7, 285–292.
- Gianetto, A., (1993), Novel cracking catalyst for reformulated gasoline, PhD thesis, University of Western Ontario, London, Canada.
- Gonzalez, L. A., Kracke, P., Green, W. H., Tester, J. W., Shafer, L. M., Timko, M. T., (2012), Oxidative desulfurization of middle-distillate fuels using activated carbon and power ultrasound, *Energy & Fuels*, 26, 5164–5176.
- Govind, N., Andzelm, J., Reindel, K., Fitzgerald, G., (2002), Zeolite-catalyzed hydrocarbon formation from methanol: density functional simulations, *International Journal of Molecular Sciences*, 3, 423–434.
- Guisnet, M., Magnoux, P., (1989), Coking and deactivation of zeolites influence of the pore structure, *Applied Catalysis*, 54, 1–27.
- Gutiérrez-Alejandre, A., Larrubia, M. A., Ramirez, J., Busca, G., (2006), FT-IR evidence of the interaction of benzothiophene with the hydroxyl groups of H-MFI and H-MOR zeolites, *Vibrational Spectroscopy*, 41, 42–47.
- Hagen, J., (2006), *Industrial catalysis: A practical approach*, second ed., Wiley-Vch., New York.
- Hernandez, E., Catlow, C., (1995), Molecular dynamics simulations of n-butane and n-hexane diffusion in silicalite, *Proceedings of the Royal Society A: Mathematical, Physical and Engineering Sciences*, 448, 143–160.
- Hernandez Enriquez, R., (2003), Catalytic de-hydrosulfidation of gasoline, MSc. thesis, University of Western Ontario, London, Canada.
- Ho, T. C., Sobel, J. E., (1991), Kinetics of dibenzothiophene hydrodesulfurization, *Journal of Catalysis*, 128, 581–584.
- Hollander, M. A., (2000), Catalytic cracking in a microriser: The different time scales of cracking and coke deposition, PhD thesis, Technische Universiteit Delft, Netherlands.
- Horvath, G., Kawazoe, K., (1983), Method for the calculation of the effective pore size distribution in molecular sieve carbon, *Journal of chemical Engineering Japan*, 16, 470–475.
- Hussain, I., Titiloye, J., (2005), Molecular dynamics simulations of the adsorption and diffusion behavior of pure and mixed alkanes in silicalite, *Microporous and Mesoporous Materials*, 85, 143–156.

Jaimes, L., (2009), Thiophene conversion under mild conditions over a ZSM-5 catalyst, A mechanistic, thermodynamic and kinetic approach, PhD thesis, University of Western Ontario, London, Canada.

Jaimes, L., Badillo, M., de Lasa, H., (2011), FCC gasoline desulfurization using a ZSM-5 catalyst Interactive effects of sulfur containing species and gasoline components, *Fuel*, 90, 2016–2025.

Jaimes, L., de Lasa, H. I., (2009), Catalytic conversion of thiophene under mild conditions over a ZSM-5 catalyst. A kinetic model, *Industrial & Engineering Chemistry Research*, 48, 7505–7516.

Jaimes, L., Ferreira, M., de Lasa, H. I., (2009), Thiophene conversion under mild conditions over a ZSM-5 catalyst, *Chemical Engineering Science*, 64, 2539–2561.

Jaimes, L., Ferreira, M., de Lasa, H. I., Tonetto, G., (2008), Desulfurization of FCC gasoline : novel catalytic processes with zeolites, *International Journal of Chemical Reactor Engineering*, 6, 1–66.

Jia, W., Murad, S., (2005), Separation of gas mixtures using a range of zeolite membranes : A molecular-dynamics study, *The Journal of Chemical Physics*, 122, 1–11.

Jianfen, F., de Graaf, B., Xiao, H. M., Njo, S. L., (1999), Molecular dynamics simulation of ethene diffusion in MFI and H[Al]ZSM-5, *Journal of Molecular Structure: THEOCHEM*, 492, 133–142.

Jiang, M., Ng, F., (2006), Adsorption of benzothiophene on Y zeolites investigated by infrared spectroscopy and flow calorimetry, *Catalysis Today*, 116, 530–536.

Jimenez-Cruz, F., Laredo, G. C., (2004), Molecular size evaluation of linear and branched paraffins from the gasoline pool by DFT quantum chemical calculations, *Fuel*, 83, 2183–2188.

Jobic, H., (2000), Diffusion of linear and branched alkanes in ZSM-5. A quasi-elastic neutron scattering study, *Journal of Molecular Catalysis A: Chemical*, 158, 135–142.

Jobic, H., Schmidt, W., Krause, C. B., Kärger, J., (2006), PFG NMR and QENS diffusion study of n-alkane homologues in MFI-type zeolites, *Microporous and Mesoporous Materials*, 90, 299–306.

Jobic, H., Theodorou, D. N., (2006), Diffusion of long n-alkanes in silicalite. A comparison between neutron scattering experiments and hierarchical simulation results, *The journal of Physical Chemistry B*, 110, 1964–1967.

Jobic, H., Theodorou, D. N., (2007), Quasi-elastic neutron scattering and molecular dynamics simulation as complementary techniques for studying diffusion in zeolites, *Microporous and Mesoporous Materials*, 102, 21–50.

Katada, N., Suzuki, K., Noda, T., Miyatani, W., Taniguchi, F., Niwa, M., (2010), Correlation of the cracking activity with solid acidity and adsorption property on zeolites, *Applied Catalysis A: General*, 373, 208–213.

Khan, A. H., Shang, J. Q., Alam, R., (2012), Ultrasound-assisted extraction for total sulphur measurement in mine tailings, *Journal of Hazardous Materials*, 235-236, 376–83.

Kilanowski, D. R., Gates, B. C., (1980), Kinetics of hydrodesulfurization of benzothiophene catalyzed by sulfided Co-Mo/Al₂O₃, *Journal of Catalysis*, 62, 70–78.

Kilanowski, D., Teeuwen, H., Beer, H., Gates, H. C., Schuit, G., Kwart, H., (1978), Hydrodesulfurization of thiophene, benzothiophene, dibenzothiophene, and related compounds catalyzed by sulfided Co-Mo/ γ -Al₂O₃, *Journal of Catalysis*, 55, 129–137.

Kim, J. W., Kim, D. J., Han, J. U., Kang, M., Kim, J. M., Yie, J. E., (2003), Preparation and characterization of zeolite catalysts for etherification reaction, *Catalysis Today*, 87, 195–203.

Kraemer, D. W., (1991), Modeling catalytic cracking in A novel Riser Simulator, PhD thesis, University of Western Ontario, London, Canada.

Krishna, R., Van Baten, J. M., (2008), Diffusion of hydrocarbon mixtures in MFI zeolite: Influence of intersection blocking, *Chemical Engineering Journal*, 140, 614–620.

Kärger, J., Pfeifer, H., (1987), NMR self-diffusion studies in zeolite science and technology, *Zeolites*, 7, 90–107.

Laredo, G. C., Altamirano, E., de los Reyes, J. A., (2003), Inhibition effects of nitrogen compounds on the hydrodesulfurization of dibenzothiophene: Part 2, *Applied Catalysis A: General*, 243, 207–214.

Laredo S, G. C., de los Reyes H, J. A., Luis Cano D, J., Jesús Castillo M, J., (2001), Inhibition effects of nitrogen compounds on the hydrodesulfurization of dibenzothiophene, *Applied Catalysis A: General*, 207, 103–112.

Leroy, F., Rousseau, B., Fuchs, A. H., (2004), Self-diffusion of n-alkanes in silicalite using molecular dynamics simulation: A comparison between rigid and flexible frameworks, *Physical Chemistry Chemical Physics*, 6, 775–783.

Lins, J. O., Nascimento, M. A., (1997), Molecular dynamics studies of light hydrocarbon diffusion in zeolites, *Molecular Engineering*, 7, 309–316.

Lippens, B., Boer, J., (1965), Studies on pore systems in catalysts: V. The t method, *Journal of Catalysis*, 4, 319–323.

Liu, Z., Ottaviani, M. F., Abrams, L., Lei, X., Turro, N. J., (2004), Characterization of the external surface of silicalites employing electron paramagnetic resonance, *Journal of Physical Chemistry A*, 108, 8040–8047.

Lugstein, A., Jentys, A., Vinek, H., (1997), n-Heptane cracking on H- and Ni-containing zeolites, *Journal of Chemical Society Faraday Transactions*, 93, 1837–1842.

Ma, X., Sprague, M., Song, C., (2005), Deep desulfurization of gasoline by selective adsorption over nickel-based adsorbent for fuel cell applications, *Industrial & Engineering Chemistry Research*, 44, 5768–5775.

Ma, X., Velu, S., Kim, J. H., Song, C., (2005), Deep desulfurization of gasoline by selective adsorption over solid adsorbents and impact of analytical methods on ppm-level sulfur quantification for fuel cell applications, *Applied Catalysis B: Environmental*, 56, 137–147.

Marcilly, C., (2001), Evolution of refining and petrochemicals: what is the place of zeolites, *Oil & Gas Science and Technology*, 56, 499–514.

McQuaid, M. J., Sun, H., Rigby, D., (2004), Development and validation of COMPASS force field parameters for molecules with aliphatic azide chains, *Journal of Computational Chemistry*, 25, 61–71.

Mitchell, S., Bonilla, A., Pérez-Ramírez, J., (2011), Preparation of organic-functionalized mesoporous ZSM-5 zeolites by consecutive desilication and silanization, *Materials Chemistry and Physics*, 127, 278–284.

Moreira, J., Serrano, B., Ortiz, A., de Lasa, H., (2012), A unified kinetic model for phenol photocatalytic degradation over TiO₂ photocatalysts, *Chemical Engineering Science*, 78, 186–203.

Nicholas, J. B., Trouw, F. R., Mertz, J. E., Iton, L. E., Hopfinger, A. J., (1993), Molecular dynamics simulation of propane and methane in silicalite, *The Journal of Physical Chemistry*, 97, 4149–4163.

Ono, Y., Kanae, K., (1991), Transformation of butanes over ZSM-5 zeolites, *Journal of Chemical Society Faraday Transactions*, 87, 663–667.

Paniv, P. M., Pyshev, S. V., Gaivanovich, V. I., Lazorko, O. I., (2006), Noncatalytic oxidation desulfurization of the kerosene cut, *Chemistry and Technology of Fuels and Oils*, 42, 159–166.

Rahman, F., Loughlin, K. F., Al-Saleh, M. a., Saeed, M. R., Tukur, N. M., Hossain, M. M., Karim, K., (2010), Kinetics and mechanism of partial oxidation of ethane to ethylene and acetic acid over MoV type catalysts, *Applied Catalysis A: General*, 375, 17–25.

Ravella, A., de Lasa, H. I., Mahay, A., (1987), Operation and testing of a novel catalytic reactor configuration for the conversion of methanol to hydrocarbons, *Industrial & Engineering Chemistry Research*, 26, 2546–2552.

Richard, F., Boita, T., Moreau, M., Bachmann, C., Pérot, G., (2007), Transformation of thiophenic compounds over HY zeolite study of the acid-catalyzed isomerization and disproportionation mechanisms by quantum chemical calculations, *Journal of Molecular Catalysis A: Chemical*, 273, 48–54.

Richard, F., Boita, T., Pérot, G., (2007), Reaction mechanism of 4,6-dimethyldibenzothiophene desulfurization over sulfided NiMoP/Al₂O₃-zeolite catalysts, *Applied Catalysis A: General*, 320, 69–79.

Roque-Malherbe, R., Wendelbo, R., Mifsud, A., Corma, A., (1995), Diffusion of aromatic hydrocarbons in H-ZSM-5, H-Beta, and H-MCM-22 zeolites, *The Journal of Physical Chemistry*, 99, 14064–14071.

Rozanska, X., Van Santen, R. A., (2003), Reaction mechanisms in zeolite catalysis, in: *Handbook of zeolite science and technology*, Marcel Dekker Inc., New York.

Rungsirisakun, R., Nanok, T., Probst, M., Limtrakul, J., (2006), Adsorption and diffusion of benzene in the nanoporous catalysts FAU, ZSM-5 and MCM-22: a molecular dynamics study, *Journal of Molecular Graphics & Modelling*, 24, 373–82.

Runnebaum, R. C., Maginn, E. J., (1997), Molecular dynamics simulations of alkanes in the zeolite silicalite: evidence for resonant diffusion effects, *The Journal of Physical Chemistry B*, 101, 6394–6408.

Saito, A., Foley, H., (1991), Curvature and parametric sensitivity in models for adsorption in micropores, *AIChE Journal*, 37, 429–436.

Sakanishi, K., Farag, H., Sato, S., Matsumura, A., Saito, I., (2003), Adsorptive removal of sulfur compounds from naphtha fractions by using carbon adsorbents, *Preprint Papers-American Chemical Society, Division of Fuel Chemistry*, 48, 524–525.

Samoletov, A. A., Dettmann, C. P., Chaplain, M. A. J., (2007), Thermostats for “slow” configurational modes, *Journal of Statistical Physics*, 128, 1321–1336.

Sastre, G., Raj, N., Catlow, C. R. A., Roque-malherbe, R., Corma, A., (1998), Selective diffusion of C8 aromatics in a 10 and 12 MR zeolite. A molecular dynamics study, *Journal of Physical Chemistry B*, 102, 3198–3209.

Satterfield, C. N., (1980), *Heterogeneous catalysis in practice*, McGraw-Hill Book Company.

Schulz, H., Bohringer, W., Ousmanov, F., Waller, P., (1999), Refractory sulfur compounds in gas oils, *Fuel Processing Technology*, 61, 5–41.

Schuring, D., (2002), *Diffusion in zeolites : towards a microscopic understanding*, PhD thesis, Eindhoven university of technology, Netherlands.

Shirazi, L., Jamshidi, E., Ghasemi, M. R., (2008), The effect of Si/Al ratio of ZSM-5 zeolite on its morphology, acidity and crystal size, *Crystal Research and Technology*, 43, 1300–1306.

Smit, B., Daniël J. C. Loyens, L., Verbist, G. L. M. M., (1997), Simulation of adsorption and diffusion of hydrocarbons in zeolites, *Faraday Discussions*, 106, 93–104.

Soleimani, M., Bassi, A., Margaritis, A., (2007), Biodesulfurization of refractory organic sulfur compounds in fossil fuels, *Biotechnology Advances*, 25, 570–96.

Song, C., (2003), An overview of new approaches to deep desulfurization for ultra-clean gasoline, diesel fuel and jet fuel, *Catalysis Today*, 86, 211–263.

Song, C., Ma, X., (2003), New design approaches to ultra-clean diesel fuels by deep desulfurization and deep dearomatization, *Applied Catalysis B: Environmental*, 41, 207–238.

Song, C., Ma, X., (2006), Ultra-clean diesel fuels by deep desulfurization and deep dearomatization of middle distillates, in: *Practical Advances in Petroleum Processing*, Springer, New York.

Song, L., Sun, Z-L., Rees, L. V. C., (2002), Experimental and molecular simulation studies of adsorption and diffusion of cyclic hydrocarbons in silicalite-1, *Microporous and Mesoporous Materials*, 55, 31–49.

Sotelo, J. L., Uguina, M. a., Águeda, V. I., (2007), Fixed bed adsorption of benzothiophene over zeolites with faujasite structure, *Adsorption*, 13, 331–339.

Stanislaus, A., Marafi, A., Rana, M. S., (2010), Recent advances in the science and technology of ultra low sulfur diesel (ULSD) production, *Catalysis Today*, 153, 1–68.

Sun, H., Ren, P., Fried, J. R., (1998), The COMPASS forcefield: parameterization and validation for polyphosphazenes, *Computational and Theoretical Polymer Science*, 8, 229–246.

Szczygieł, J., Szyja, B., (2005), Computer simulated diffusion of C7 hydrocarbons in microporous materials: molecular modeling, *Microporous and Mesoporous Materials*, 83, 85–93.

Taniguchi, M., Imamura, D., Ishige, H., Ishii, Y., Murata, T., Hidai, M., Tatsumi, T., (1999), Hydrodesulfurization of benzothiophene over zeolite-supported catalysts prepared from Mo and Mo – Ni sulfide clusters, *Journal of Catalysis*, 187, 139–150.

Tepper, H., (2001), Molecular dynamics of crystal growth and transport in zeolites, PhD thesis, Univeristy of Twente, Netherlands.

Tonetto, G., Atias, J., de Lasa, H. I., (2004), FCC catalysts with different zeolite crystallite sizes: acidity, structural properties and reactivity, *Applied Catalysis A: General*, 270, 9–25.

Tonetto, G. M., Ferreira, M. L., Atias, J. A., de Lasa, H. I., (2006), Effect of steaming treatment in the structure and reactivity of FCC catalysts, *AIChE Journal*, 52, 754–768.

Treacy, M. M. J., Higgins, J. B., (2001), Collection of simulated XRD powder patterns for zeolites, fourth ed., Elsevier.

Trout, B. L., Chakraborty, A. K., Bell, A. T., (1997), Diffusion and reaction in ZSM-5 studied by dynamic Monte Carlo, *Chemical Engineering Science*, 52, 2265–2276.

Tukur, N., Alkhattaf, S., (2005), Catalytic cracking of n-dodecane and alkyl benzenes over FCC zeolite catalysts: time on stream and reactant converted models, *Chemical Engineering and Processing*, 44, 1257–1268.

Uguina, M., Sotelo, J., Rodriguez, a, Gomezcivicos, J., Lazaro, J., (2006), Liquid adsorption of linear and branched paraffins onto microporous adsorbents: influence of adsorbent structure and Si/Al molar ratio, *Separation and Purification Technology*, 51, 72–79.

Valla, J. A., Mouriki, E., Lappas, A. A., Vasalos, I. A., (2007), The effect of heavy aromatic sulfur compounds on sulfur in cracked naphtha, *Catalysis Today*, 127, 92–98.

Valla, J., Lappas, A., Vasalos, I., (2006), Catalytic cracking of thiophene and benzothiophene: mechanism and kinetics, *Applied Catalysis A: General*, 297, 90–101.

Verlet, L., (1967), Computer experiments on classical fluids. I. Thermodynamical properties of Lennard-Jones molecules, *Physical Review*, 159, 98–103.

Vrinat, M. L., (1983), The kinetics of the hydrodesulfurization process - A review, *Applied Catalysis*, 6, 137–158.

- Wang, H., Prins, R., (2008), HDS of benzothiophene and dihydrobenzothiophene over sulfided Mo/ γ -Al₂O₃, *Applied Catalysis A: General*, 350, 191–196.
- Wang, Y., Latz, J., Dahl, R., Pasel, J., Peters, R., (2009), Liquid phase desulfurization of jet fuel by a combined pervaporation and adsorption process, *Fuel Processing Technology*, 90, 458–464.
- Wilson, W. H., Klee, M. S., (1997), Analysis of sulfur and phosphorus compounds with a Flame Photometric Detector on the Agilent 6890 series gas chromatograph, Application report, Agilent Technologies Inc., USA.
- Woltz, C., (2005), Kinetic studies on alkane hydroisomerization over bifunctional catalysts, PhD thesis, Technische Universität München, Germany.
- Wu, P., Debebe, A., Ma, Y. H., (1983), Adsorption and diffusion of C₆ and C₈ hydrocarbons in silicalite, *Zeolites*, 3, 118–122.
- Xiao, J., (1990), The diffusion mechanism of hydrocarbons in zeolites, PhD thesis, Massachusetts Institute of Technology, United States.
- Xiao, J., Wei, J., (1992a), Diffusion mechanism of hydrocarbons in zeolite I. Theory, *Chemical Engineering Science*, 47, 1123–1141.
- Xiao, J., Wei, J., (1992b), Diffusion mechanism of hydrocarbons in zeolites—II. Analysis of experimental observations, *Chemical Engineering Science*, 47, 1143–1159.
- Xue, M., Chitrakar, R., Sakane, K., Hirotsu, T., Ooi, K., Yoshimura, Y., Feng, Q., (2005), Selective adsorption of thiophene and 1-benzothiophene on metal-ion-exchanged zeolites in organic medium, *Journal of Colloid and Interface Science*, 285, 487–92.
- Yu, S., Li, W., Iglesia, E., (1999), Desulfurization of thiophene via hydrogen transfer from alkanes on cation-modified H-ZSM5, *Journal of Catalysis*, 187, 257–261.
- Yu, S., Waku, T., Iglesia, E., (2003), Catalytic desulfurization of thiophene on H-ZSM5 using alkanes as co-reactants, *Applied Catalysis A: General*, 242, 111–121.
- Zhao, H., (2009), Catalytic hydrogenation and hydrodesulfurization of model compounds, PhD thesis, Virginia Polytechnic Institute and State University, United States.
- Zheng, S., (2002), Surface modification of HZSM-5 zeolites. PhD thesis, Technische Universität München, Germany.

APPENDIX A.

MD Simulation Parameters

A.1 The Forcefield

The purpose of a forcefield is to describe the potential energy surface of entire classes of molecules with reasonable accuracy. In a sense, the forcefield extrapolates from the empirical data of the small set of models used to parameterize it, a larger set of related models. Some forcefields aim for high accuracy for a limited set of elements, thus enabling good predictions of many molecular properties. Others aim for the broadest possible coverage of the periodic table, with necessarily lower accuracy.

A.1.1 COMPASS Forcefield

COMPASS is a powerful forcefield supporting atomistic simulations of condensed phase materials. COMPASS stands for condensed-phase optimized molecular potentials for atomistic simulation studies. COMPASS is the first ab initio forcefield that has been parameterized and validated using condensed-phase properties, in addition to various ab initio and empirical data for molecules in isolation. Consequently, this forcefield enables accurate and simultaneous prediction of structural, conformational, vibrational, and thermophysical properties for a broad range of molecules in isolation and in condensed phases, and under a wide range of conditions of temperature and pressure.

A.2 NVT Ensemble

NVT (constant number of particles, constant volume, and constant temperature dynamics) allow the system to exchange heat with the environment at a controlled

temperature. The initial temperature and the initial distribution of atomic velocities in a system are related through the Maxwell-Boltzmann equation:

$$f(v) = \left(\frac{m}{2\pi K_B T} \right)^{3/2} \exp\left(\frac{-mv^2}{2K_B T} \right) 4\pi v^2 \quad (\text{A.1})$$

This well known formula expresses the probability $f(v)$ that a molecule of mass m has a velocity of v when it is at temperature T , with K_B here representing Boltzmann constant ($1.38 \times 10^{-23} \text{ m}^2 \text{ Kg} / \text{s}^2 \text{ K}$). The x , y , z components of the velocities have Gaussian distributions $g(v)$:

$$g(v_x) dv_x = \left(\frac{m}{2\pi K_B T} \right)^{1/2} \exp\left(\frac{mv_x^2}{2K_B T} \right) dv_x \quad (\text{A.2})$$

The initial velocities are generated from the Gaussian distribution of v_x , v_y , and v_z . The Gaussian distribution is in turn generated using a random number generator and a random number seed.

A.2.1 Temperature Calculations

Temperature is a thermodynamic quantity, which is meaningful only at equilibrium. It is related to the average kinetic energy of the system and can be calculated from the total kinetic energy and the total number of degrees of freedom as:

$$\frac{(3N - 3)K_B T}{2} = \sum_{i=1}^N \frac{m_i v_i^2}{2} \quad (\text{A.3})$$

where m is the mass of molecule i , with a velocity of v when it is at temperature T , with K_B here representing Boltzman constant ($1.38 \times 10^{-23} \text{ m}^2 \text{ Kg} / \text{s}^2 \text{ K}$), and N is the number of molecules in the system.

A.2.2 Temperature Control

Although the initial velocities are generated so as to produce a Maxwell-Boltzmann distribution at the desired temperature, the distribution does not remain constant as the simulation continues. This is especially true when the system does not start at a minimum-energy configuration of the structure. This situation often occurs since structures are commonly minimized only enough to eliminate any hot spots. During dynamics, kinetic and potential energy are exchanged and the temperature changes as a consequence. To maintain the correct temperature, the computed velocities have to be adjusted appropriately. In addition to maintaining the desired temperature, the temperature-control mechanism must produce the correct statistical ensemble. This means that the probability of occurrence of a certain configuration obeys the laws of statistical mechanics. The temperature-control methods, or thermostats, considered in materials studio software are: Direct velocity scaling, Berendsen, Nosé, Andersen, and Nosé-Hoover-Langevin (NHL) . In this study all MD runs were conducted using Nosé-Hoover-Langevin (NHL) thermostat.

A.2.2.1 Nosé-Hoover-Langevin (NHL)

The Nosé-Hoover-Langevin algorithm provides a reliable thermostat for systems that are at equilibrium, or close to it. The main idea behind Nosé-Hoover-Langevin dynamics is that an additional (fictitious) degree of freedom is added to the structure, to represent

the interaction of the structure with the heat bath. More details on this method of temperature control can be found in the work done by Samoletov et al. (2007).

A.3 NVE Ensemble

The constant energy, constant volume ensemble (NVE), also known as the microcanonical ensemble, is obtained by solving the standard Newton equation without any temperature and pressure control. Energy is conserved when this (adiabatic) ensemble is generated. However, because of rounding and truncation errors during the integration process, there is always a slight fluctuation, or drift, in energy. True constant energy conditions (i.e., without temperature control) are not recommended for the equilibration phase of the simulation because, without the energy flow facilitated by temperature control, the desired temperature cannot be achieved. However, during the data collection phase, if you are interested in exploring the constant energy surface of the conformational space or if, for some other reason, you do not want the perturbation introduced by temperature bath coupling, this is a useful ensemble.

A.3.1 Equations of Motion

In its simplest form, molecular dynamics solves Newton's familiar equation of motion:

$$F_i(t) = m_i a_i(t) \tag{A.4}$$

where F_i is the force, m_i is the mass, a_i is the acceleration of atom i , and t is the time. The force on atom i can be computed directly from the derivative of the potential energy V with respect to the coordinate r_i as:

$$-\frac{\partial V}{\partial r_i} = m_i \frac{\partial^2 r_i}{\partial t^2} \quad (\text{A.5})$$

The classical equations of motion are deterministic. This means that, once the initial coordinates and velocities are known, the coordinates and velocities at a later time can be determined. The coordinates and velocities for a complete dynamics run are called the *trajectory*. The standard method of solving an ordinary differential equation such as numerically is the finite-difference method. Given the initial coordinates and velocities and other dynamic information at time t , the positions and velocities at time $t + \Delta t$ are calculated. The time step Δt depends on the integration method as well as the system itself. Although the initial coordinates are determined in the input file or from a previous operation such as minimization, the initial velocities are randomly generated at the beginning of a dynamics run, according to the desired temperature. Therefore, dynamics runs *cannot* be repeated exactly, except for forcefield engines that allow you to set the random number seed to the value that was used in a previous run.

A.3.2 Criteria for Molecular Dynamics Integrators

Molecular dynamics is usually applied to a large model. Energy evaluation is time consuming and the memory requirement is large. To generate the correct statistical ensembles, energy conservation is also important. Thus, the basic criteria for a good integrator for molecular simulations are as follows:

- It should be fast, ideally requiring only one energy evaluation per time step.
- It should require little computer memory.
- It should permit the use of a relatively long time step.

- It must show good conservation of energy.

A.3.3 Integrators in Materials Studio

The integrators provided in Materials Studio were chosen based on the above criteria. Only the dynamics algorithms used in Materials Studio are considered here. Variants of the Verlet (1967) algorithm of integrating the equations of motion are perhaps the most widely used method in molecular dynamics. The advantages of Verlet integrators are that these methods require only one evaluation of energy per step. Also, they require only modest memory, and allow a relatively large time step to be used.

A.3.3.1 Verlet Velocity Integrator

The Verlet velocity algorithm overcomes the out-of-synchrony shortcoming of the Verlet leapfrog method. The Verlet velocity algorithm is as follows:

$$r(t + \Delta t) = r(t) + \Delta t v(t) + \frac{\Delta t^2 a(t)}{2} \quad (\text{A.6})$$

$$a(t + \Delta t) = \frac{f(t + \Delta t)}{m} \quad (\text{A.7})$$

$$v(t + \Delta t) = v(t) + \frac{1}{2} \Delta t [a(t) + a(t + \Delta t)] \quad (\text{A.8})$$

where $r(t)$, $v(t)$, and $a(t)$, respectively, the position, velocity, and acceleration at time t .

Appendix B.

Assessment of Volume

A critical parameter in the CREC Riser Simulator is the volume of both the reactor and the vacuum box. The volumes of these two chambers are needed for the mass balance closure calculations, adsorption constants calculations, and in kinetic modeling.

B.1 Reactor Volume

The volume of the reactor is calculated by injecting a known amount of a chemical compound (i.e. air or any hydrocarbon) using a calibrated gas syringe into the reactor, which is isolated from other compartments of the system. Upon injection, the resultant pressure increase in the reactor is noted. Knowing the volume of the compound injected and its temperature as well as reactor temperature, the volume of the reactor can be assessed from the pressure readings.

If air at room temperature is the compound of choice to be used for the reactor volume assessment, equation B.1, based on the ideal gas law, can be used if the reactor is also at room temperature:

$$V_R = \frac{V_{\text{injected}} P_{\text{atm}}}{P_{\text{final}} - P_{\text{initial}}} \quad (\text{B.1})$$

where V_R is the reactor volume, V_{injected} is the volume of air injected, P_{final} and P_{initial} are the reactor final and initial pressure, respectively, and P_{atm} is the atmospheric pressure. Table B.1 shows the values of pressure versus volume of air injected as well as the calculated reactor volume.

Table B.1. Determination of the reactor volume

Volume of Air injected (cm³)	Initial Reactor Pressure (psia)	Final Reactor Pressure (psia)	Reactor Volume (cm³)
10	12.79	15.44	55.74
10	12.79	15.44	55.74
15	12.8	16.72	56.52
15	12.79	16.72	56.37
20	12.81	18.05	56.37
20	12.81	18.04	56.48
30	12.8	20.61	56.73
30	12.79	20.61	56.66
Average			56.55

B.2 Vacuum Box Volume

In a similar manner to the reactor volume determination, the vacuum box volume can be assessed. Using a calibrated syringe, air at room temperature with different volumes is injected directly to the vacuum box which is isolated from the reactor. The vacuum box temperature is kept at room temperature. Hence, equation B.2 can be used to calculate the vacuum box volume:

$$V_{VB} = \frac{V_{\text{injected}} P_{\text{atm}}}{P_{\text{final}} - P_{\text{initial}}} \quad (\text{B.2})$$

where V_{VB} is the vacuum box volume, V_{injected} is the volume of air injected, P_{final} and P_{initial} are the vacuum box final and initial pressure, respectively, and P_{atm} is the atmospheric pressure. Table B.2 shows the values of pressure versus volume of air injected as well as the calculated vacuum box volume.

Table B.2. Determination of the vacuum box volume

Volume of Air injected (cm³)	Initial VB Pressure (psia)	Final VB Pressure (psia)	Vacuum Box Volume (cm³)
50	13	13.64	1153.91
50	13.01	13.65	1153.91
40	13	13.51	1158.43
40	13	13.52	1136.15
30	13	13.38	1166.05
30	13	13.38	1166.05
20	13.01	13.27	1136.15
10	13	13.13	1136.15
		Average	1150.85

Appendix C.

Benzothiophene Calibration Curve

The benzothiophene calibration curve that correlates its concentration with FPD detector chromatogram area was determined using benzothiophene/n-dodecane mixtures and the GC/FID/FPD system. It has to be mentioned that when conducting the experiments in the CREC Riser Simulator, Argon gas available in the system (reactor and vacuum box) is diluting the sample going to GC/FID/FPD system. So, one has to consider this fact when establishing any calibration curve. However, direct relation with initial benzothiophene and FPD detector signal area can be considered if the calibration curve is generated using direct injection to the GC/FID/FPD system.

For this purpose, samples of different initial benzothiophene concentrations (0, 0.5, 2, 4, and 8 wt % with the balance being n-dodecane) were prepared. About 0.1 μL of each sample was injected directly to the GC/FID/FPD system back inlet using a calibrated gas tight Hamilton syringe. The GC method used for to establish the calibration curve was the same one used for the analysis which is described in the experimental part (Chapter 5) of this thesis. Every direct injection run was repeated at least three times to secure reproducibility of the results. Equation C.1 and based on the fact that FPD detector response to sulfur species is of a second order (Wilson & Klee, 1997), reports the calibration curve obtained from benzothiophene initial concentration versus FPD chromatogram area data (Figure C.1). The proposed second order polynomial adequately represents the data with its determination coefficient R^2 of 0.998.

$$Y = 3 \times 10^{-21} X^2 + 2 \times 10^{-11} X - 0.0814 \quad (\text{C.1})$$

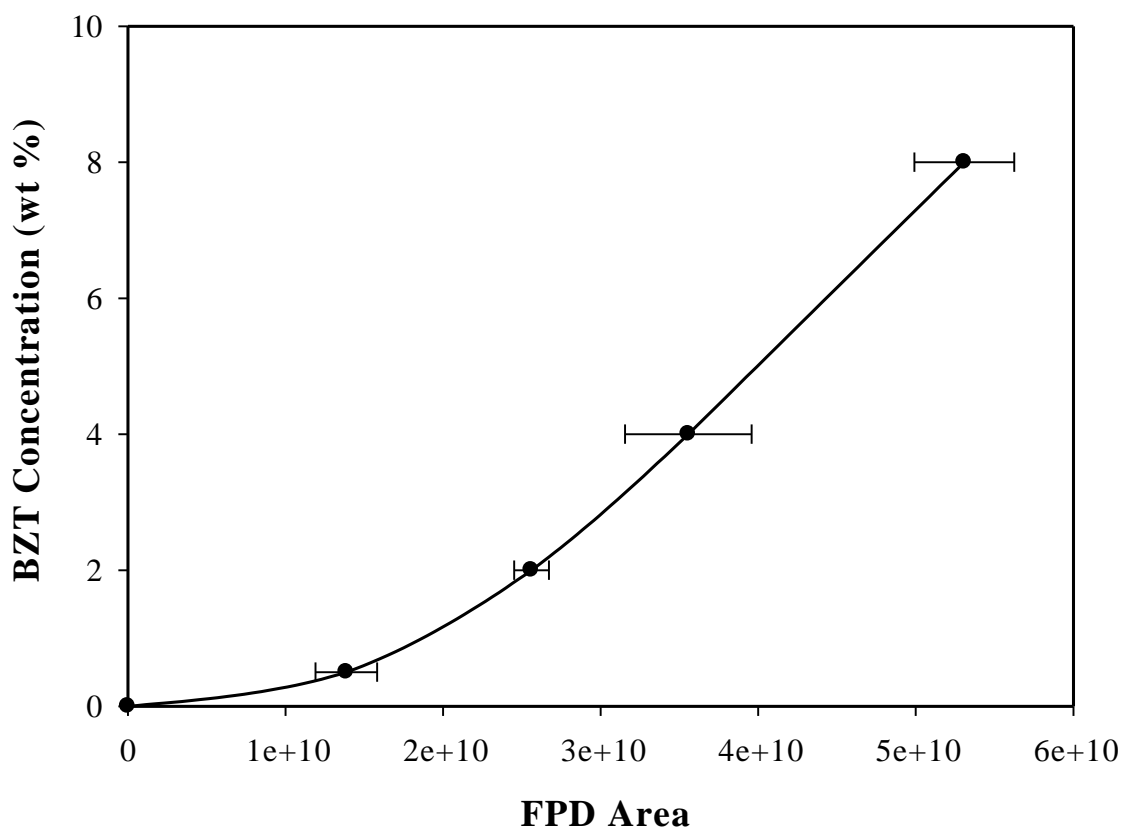


Figure C.1. FPD detector calibration curve for benzothiophene. Error bars correspond to standard deviations of three repeats.

It was noticed that the gas phase sulfur containing compounds (alkyl-BZT) produced from the reaction of 6 wt % BZT n-C12 mixture are very low in concentration and cannot be detected using FPD detector. On the other hand, FID showed reasonable peaks for these compounds which can be used for their quantification. FID has a response factor (RSF) of 1 for hydrocarbon compounds only. However, FID can be used to quantify sulfur containing compounds if the RSF for them is known. For example, Dietz (1967)

and Hernandez Enriquez (2003) found that FID detector has a RSF of 0.57 and 0.45 for thiophene and ethyl mercaptan, respectively.

For the purpose of this study, FID response factor for benzothiophene was determined in the samples containing 6 wt % BZT and using n-C₁₂ as an internal standard. About 8 direct injections of 0.1 μ L to the GC/FID/FPD system back inlet were conducted. For each run, the FID chromatogram area was recorded and equation C.2 was applied to calculate the RSF for benzothiophene.

$$\text{RSF} = (A_{\text{BZT}}/C_{\text{BZT}})/(A_{\text{C}_{12}}/C_{\text{C}_{12}}) \quad (\text{C.2})$$

where A_{BZT} and $A_{\text{C}_{12}}$ are the FID chromatogram peak areas for benzothiophene and n-dodecane, respectively. Similarly, C_{BZT} and $C_{\text{C}_{12}}$ are the initial concentrations of benzothiophene and n-dodecane in the mixture (wt %), respectively. The average FID RSF for benzothiophene was found to be about 0.81 as reported in Table C.1.

Table C.1. Data for FID detector response factor of benzothiophene.

Injection #	Calculated RSF
1	0.80879
2	0.80836
3	0.80685
4	0.80787
5	0.80545
6	0.80675
7	0.80561
8	0.80590
Average	0.80695

Finally, the determined RSF for BZT was used to quantify the sulfur containing compounds detected by FID (Alkyl-BZT) incorporating the molecular weights ratio as a correction factor.

Appendix D.

Mass Balance

The mass balance closure was defined as:

$$MB = \frac{m_i - m_p - m_c}{m_i} \times 100 \quad (D.1)$$

where

MB: mass balance closure (%)

m_i : total mass of reactant injected (g)

m_p : total mass of reaction products in gas phase (g)

m_c : weight of coke over catalyst (g)

The exact amount of reactant injected was calculated as the difference between the mass of the syringe before (m_{bef}) and after (m_{aft}) performing the injection.

$$m_i = m_{bef} - m_{aft} \quad (D.2)$$

The mass of products was determined by calculating the total number of moles of products in the system using ideal gas law and the average molecular weight of product mixture in an Argon free basis. Equation D.3 was used to calculate products total number of moles from the reactor and equation D.4 was used to calculate products total number of moles from the whole system (reactor and vacuum box).

$$n_{p,r} = \frac{(P_{r,f} - P_{r,i})V_R}{RT_R} \quad (D.3)$$

$$n_{p,s} = \frac{(P_{r,fe} - P_{r,i})V_R}{RT_R} + \frac{(P_{VB,f} - P_{VB,i})V_{VB}}{RT_{VB}} \quad (D.4)$$

where

$n_{p,r}$: products total number of moles from the reactor (mole)

$n_{p,s}$: products total number of moles from the system (mole)

$P_{r,f}$: reactor final pressure (psia)

$P_{r,i}$: reactor initial pressure (psia)

$P_{r,fe}$: final equilibrium reactor pressure after evacuation of products to vacuum box (psia)

$P_{VB,f}$: vacuum box final pressure (psia)

$P_{VB,i}$: vacuum box initial pressure (psia)

V_R : reactor volume (cm³)

V_{VB} : vacuum box volume (cm³)

R : universal gas constant (1205.91 cm³ psia /gmole K)

T_R : reactor temperature (K)

T_{VB} : vacuum box temperature (K)

The average molecular weight of the products mixture was calculated using the molecular weight of the individual species and the weight fractions as follows:

$$MW_p = \frac{1}{\sum \frac{w_i}{MW_i}} \quad (D.5)$$

where

MW_p : average molecular weight of the products mixture (g/gmol)

w_i : weight fraction of product i

MW_i : molecular weight of product i (g/gmol)

The weight fraction of each hydrocarbon species was calculated by normalizing the FID chromatogram peak areas and using the response factor, and the weight fraction of BZT sulfur species was calculated the FPD chromatogram peak area and calibration curve.

Finally, the mass of the products from the reactor ($m_{p,r}$) and from the system ($m_{p,s}$) can be calculated respectively, as follows:

$$m_{p,r} = n_{p,r} \times MW_p \quad (D.6)$$

$$m_{p,s} = n_{p,s} \times MW_p \quad (D.7)$$

Table D.1 reports the mass balance calculations for thermal cracking of pure n-dodecane samples while Table D.2 reports the mass balance calculations for thermal cracking of 6 wt % benzothiophene mixture.

Table D.1. Mass balance data for thermal cracking runs of pure n-dodecane samples at 450 °C and 7 seconds contact time.

Run number	Run 1	Run 2	Run 3
Sample name	TR-R1-1	TR-R1-2	TR-R1-3
m_{bef} , g	19.700	19.699	19.699
m_{aft} , g	19.543	19.551	19.557
m_{i} , g	0.157	0.148	0.142
T_{R} , °C	451	449	452
T_{VB} , °C	285	290	291
$P_{\text{r,i}}$, psia	14.80	14.90	14.90
$P_{\text{r,f}}$, psia	28.30	27.70	27.40
$P_{\text{r,fe}}$, psia	4.34	4.18	4.53
$P_{\text{VB,i}}$, psia	3.81	3.70	3.93
$P_{\text{VB,f}}$, psia	4.72	4.62	4.80
$n_{\text{p,r}}$, mol	0.00087	0.00083	0.00081
$n_{\text{p,s}}$, mol	0.00088	0.00086	0.00080
MW_{p} , g/gmol	169.076	169.082	169.123
$m_{\text{p,r}}$, g	0.148	0.141	0.137
$m_{\text{p,s}}$, g	0.143	0.120	0.127
coke on catalyst, g	n/a	n/a	n/a
MB closure	5.853	5.041	3.725

Table D.2. Mass balance data for thermal cracking runs of 6 wt % benzothiophene / 94 wt % n-dodecane mixture samples at 450 °C and 7 seconds contact time.

Run number	Run 1	Run 2	Run 3
Sample name	TR-R2-1	TR-R2-2	TR-R2-3
m_{bef} , g	19.700	19.705	19.700
m_{aft} , g	19.567	19.567	19.568
m_{i} , g	0.133	0.138	0.132
T_{R} , °C	451	449	450
T_{VB} , °C	292	293	293
$P_{\text{r,i}}$, psia	15.00	15.00	14.90
$P_{\text{r,f}}$, psia	27.1	27.2	27.3
$P_{\text{r,fe}}$, psia	4.55	4.21	4.33
$P_{\text{VB,i}}$, psia	3.95	3.68	3.75
$P_{\text{VB,f}}$, psia	4.81	4.54	4.59
$n_{\text{p,r}}$, mol	0.00078	0.00079	0.00080
$n_{\text{p,s}}$, mol	0.0007	0.0007	0.0007
MW_{p} , g/gmol	166.526	166.364	167.53
$m_{\text{p,r}}$, g	0.130	0.132	0.135
$m_{\text{p,s}}$, g	0.121	0.122	0.122
coke on catalyst, g	n/a	n/a	n/a
MB closure	1.892	4.494	-2.054

Table D.3 reports selected mass balance calculations for catalytic cracking of pure n-dodecane samples while Table D.4 reports selected mass balance calculations for catalytic runs of 6 wt % benzothiophene mixture.

Table D.3. Mass balance data for catalytic cracking runs of pure n-dodecane samples at 350 °C, cat/oil = 5, and 7 seconds contact time.

Run number	Run 1	Run 2	Run 3
Sample name	C12350_7_4	C12350_7_5	C12350_7_6
m_{bef} , g	19.569	19.568	19.569
m_{aft} , g	19.405	19.405	19.406
m_{i} , g	0.164	0.163	0.163
T_{R} , °C	350	350	350
T_{VB} , °C	265	268	267
$P_{\text{r,i}}$, psia	14.8	14.8	14.8
$P_{\text{r,f}}$, psia	26.5	26.9	26.6
$P_{\text{r,fe}}$, psia	4.53	4.78	4.54
$P_{\text{VB,i}}$, psia	3.17	3.24	3.21
$P_{\text{VB,f}}$, psia	4.19	4.23	4.22
$n_{\text{p,r}}$, mol	0.00088	0.00091	0.00089
$n_{\text{p,s}}$, mol	0.001	0.001	0.001
MW_{p} , g/gmol	150.58	151.11	152.70
$m_{\text{p,r}}$, g	0.138	0.133	0.136
$m_{\text{p,s}}$, g	0.156	0.150	0.154
coke on catalyst, g	0.0089	0.0089	0.0089
MB closure	-0.460	2.674	-0.214

Table D.4. Mass balance data for catalytic runs of 6 wt % benzothiophene / 94 wt % n-dodecane mixture samples at 350 °C, cat/oil = 5, and 7 seconds contact time.

Run number	Run 1	Run 2	Run 3
Sample name	6%B350_7_4	6%B350_7_5	6%B350_7_6
m_{bef} , g	19.583	19.584	19.582
m_{aft} , g	19.415	19.416	19.415
m_{i} , g	0.168	0.168	0.167
T_{R} , °C	350	350	350
T_{VB} , °C	267	266	268
$P_{\text{r,i}}$, psia	14.7	14.7	14.8
$P_{\text{r,f}}$, psia	27.6	29.8	28.1
$P_{\text{r,fe}}$, psia	4.52	4.57	4.57
$P_{\text{VB,i}}$, psia	3.17	3.12	3.22
$P_{\text{VB,f}}$, psia	4.32	4.30	4.38
$n_{\text{p,r}}$, mol	0.00097	0.00113	0.00100
$n_{\text{p,s}}$, mol	0.00107	0.00132	0.00127
MW_{p} , g/gmol	124	123	125
$m_{\text{p,r}}$, g	0.120	0.139	0.125
$m_{\text{p,s}}$, g	0.156	0.162	0.159
coke on catalyst, g	0.0098	0.0098	0.0098
MB closure	1.31	-2.37	-0.79

Appendix E.

Conversion and Products Distribution

E.1 Conversion Calculations

The “1” species percentual conversion of chemical species such as benzothiophene can be calculated using GC-MS data and TOC analysis as follows:

$$X_1 = \left(\frac{W_{1,conv}}{W_{1,initial}} \right) \times 100 \quad (E.1)$$

where

X_1 : conversion of “1” reactant species (%)

$W_{1,conv}$: weight of “1” species converted (g)

$W_{1,initial}$: weight of “1” species at initial or feed conditions (g)

Regarding $W_{1,initial}$, the initial weight of “1” species injected (fed) in the CREC Riser Simulator prior to the catalytic reaction also can be calculated as follows:

$$W_{1,initial} = y_{1,feed} (m_{before} - m_{after}) \quad (E.2)$$

with m_{before} representing the initial mass of the feed syringe before an injection, m_{after} the final mass of the feed syringe after an injection and $y_{1,feed}$ is the weight fraction of the “1” species in the feed.

Given all species are contained in the CREC Riser Simulator during the reaction with no gas phase leaking, one can also state:

$$\sum W_p = (m_{\text{before}} - m_{\text{after}}) - W_{\text{coke}} \quad (\text{E.3})$$

with $\sum W_p$ representing all chemical species in gas phase including all products and unconverted reactants after a set reaction period in the CREC Riser Simulator unit.

Regarding the $W_{1,\text{conv}}$ mass converted of “1” species after a given reaction period, it can be calculated as:

$$W_{1,\text{conv}} = W_{1,\text{coke}} + \sum W_{1,j} \quad (\text{E.4})$$

with $W_{1,\text{coke}}$ being the weight of “1” species (e.g. benzothiophene) converted into coke and $W_{1,j}$ the weight “j” products that can be traced to “1” converted species remaining in the gas phase.

Furthermore W_{coke} , the mass of coke formed can be assessed from TOC analysis as:

$$W_{\text{coke}} = \left(\frac{W_{\text{TOC}}}{W_{\text{sample}}} \right) \times W_{\text{cat}} \quad (\text{E.5})$$

with W_{TOC} being the weight of coke from TOC analysis, W_{sample} the weight of catalyst used in the TOC analysis and W_{cat} the weight of catalyst used in the Riser Simulator.

And based on that, the amount of “1” species converted into coke can be determined as:

$$W_{1,\text{coke}} = W_{\text{coke}} - W_{2,\text{coke}} \quad (\text{E.6})$$

with $W_{2,\text{coke}}$ being the coke formed during experiments developed at the same conditions (temperature, reactant partial pressure, contact time) using pure C12. This approximation is considered adequate given the 15.6 C₁₂/benzothiophene feed weight ratio.

Thus, and in order to be able to use equation (E.4), the weight fractions for “j” species in the gas phase that can be traced to the “1” reactant, can be calculated using the individual weight fractions from GC-MS analysis and the ΣW_p as per equation (E.3)

$$y_{1,j} = \frac{A_{1,j}}{A_T} = \frac{W_{1,j}}{\Sigma W_p} \quad \text{or} \quad W_{1,j} = y_{1,j} \times \Sigma W_p \quad (\text{E.7})$$

With $y_{i,j}$ being the weight fraction of product “j” that can be traced to reactant “1”, $A_{1,j}$ the GC chromatogram area of product “j” that can be traced to reactant “1” and A_T the sum of all GC chromatogram areas for all products.

Thus, calculating $W_{i,j}$ as in equation (E.7), $W_{i,\text{coke}}$ as in equation (E.6), the $W_{i,\text{conv}}$ (refer to equation (E.1)) provides the percentual conversion X_i for every single run.

E.2 Product Distributions

Tables E.1 to E.2 report the main products from thermal cracking of pure n-dodecane and 6 wt % benzothiophene samples, respectively.

Tables E.3 to E.5 report the main products from catalytic cracking of pure n-dodecane samples at different temperatures (450 °C, 425 °C, and 400 °C) and 5 seconds reaction time.

Table E.1. Product distribution from thermal cracking runs of pure n-dodecane samples at 450 °C and 7 seconds contact time.

Product #	Ret. Time	Product name	Sample name		
			TR-R1-1 Wt%	TR-R1-2 Wt%	TR-R1-3 Wt%
1	3.847	propane	0.074769	0.071984	0.074843
2	4.014	2-methylpropene	0.082766	0.081504	0.069855
3	4.291	butane	0.001688	0.00157	0.025096
4	4.451	2-butene	0.026634	0.028826	0.001073
5	4.527	1-butene	0.001791	0.001411	0.007512
6	4.604	1-pentene	0.008431	0.009561	0.007487
7	4.731	pentane	0.008537	0.009827	0.014701
8	5.597	2-pentene	0.015265	0.014455	0.002441
9	5.818	2-methylbutene	0.004598	0.004271	0.009719
10	5.958	dimethylcyclopropene	0.01376	0.012406	0.00308
11	8.614	1-hexene	0.013955	0.017323	0.00762
12	9.166	hexane	0.002925	0.003323	0.021325
13	9.406	2-hexene	0.005172	0.003876	0.003971
14	13.859	heptene	0.010831	0.012696	0.014132
15	31.041	2,6-dimethyldecane	0.083648	0.083657	0.083174
16	31.239	3-methylundecane	0.335773	0.336953	0.336396
17	31.449	3-dodecene	0.031565	0.019982	0.0268
18	31.728	n-dodecane	99.27242	99.28273	99.2868
19	31.795	2-dodecene	0.005472	0.003646	0.003974
Average MW (g/mol)			169.0764	169.0824	169.1233

Table E.2. Product distribution from thermal cracking runs of 6 wt % benzothiophene / 94 wt % n-dodecane mixture samples at 450 °C and 7 seconds contact time.

Product #	Ret. Time	Product name	Sample name		
			TR-R2-1 Wt%	TR-R2-2 Wt%	TR-R2-3 Wt%
1	3.851	propane	0.141538	0.152288	0.160794
2	4.02	2-methylpropene	0.113883	0.115316	0.116405
3	4.456	butene	0.051145	0.038824	0.050357
4	4.607	1-pentene	0.010488	0.009328	0.00733
5	4.739	pentane	0.010025	0.008746	0.007038
6	5.603	2-pentene	0.030911	0.033693	0.035058
7	5.815	2-methylbutene	0.00407	0.004337	0.003198
8	5.966	dimethylcyclopropene	0.013581	0.014198	0.010684
9	6.255	1-hexene	0.007757	0.006415	0.004332
10	8.61	hexane	0.036513	0.045348	0.039488
11	9.412	2-hexene	0.007188	0.007483	0.005064
12	13.859	heptene	0.033011	0.038658	0.029546
13	19.372	octene	0.02955	0.03657	0.029173
14	25.525	nonene	0.027433	0.035694	0.027644
15	28.285	undecene	0.024494	0.033331	0.02527
16	31.041	2,6-dimethyldecane	0.079126	0.079746	0.018089
17	31.239	3-methylundecane	0.321518	0.320598	0.07032
18	31.462	benzothiophene	4.257462	4.518783	1.679053
19	31.715	n-dodecane	94.79635	94.49681	97.6761
20	31.787	2-dodecene	0.003958	0.003838	0.005051
Average MW (g/mol)			166.5267	166.364	167.5358

Table E.3. Product distribution from a catalytic cracking run of pure n-dodecane sample at 450 °C, cat/oil = 5, and 5 seconds reaction time.

		Sample name	C1245052
Product #	Ret. Time	Product name	Wt %
1	2.117	propane	5.0920256
2	2.201	isobutane	4.8393177
3	2.351	2-methylbutane	0.6321477
4	2.431	pentane	0.7787812
5	2.471	1-pentene	0.1598407
6	2.523	2-pentene	0.4858383
7	2.72	1-hexene	0.0275261
8	2.782	2-methylpentane	0.1906406
9	2.892	3-methylpentane	0.05288
10	2.959	3-methylpentene	0.0863663
11	3.036	hexane	0.1811708
12	3.128	2-methylpentene	0.1494
13	3.209	2-hexene	0.0221902
14	3.277	3-methylpentene	0.0562825
15	3.366	methylcyclopentane	0.0955191
16	3.703	3-methylcyclopentene	0.0458682
17	3.859	benzene	0.109795
18	3.917	3-methylhexane	0.0339016
19	4.078	4-methylhexane	0.0225838
20	4.411	heptene	0.0552942
21	4.607	heptane	0.0715697
22	4.715	dimethylcyclopentene	0.0393434
23	6.832	toluene	0.4238282
24	8.153	octene	0.0415382
25	8.673	octane	0.0353283
26	12.281	ethylbenzene	0.0780415
27	12.646	p-xylene	0.3907668
28	13.6	1,2-dimethylbenzene	0.0993508
29	13.694	propylbenzene	0.0384965
30	16.295	1-ethyl-2-methyl benzene	0.1372219
31	17.773	1,3,5-trimethyl benzene	0.0698189
32	17.841	trimethyl benzene	0.0377802
33	25.249	2,6-dimethyldecane	0.0812679
34	25.486	3-methylundecane	0.3016657
35	26.064	dodecane	85.036612
		Average MW (g/mol)	131.83666

Table E.4. Product distribution from a catalytic cracking run of pure n-dodecane sample at 425 °C, cat/oil = 5, and 5 seconds contact time.

		Sample name	C1242551
Product #	Ret. Time	Product name	Wt %
1	2.109	propane	4.4527606
2	2.156	isobutane	1.7167328
3	2.194	butane	3.6006948
4	2.344	2-methylbutane	0.7499716
5	2.424	pentane	0.9947802
6	2.463	1-pentene	0.2016621
7	2.515	2-pentene	0.6327744
8	2.713	1-hexene	0.0324742
9	2.775	2-methylpentane	0.2613774
10	2.885	3-methylpentane	0.0724827
11	2.948	3-methylpentene	0.0591406
12	3.029	hexane	0.2723005
13	3.122	2-methylpentene	0.1509432
14	3.159	3-methylpentene	0.0592617
15	3.203	2-hexene	0.0288812
16	3.271	3-methylpentene	0.0825957
17	3.36	methylcyclopentane	0.082438
18	3.401	3-methylcyclopentene	0.0280747
19	3.697	3-methylcyclopentene	0.059584
20	3.853	benzene	0.0673315
21	3.911	2-methylhexane	0.057045
22	4.073	3-methylhexane	0.03698
23	4.245	3-methylcyclopentene	0.0140739
24	4.602	heptane	0.0895029
25	4.711	dimethylcyclopentene	0.0753154
26	6.829	toluene	0.2701045
27	8.672	octane	0.033102
28	12.284	ethylbenzene	0.0650789
29	12.648	p-xylene	0.2709539
30	13.603	1,2-dimethylbenzene	0.0629559
31	16.298	1-ethyl-2-methylbenzene	0.086252
32	16.349	1,3,5-trimethylbenzene	0.0513751
33	17.778	1,2,3-trimethylbenzene	0.0602835
34	25.251	2,6-dimethyldecane	0.0822528
35	25.488	3-methylundecane	0.303272
36	26.065	n-dodecane	84.83519
		Average MW (g/mol)	132.42689

Table E.5. Product distribution from a catalytic cracking run of pure n-dodecane sample at 400 °C, cat/oil = 5, and 5 seconds contact time.

		Sample name	C1240051
Product #	Ret. Time	Product name	Wt %
1	2.111	propane	2.7546403
2	2.195	isobutane	4.3685081
3	2.346	2-methylbutane	0.7009607
4	2.426	pentane	1.0146609
5	2.464	1-pentene	0.1808349
6	2.517	2-pentene	0.6589435
7	2.714	1-hexene	0.0296735
8	2.776	2-methylpentane	0.2849069
9	2.885	3-methylpentane	0.0783916
10	2.949	3-methylpentene	0.0777812
11	3.03	hexane	0.3230357
12	3.122	2-methylpenetene	0.1783865
13	3.159	3-methylpentene	0.064467
14	3.202	2-hexene	0.0290094
15	3.271	3-methylpenetene	0.0973761
16	3.36	methylcyclopentane	0.0579397
17	3.4	3-methylcyclopentene	0.0369306
18	3.696	3-methylcyclopentene	0.0494672
19	3.852	benzene	0.0318886
20	3.91	2-methylhexane	0.0750871
21	4.072	3-methylhexane	0.0428549
22	4.405	1-heptene	0.0391342
23	4.599	heptane	0.1003623
24	4.709	dimethylcyclopentene	0.0867423
25	5.211	2-heptene	0.027543
26	6.341	dimethylcyclopentene	0.0198882
27	6.825	toluene	0.0958316
28	8.661	octane	0.035375
29	12.642	p-xylene	0.0962021
30	13.598	1,2-dimethylbenzene	0.0212316
31	16.292	1-ethyl2-methylbenzene	0.0123133
32	17.771	1,3,5-trimethylbenzene	0.0133223
33	25.248	2,6-dimethyldecane	0.0849596
34	25.486	3-methylundecane	0.3147696
35	26.067	n-dodecane	87.916581
		Average MW (g/mol)	139.99462

In addition, Figures E.1 to E.3 demonstrate a comparison between the product distribution from catalytic cracking runs of pure n-dodecane samples at different temperatures, different contact times, and $\text{cat/oil} = 5$. It is important to mention that the unconverted fraction of n-dodecane is not reflected in these Figures.

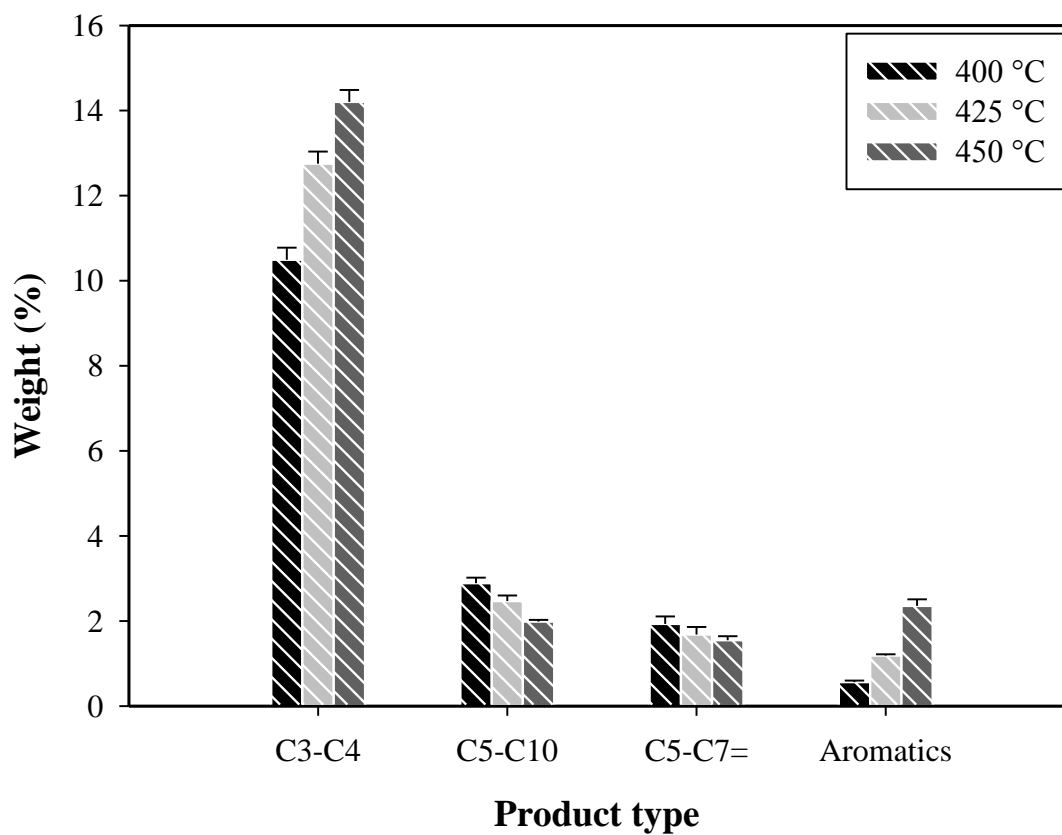


Figure E.1. Product distribution from catalytic cracking runs of pure n-dodecane samples at 7 seconds contact times and temperatures between 400 °C - 450 °C.

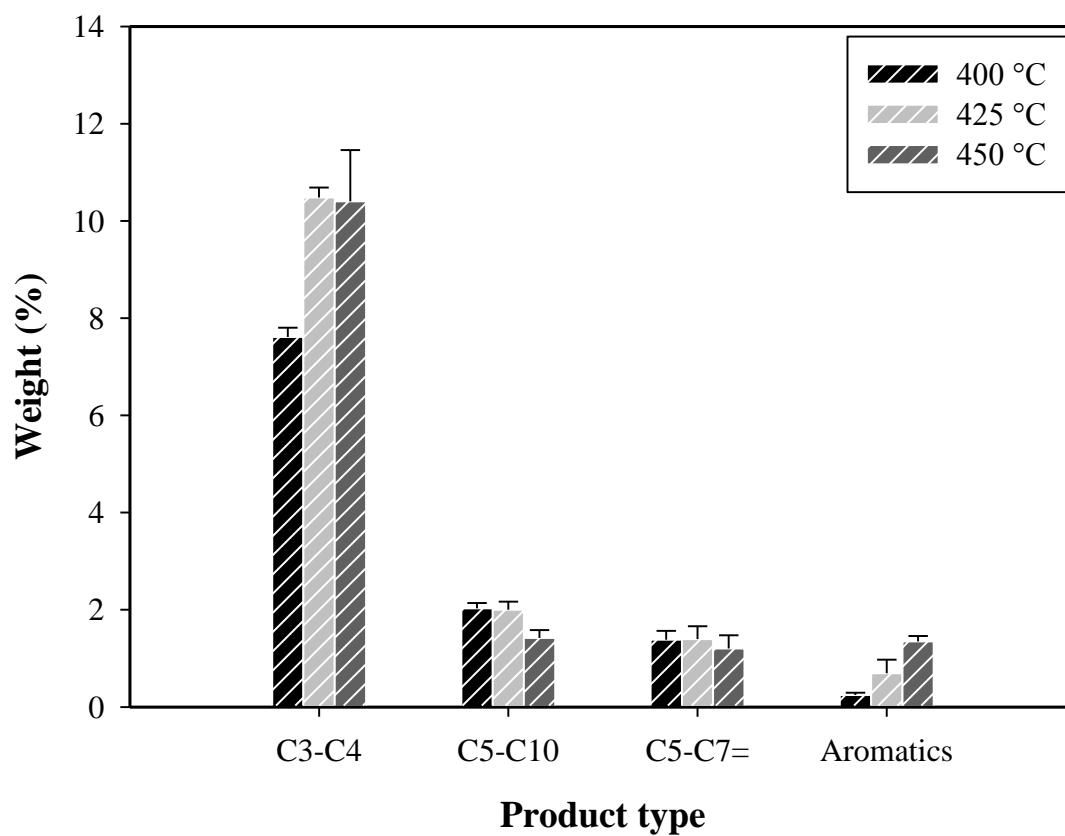


Figure E.2. Product distribution from catalytic cracking runs of pure n-dodecane samples at 5 seconds contact times and temperatures between 400 °C - 450 °C.

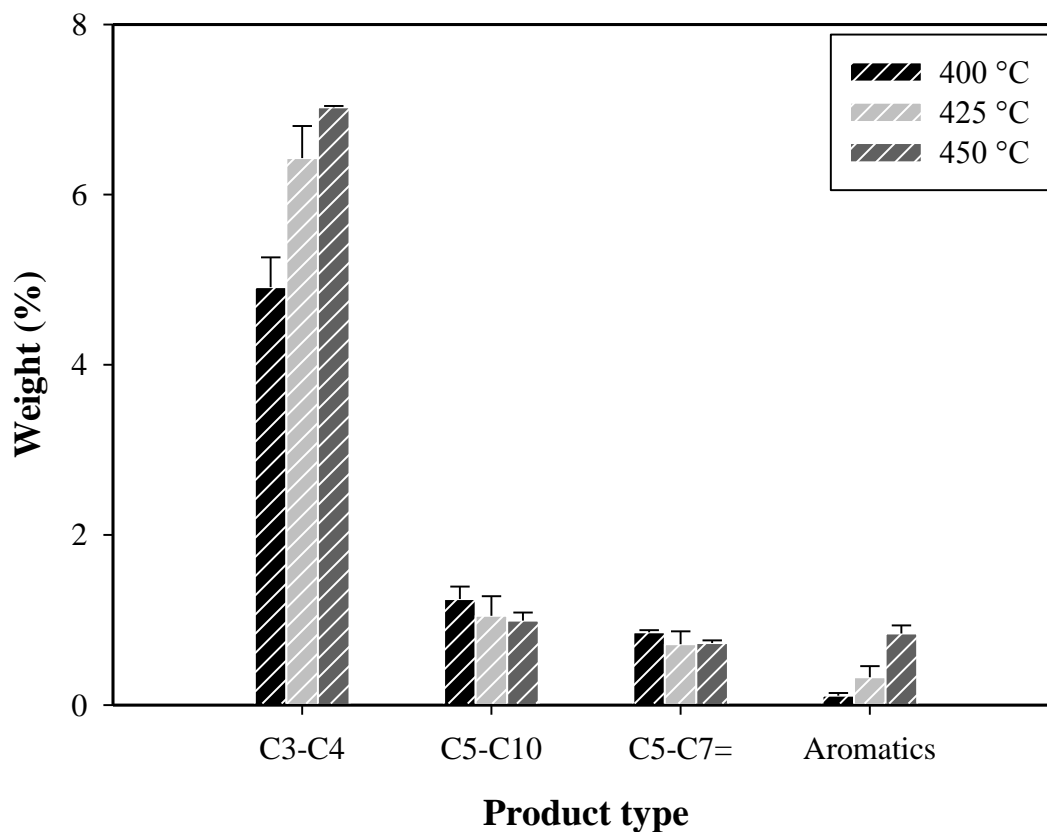


Figure E.3. Product distribution from catalytic cracking runs of pure n-dodecane samples at 3 seconds contact times and temperatures between 400 °C - 450 °C.

Tables E.6 to E.8 report the main products from catalytic conversion of 6 wt % benzothiophene / 94 wt % n-dodecane samples at different reaction temperatures (450 °C, 425 °C, and 400 °C) and 7 seconds reaction time.

Table E.6. Product distribution from a catalytic run of 6 wt % benzothiophene / 94 wt % n-dodecane samples at 450 °C, cat/oil = 5, and 7 seconds contact time.

		Sample name	6%B45071
Product #	Ret. Time	Product name	Wt %
1	2.071	propane	6.2972398
2	2.116	isobutane	2.105098
3	2.154	butane	4.0617207
4	2.301	2-methylbutane	0.8610961
5	2.379	pentane	1.0164742
6	2.418	1-pentene	0.2334612
7	2.468	2-pentene	0.5580938
8	2.662	1-hexene	0.0359419
9	2.722	2-methylpentane	0.2667523
10	2.829	3-methylpentane	0.0770067
11	2.895	2-hexene	0.1030293
12	2.971	hexane	0.2481009
13	3.06	2-methyl2-pentene	0.1514671
14	3.099	3-hexene	0.0469237
15	3.14	3-methyl2-pentene	0.037704
16	3.207	3-methyl2-pentene	0.0626766
17	3.293	methylcyclopentane	0.1374551
18	3.624	2-methylcyclopentene	0.0604274
19	3.775	benzene	0.1404956
20	3.832	2-methylhexane	0.0503914
21	3.99	3-methylhexane	0.0366031
22	4.159	3-methylcyclopentene	0.0210525
23	4.22	1,3-dimethylcyclopentane	0.0207567
24	4.316	1,2-dimethylcyclopentane	0.068851
25	4.509	heptane	0.1061442
26	4.613	heptene	0.0476625
27	5.106	methylcyclohexane	0.0288674
28	6.686	toluene	0.5486866
29	7.979	nonene	0.0468946
30	8.49	octane	0.0559319
31	12.145	ethylbenzene	0.1234728
32	12.521	p-xylene	0.5490348
33	13.49	1,3-dimethylbenzene	0.1400378
34	13.591	nonane	0.0404
35	13.917	trimethylnonane	0.0244466
36	16.176	1-ethyl3methylbenzene	0.2262795
37	17.634	1,2,3-trimethylbenzene	0.1030653
38	17.705	1,3,5-trimethylbenzene	0.0331336
39	25.211	3,6-dimethyldecane	0.0789883

40	25.45	3-methylundecane	0.2837272
41	25.732	benzothiophene	3.58
42	26.022	n-dodecane	77.225996
43	26.392	2-methylbenzothiophene	0.0153382
44	26.65	3-methylbenzothiophene	0.0038404
45	26.943	4-methylbenzothiophene	0.0026518
46	27.089	5-methylbenzothiophene	0.0178417
47	27.691	7-ethylbenzothiophene	0.0051496
48	27.997	2-ethylbenzothiophene	0.0026441
49	28.559	2-propylbenzothiophene	0.0109473
Average MW (g/mol)			124.47939

Table E.7. Product distribution from a catalytic run of 6 wt % benzothiophene / 94 wt % n-dodecane samples at 425 °C, cat/oil = 5, and 7 seconds contact time.

		Sample name	6%B42571
Product #	Ret. Time	Product name	Wt %
1	2.056	propane	4.3802274
2	2.137	butane	5.5262462
3	2.283	2-methylbutane	0.7730948
4	2.361	pentane	1.358395
5	2.449	1-pentene	0.7436756
6	2.64	1-hexene	0.0382297
7	2.7	2-methylpentane	0.286591
8	2.806	3-methylpentane	0.0772665
9	2.87	hexene	0.121689
10	2.946	hexane	0.3086889
11	3.035	2-methyl2-pentene	0.1834372
12	3.071	3-hexene	0.0706477
13	3.114	3-methyl2-pentene	0.034085
14	3.18	3-methyl2-pentene	0.0981449
15	3.266	methylcyclopentane	0.1255836
16	3.594	3-methylcyclopentene	0.0693288
17	3.746	benzene	0.0581797
18	3.802	2-methylhexane	0.0652547
19	3.961	3-methylhexane	0.0389978
20	4.129	3-methylcyclopentene	0.0182898
21	4.19	1,3-dimethylcyclopentane	0.0174884
22	4.284	1,2-dimethylcyclopentane	0.0751331
23	4.475	heptane	0.0992834
24	4.58	heptene	0.0752634
25	5.069	methylcyclohexane	0.0297635

26	6.165	1-methylcyclohexene	0.029244
27	6.637	toluene	0.2004299
28	7.907	nonene	0.0509148
29	8.415	octane	0.0432114
30	12.098	ethylbenzene	0.0542279
31	12.474	p-xylene	0.2173444
32	13.452	1,3-dimethylbenzene	0.0572056
33	13.552	nonane	0.0501744
34	16.136	1-ethyl4methylbenzene	0.0734593
35	16.185	1-ethyl3methylbenzene	0.046467
36	17.589	1,2,3-trimethylbenzene	0.0505854
37	17.661	1,3,5-trimethylbenzene	0.0485079
38	25.196	3,6-dimethyldecane	0.0802169
39	25.438	3-methylundecane	0.2972408
40	25.718	benzothiophene	3.97
41	26.012	n-dodecane	80.012453
42	26.381	2-methylbenzothiophene	0.0073167
43	26.638	3-methylbenzothiophene	0.0020248
44	26.936	4-methylbenzothiophene	0.0011529
45	27.077	5-methylbenzothiophene	0.0006958
46	27.869	7-ethylbenzothiophene	0.0121281
47	28.327	2-ethylbenzothiophene	0.0073475
48	28.559	2-propylbenzothiophene	0.0146850
Average MW (g/mol)			130.43119

Table E.8. Product distribution from a catalytic run of 6 wt % benzothiophene / 94 wt % n-dodecane samples at 400 °C, cat/oil = 5, and 7 seconds contact time.

		Sample name	6%B40071
Product #	Ret. Time	Product name	Wt %
1	2.129	propane	3.367627
2	2.176	isobutane	1.498797
3	2.213	butane	3.735808
4	2.365	2-methylbutane	0.781437
5	2.446	pentane	1.251788
6	2.485	2-pentene	0.228447
7	2.537	1-hexene	0.838822
8	2.736	2-methylpentane	0.037501
9	2.798	3-methylpentane	0.331564
10	2.908	hexene	0.086595
11	2.974	hexane	0.111464
12	3.054	2-methyl2-pentene	0.390216
13	3.147	3-hexene	0.223372
14	3.184	3-methyl2-pentene	0.081378
15	3.228	3-methyl2-pentene	0.036762
16	3.296	2-methylcyclopentane	0.121801
17	3.386	3-methylcyclopentane	0.071283
18	3.428	2-methylcyclopentene	0.047642
19	3.725	benzene	0.068944
20	3.881	2-methylhexane	0.033782
21	3.94	3-methylhexane	0.090444
22	4.103	3-methylcyclopentene	0.051713
23	4.276	1,2-dimethylcyclopentane	0.017605
24	4.438	1,3-dimethylcyclopentane	0.064736
25	4.635	1,2-dimethylcyclopentane	0.123241
26	4.745	heptane	0.121879
27	4.95	heptene	0.014176
28	5.248	2-methylcyclohexane	0.031593
29	6.388	3-methylcyclohexane	0.028981
30	6.876	toluene	0.094861
31	8.203	nonene	0.036058
32	8.728	octane	0.043499
33	12.325	ethylbenzene	0.026258
34	12.689	p-xylene	0.097136
35	13.637	1,3-dimethylbenzene	0.029089
36	13.726	nonane	0.03968
37	16.336	1-ethyl3methylbenzene	0.012187
38	17.823	1,2,3-trimethylbenzene	0.029235
39	17.888	1,3,5-trimethylbenzene	0.037506

40	25.269	3,6-dimethyldecane	0.082337
41	25.505	3-methylundecane	0.303485
42	25.788	benzothiophene	4.54
43	26.071	n-dodecane	80.72772
44	26.989	2-methylbenzothiophene	0.00185
45	27.126	3-methylbenzothiophene	0.000547
46	27.91	5-methylbenzothiophene	0.000499
47	28.156	7-ethylbenzothiophene	0.002017
48	28.316	2-ethylbenzothiophene	0.002266
49	28.515	2-propylbenzothiophene	0.004376
Average MW (g/mol)			133.84994

Appendix F.

Kinetic Modeling Parameters

F.1 Langmuir-Hinshelwood Mechanism Derivation

For a reaction to occur between adsorbed benzothiophene (BZT) molecule and adsorbed n-dodecane (C12) molecule, we can write:



where S representing the catalytic active site on which adsorption process is taking place.

Performing a site balance for the catalyst surface sites will result in:

$$\Theta_{\text{BZT}} + \Theta_{\text{C12}} + \Theta_{\text{V}} = 1 \quad (\text{F.4})$$

where, Θ_{BZT} is the fraction of sites occupied by benzothiophene, Θ_{C12} is the fraction of sites occupied by n-dodecane, and Θ_{V} is the fraction of empty sites.

Hence, we can write:

$$\Theta_{\text{BZT}} = K_{\text{BZT}} C_{\text{BZT}} \Theta_{\text{V}} \quad (\text{F.5})$$

$$\Theta_{\text{C12}} = K_{\text{C12}} C_{\text{C12}} \Theta_{\text{V}} \quad (\text{F.6})$$

where, K_{BZT} and C_{BZT} are the adsorption constant and concentration for benzothiophene species, respectively. Similarly, K_{C12} and C_{C12} are the adsorption constant and concentration for n-dodecane species, respectively.

Adding equations F5 and F6 will give:

$$\Theta_{BZT} + \Theta_{C12} = K_{BZT}C_{BZT}\Theta_V + K_{C12}C_{C12}\Theta_V \quad (F.7)$$

Now, adding +1 to both sides and multiplying by -1 will give:

$$1 - \Theta_{BZT} - \Theta_{C12} = 1 - \Theta_V(K_{BZT}C_{BZT} + K_{C12}C_{C12}) \quad (F.8)$$

The left hand side is basically Θ_V from equation F.4 and combining with the right hand side that contains Θ_V will give:

$$\Theta_V + \Theta_V(K_{BZT}C_{BZT} + K_{C12}C_{C12}) = 1 \quad (F.9)$$

As a result:

$$\Theta_V = \frac{1}{(1 + K_{BZT}C_{BZT} + K_{C12}C_{C12})} \quad (F.10)$$

Substituting equation F.10 into equations F.5 and F.6 will give respectively:

$$\Theta_{BZT} = \frac{K_{BZT}C_{BZT}}{(1 + K_{BZT}C_{BZT} + K_{C12}C_{C12})} \quad (F.11)$$

$$\Theta_{C12} = \frac{K_{C12}C_{C12}}{(1 + K_{BZT}C_{BZT} + K_{C12}C_{C12})} \quad (F.12)$$

The next step is writing the rate equations for BZT and C12 disappearances. It is worth to mention that products from the catalytic reaction are of two kinds: (i) alkylated benzothiophene (in gas phase and coke on catalyst) which produced by reacting an adsorbed benzothiophene with a cracked product (olefin) from adsorbed C12, and (ii) cracked products of C12 which produced by cracking of adsorbed C12 only. The first reaction is called bimolecular reaction where the second one is called unimolecular reaction. Keeping this in mind, one can write the reaction rate equations for BZT and C12 according to Langmuir-Hinshelwood formulations as follows:

$$-r_{\text{BZT}} = k_{\text{BZT}} \Theta_{\text{BZT}} \Theta_{\text{C12}} \quad (\text{F.13})$$

where, r_{BZT} is reaction rate of BZT with its rate constant k_{BZT} .

Substituting equation F.11 and F.12 into equation F.13 will give the final rate expression for benzothiophene as:

$$-r_{\text{BZT}} = \frac{k_{\text{BZT}} K_{\text{BZT}} C_{\text{BZT}} K_{\text{C12}} C_{\text{C12}}}{(1 + K_{\text{BZT}} C_{\text{BZT}} + K_{\text{C12}} C_{\text{C12}})^2} \quad (\text{F.14})$$

However, for cracking of C12 we can only write:

$$-r_{\text{C12}} = k_{\text{C12}} \Theta_{\text{C12}} \quad (\text{F.15})$$

where, r_{C12} is reaction rate for C12 cracking with its rate constant k_{C12} .

Similarly, substituting equation F.12 into equation F.15 will give the final rate expression for C₁₂ as:

$$-r_{C12} = \frac{k_{C12}K_{C12}C_{C12}}{(1 + K_{BZT}C_{BZT} + K_{C12}C_{C12})} \quad (F.16)$$

CURRICULUM VITAE

- Name:** Saad A. Al-Bogami
- Post Secondary Education:**
- January 2009 - April 2013
Doctor of Philosophy (PhD)
Chemical and Biochemical Engineering
University of Western Ontario, London, Ontario, Canada
- September 2007 - December 2008
Master's of Engineering (MEng)
Chemical and Petroleum Engineering
University of Calgary, Calgary, Alberta, Canada
- September 1998 – December 2002
Bachelor of Engineering Science (BESc)
Chemical Engineering
KFUPM, Dhahran, Saudi Arabia
- Related Work Experience:**
- September 2011 – December 2011
Teaching Assistant
Chemical and Biochemical Engineering Department
University of Western Ontario, London, Ontario, Canada
- September 2005 – August 2007
Lab Scientist / Research & Development Centre
Saudi Aramco Oil Company
Dhahran, Saudi Arabia
- March 2004 – August 2005
Operation Engineer / Yanbu Refinery
Saudi Aramco Oil Company
Yanbu, Saudi Arabia
- January 2003 – February 2004
Chemical Engineer
Professional Development Program
Saudi Aramco Oil Company
Dhahran, Saudi Arabia

List of Publications:**Journal Articles:**

S. A. Al-Bogami, H. de Lasa, “Catalytic Conversion of Benzothiophene Over a H-ZSM-5 Based Catalyst”, in press, *Fuel*, **2012**.

M.L. Ferreira, **S. A. Al-Bogami**, L. Jaimes, H. de Lasa, “Diffusion of Octane and Thiophene in Silicalite (MFI): A Molecular Dynamics (MD) Study”, submitted to *Microporous and Mesoporous Materials*.

S. A. Al-Bogami, M.L. Ferreira, H. de Lasa, “Self Diffusivity of n-Dodecane and Benzothiophene in ZSM-5 Zeolite; A Molecular Dynamics (MD) Study”, submitted to *Chemical Engineering Science*, **2012**.

S. A. Al-Bogami, H. de Lasa, “Catalytic Conversion of Benzothiophene Over a H-ZSM-5 Based Catalyst: A Kinetic Model”, submitted to *Industrial and Engineering Chemistry Research*, **2013**.

Conference Presentations:

S. A. Al-Bogami, M.L. Ferreira, H. de Lasa, “Hydrocarbon Desulfurization using ZSM-5 Zeolite: Self Diffusivity of n-Dodecane and Benzothiophene using Molecular Dynamics Simulation”, 61st Canadian Chemical Engineering Conference, London, Ontario, Canada, October 23-26, **2011**.

M.L. Ferreira, L. Jaimes, **S. A. Al-Bogami**, H. de Lasa, “Diffusion of Octane and Thiophene in Silicalite (MFI): Molecular Dynamics Study”, 17th Argentinian Catalysis Congress, Salta, Argentina, October 17-20, **2011**.

S. A. Al-Bogami, M.L. Ferreira, H. de Lasa, “Hydrocarbon Desulfurization using ZSM-5 Zeolite: Self Diffusivity of n-Dodecane and Benzothiophene using Molecular Dynamics Simulation”, 22nd Canadian Symposium on Catalysis, Quebec City, Quebec, Canada, May 13-16, **2012**.

S. A. Al-Bogami, M.L. Ferreira, H. de Lasa, “Molecular Dynamics Study of Benzothiophene and Dodecane Diffusion in Silicalite”, 23rd Iberoamerican Congress on Catalysis (CICAT 2012), Santa Fe, Argentina, September 2-7, **2012**.

S. A. Al-Bogami, H. de Lasa, “Benzothiophene Conversion Over a ZSM-5 Catalyst under Mild FCC Conditions: A Novel Approach for Light Diesel Desulfurization”, 62nd Canadian Chemical Engineering Conference, Vancouver, British Columbia, Canada, October 14-17, **2012**.

S. A. Al-Bogami, H. de Lasa, “Reactivity and Kinetics of Benzothiophene Conversion Over a H-ZSM5 Based Catalyst”, 3rd North American Symposium on Chemical Reaction Engineering (NASCRE-3), Houston, USA, March 17-20, **2013**.